

EXPERIMENTAL AND COMPUTATIONAL
INVESTIGATION OF SNOW MELTING
ON HEATED HORIZONTAL
SURFACES

By

SEAN LYNN HOCKERSMITH

Bachelor of Science

Oklahoma State University

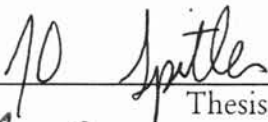
Stillwater, Oklahoma

1999

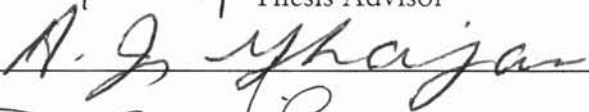
Submitted to the Faculty of the
Graduate College of the
Oklahoma State University
in partial fulfillment of
the requirements for
the Degree of
MASTER OF SCIENCE
December, 2002

EXPERIMENTAL AND COMPUTATIONAL
INVESTIGATION OF SNOW MELTING
ON HEATED HORIZONTAL
SURFACES

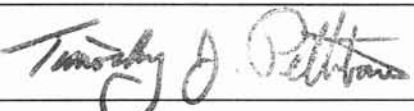
Thesis Approved:



Thesis Advisor







Dean of the Graduate College

ACKNOWLEDGEMENTS

I wish to thank Dr. Jeff Spitler for his guidance and trust, allowing me the creative freedom to make key decisions on the format and features. I wish to also thank Dr. Simon Rees for his help and my committee members for their time and patience. Dr. Samuel Colbeck of the Cold Regions Research and Engineering Laboratory also provided several papers and direction during the early stages and I would like to thank him.

Perhaps the greatest importance has been the love, support, and patience of my family. I would like to thank my parents Benny and Lenita Hockersmith for their continued support and patience throughout my life that has enable me to be where I am today.

Finally, I wish to thank all the faculty members and staff of the School of Mechanical and Aerospace Engineering and the School of Chemical Engineering for their support and guidance.

TABLE OF CONTENTS

<u>Chapter</u>	<u>Page</u>
CHAPTER 1	1
INTRODUCTION	1
1.1 Background	1
1.2 Thesis Organization.....	3
CHAPTER 2	5
LITERATURE REVIEW	5
2.1 Outline	5
2.2 Snowmaking.....	5
2.3 Snow/Ice Physical Properties	7
2.4 Heat Transfer / Heat Balance	11
2.4.1 Surface Convection	11
2.4.2 Natural Internal Convection.....	16
2.4.3 Radiation	20
2.5 Water Flow	29
2.6 Snow Metamorphism	35
2.7 Snow Melting from the Bottom	39
2.8 Road Effects	47
CHAPTER 3	48
NUMERICAL MODEL.....	48
3.1 Overview	48
3.2 Model	48
3.3 Boundary condition model.....	49
3.4 Model Detail Considerations.....	50
3.5 Geometry.....	51
3.6 Mass Transfer.....	53
3.7 Heat Transfer.....	54
3.8 Mathematical Model	56
3.9 Model Changes.....	64
CHAPTER 4	70
EXPERIMENTAL APPARATUS	70
4.1 Introduction	70
4.2 Snow Making/ Environmental Chamber.....	70
4.2.1 Top Section	74
4.2.2 Middle Section	77
4.2.3 Bottom Section.....	81
4.3 Snow Making Equipment.....	84
4.4 Mechanical Refrigeration Setup.....	89
4.5 Chamber Thermocouple Placement	95
4.6 Snow-melting apparatus.....	96
4.7 Weight Measurement	102

4.8 Height Measurement	103
4.9 Instrument Calibration.....	103
CHAPTER 5	104
RESULTS AND DISCUSSION.....	104
5.1 Experimental Procedure	104
5.1.1 Snow-Making Procedure.....	106
5.2 Preliminary Experiments.....	106
5.2.1 Uneven melting/Hot spots on the plate	107
5.2.2 Water drainage experiment	109
5.2.3 Capillary Height	110
5.2.4 Plate Temperature – Qualitative Analysis.....	113
5.2.5 Plate Temperature - Quantitative Analysis	117
5.2.6 Crystal Size	118
5.3 Snow Melting Results	120
5.4 Thermodynamic Melt Time	128
5.5 Melt water Runoff.....	131
5.6 Qualitative discussion of snow melt.....	133
5.7 Practical Guidance.....	135
5.8 Additional Modeling	137
CHAPTER 6	138
CONCLUSIONS AND RECOMMENDATIONS.....	138
6.1 Conclusions	138
6.2 Recommendations	139
BIBLIOGRAPHY	141
APPENDIX A	146
INSTRUMENT CALIBRATION	146
APPENDIX B.....	149
ERROR ANALYSIS/ UNCERTAINTY ANALYSIS	149
B.1: Overview	149
B.2: Model.....	149
B.2.1: Mass of Snow	149
B.2.2: Melt Time	161
B.2.8: Camera Light	162
B.2.9: Convection Heat Flux.....	156
B.2.10: Radiation Heat Flux.....	163
B.2.11: Apparatus Radial Heat Gain	165
B.2.12: Heat Gain from Backside of Plate	166
B.2.13: Initial Conditions	166
B.2.14: Heat Storage	167
B.2.15: Overall Numerical Uncertainty	170
B.3: Experimental Uncertainty.....	171
B.4: Uncertainty Summary.....	180
APPENDIX C	181
WATER SATURATION LAYER MODEL	181
Procedure.....	182
Results	183

APPENDIX D	189
OTHER EXPERIMENTAL DATA	189

LIST OF TABLES

<u>Table</u>	<u>Page</u>
Table 2.3-1: Representative Physical Property Data, Yen (1981)	10
Table 3.3-1: Possible Boundary Conditions at the end of the time step vs. Current Environmental Conditions (Spitler, et al. 2001)	50
Table 5.3-1: Melt Time Comparison	123
Table 5.3-2: Corrected Melt Time Comparison	125

LIST OF FIGURES

<u>Figure</u>	<u>Page</u>
Figure 3.2-1: Grid generated of the bridge deck and embedded pipes (Spitler, et al. 2001)	49
Figure 3.5-1: Snow/Slush Layer Diagram.....	52
Figure 3.6-1: Mass Balance.....	54
Figure 3.7-1: Overall Heat Transfer Balance	56
Figure 3.8-1: Schematic representation of heat transfer in the two-node snowmelt model (Spitler, et al. 2001).....	57
Figure 3.9-1: Reradiating Surface Node Diagram	67
Figure 4.2-1 Concrete Test Slab.....	71
Figure 4.2-2: Side View of Chamber (inside dimensions are noted).....	73
Figure 4.2-3: Environmental Chamber	74
Figure 4.2-4: Chamber Roof viewed from the inside.....	76
Figure 4.2-5: Air return in the sidewall of the top section	77
Figure 4.2-6: Middle Section Breakdown in two L's	78
Figure 4.2-7: Snowmaking holes in side wall	79
Figure 4.2-8: Window and Insulative Plug	80
Figure 4.2-9: One side of the chamber (note the location of the snow making equipment)	81
Figure 4.2-10: Bottom Section and doors	82
Figure 4.2-11: Drainage Channel	83
Figure 4.2-12: Air Diffuser	84
Figure 4.3-1: Snowmaking Nozzle.....	86
Figure 4.3-2: Snowmaking Control Box	87
Figure 4.3-3: Snowmaking Setup.....	88
Figure 4.3-4: Liquid Nitrogen Nozzle and Snow Making Nozzle from the Inside of Chamber	89
Figure 4.4-1: Mechanical Refrigeration Setup.....	90
Figure 4.4-2: Inside of Fan Box	91
Figure 4.4-3: Fan Box	92
Figure 4.4-4: Empty Heat Exchanger Box	93
Figure 4.4-5: Heat Exchanger Coil	93
Figure 4.4-6: Heat Exchanger Box.....	94
Figure 4.4-7: Heat Exchanger Box with Chillers.....	95
Figure 4.6-1: Plexiglas Tube Fitted with Aluminum Plate	97
Figure 4.6-2: Nichrome wire coiled and expoxied to the plate.....	98
Figure 4.6-3: Heated Plate Setup.....	99
Figure 4.6-4: Layer profile of heated plate	101
Figure 4.6-5: Final Heated Plate Setup	101
Figure 4.6-6: Insulation Around Plexiglas Tube.....	102
Figure 5.2-1: Hot Spot Temperature Profile	108
Figure 5.2-2: Plate Temperature Profile after Thickening	109
Figure 5.2-3: Capillary height measurement (density=250 kg/m ³).....	111

Figure 5.2-4: Experimental Saturated Height	113
Figure 5.2-5: General Temperature Profile with Water Run-off	114
Figure 5.2-6: Crystal size (close up)	119
Figure 5.2-7: Crystal size	120
Figure 5.3-1: Model vs. Experimental Height Validation (789 W/m ²).....	122
Figure 5.3-2: Model Melt Time Comparison.....	126
Figure 5.3-3: Model vs. Experimental Melt Time	127
Figure 5.3-4: Model vs. Experimental Melt Time Modified for Inhomogeneity.....	128
Figure 5.4-1: Thermodynamic, Model, and Experimental Melt Time vs. Heat Flux	130
Figure 5.5-1: Experimental vs. Model Melt Water Run-off (789 W/m ²)	132

CHAPTER 1

INTRODUCTION

1.1 Background

Snow, in its pure form, is simple porous ice. Although snow can be described simply, snowmaking and snow melting are not quite so easily analyzed. Snow is formed naturally by the collection of fallen ice crystals, which in turn collect on the ground and form the highly porous snow, as we know it. Snow is quite a broad word for the deposited ice crystals. If you ask school children, they will tell you there is a difference in snow because some snow forms snowballs quite easily and some snow will not. Some ice crystals are quite large and very elegant and some are small. Snow can be compacted, it can contain impurities, e.g. acid snow, and it can have different strength characteristics. Over time the deposited snow can undergo a wide range of changes. One of the most important is called snow metamorphism where the large snow crystals grow in size at the expense of the smaller crystals. This has been implicated as a precursor for avalanches. Rain can form a hard ice layer within the snow, or solar radiation can melt the top layer of snow and then, overnight, refreeze into a hard ice layer. Snow can partially melt and form a slush layer. Most of these changes in snow have one aspect in common, they take place over time and, more specifically, the time scale is measured in days. In each case, snow is defined primarily by the size and shape of the individual

grain; the other primary physical characteristics are density, grain size, grain shape, liquid water content, hardness index, and snow temperature all of which have been adopted as the *International Classification for Seasonal Snow on the Ground* (Colbeck, et al. 1991).

Airports must remove the snow from the runways and from the airplane wings; roads/highways must be cleared for normal driving and special care must be taken with bridges, because the bridges are exposed on all sides to the atmosphere; thus, bridge decks will freeze at a much faster rate. As the snow melts on the bridge and becomes slush or water, the possibility of ice forming on the bridge increases, which produces a very unsafe scenario for motorists.

A current road/bridge de-icing practice involves the widespread use of salt. Salt interacts with water/ice and causes a freezing point depression, which in most cases will melt the ice or and prevent ice from forming. Salt will work except where the temperature is very low. Salt is typically the de-icer of choice because of its relative inexpensive initial cost; however the salt will damage the bridge deck over time by corroding the rebar within the concrete. The salt will also be picked up by vehicles which in time will corrode the metal. The cost of replacement of the bridge deck is often very large and therefore, if an alternative means could be found to prevent ice on the bridge-deck, savings could be realized. Sand is also sometimes used on snow and ice, however sand works more as a traction aid than a snow melting mechanism.

One alternative method involves embedding the bridge-deck with a network of hydronic tubing to facilitate snow melting. Historically, sidewalks and onramps (Bienert, et al. 1974) have been fitted with hydronic tubing to remove snow and ice. This is similar to technology that has been used to provide radiant heating in houses. To keep the bridge

from freezing, a warm liquid must be circulated through the pipes. The liquid may be heated with a boiler or a ground source heat pump system and gives the capability to keep the bridge free of ice. The pairing of a ground source heat pump and hydronic tubing embedded in the bridge deck was put together by researchers at Oklahoma State University (Chiasson and Spitler, 2000) and is called the “smart bridge”. To evaluate the effectiveness of the “smart bridge”, numerical models must be created for all the main parts of the system, i.e. heat pump, bridge deck with snow and ice melting, and a ground loop heat exchanger. The numerical models can then be used to predict the response time of the system. These models can also be used to help train a neural network so that a “smart” controller can be developed to predict and respond to the ever-changing weather conditions.

1.2 Thesis Organization

This thesis is organized as follows. The following chapter, Chapter II, will provide a review of the literature relating to snow melting, both from a modeling viewpoint and from a heat transfer aspect. The level of detail of the information varies from very gross approximations to very detailed crystal level. Chapter III will present the numerical model utilized as the snow-melting algorithm. Only the snow-melting portion of the numerical model will be discussed. Chapter IV will present the experimental apparatus for making snow, as well as the snow melting apparatus used to validate the numerical model. Chapter V covers the experimental results of the snow melting with emphasis on snow melting time and water runoff. The thesis will be wrapped up in Chapter VI, where the conclusions and recommendations will be discussed. Appendix A

covers the calibration of the test equipment. An uncertainty analysis was completed and can be found in Appendix B. A separate water saturation layer height model was developed and tested in Appendix C. Appendix D includes the experimental data and the numerical comparison for each of the heat fluxes studied.

CHAPTER 2

LITERATURE REVIEW

2.1 Outline

The following literature review section provides an overview of the literature related to snowmaking, snow properties, snow melting, and snow making. First, a brief explanation on natural and artificial snow making procedures will be presented. Then, general snow properties and the current classification system will be reviewed. Following these somewhat general sections, heat transfer mechanisms involved in snow melting will be reviewed. A snow specific phenomenon called metamorphism will be discussed and finally, the literature directly related to melting snow on heated horizontal surfaces will be discussed.

2.2 Snowmaking

Because artificial snowmaking is more of an art than a science, and because snowmaking has important commercial applications, snowmaking processes are usually proprietary. The general principles of snowmaking are similar between the different processes, which tend to follow natural snow making principles. Natural snow is formed in the atmosphere when water vapor, found in clouds, sublimates into ice crystals. Just as rain needs a seed to start growth, so do ice crystals, and usually these seeds are found in nature to be dirt or smoke particles. As the crystals freeze, they begin to grow, and the mass of ice causes the ice crystals to fall to the earth. As the crystals fall, they continue

to grow until they reach the earth. New fallen snow is highly faceted and has a very low density when compared to aged ground snow (Colbeck, 1991).

To make snow without the use of clouds, several aids can be utilized to enhance the snowmaking. Instead of natural smog, soot, or dust, artificial seeds can range from powdered substances to bacteria strains. In climates in which the outdoor temperature is sufficiently low, liquid water can simply be atomized, to form a fine mist of water, and blown sufficiently high in the air so that the water has time to freeze. If the outdoor temperature will not allow for water only systems, the water may be mixed with compressed air before leaving the nozzle. The expansion of the compressed air removes enough heat from the water so that the growth of ice crystals is significantly accelerated (Shea, 1999). One such report of snowmaking is by a Virginia Tech student whose project was to monitor the efficiency of snow cover on the “smart road” (Shea, 1999). This projects’ main objective is to monitor the effects of snow on road conditions. To do this, a network of snowmaking towers were positioned on a road section such that snow could be made anytime during the winter months of the year. Several general snow measurement criteria were set along with a way of measuring the efficiency of the coverage of the snow guns.

A group of senior mechanical engineering students at Oklahoma State University were tasked to develop a laboratory scale snowmaking device (Longwill, et al. 1999). The density of the snow was set as a criteria for measuring the quality of the snow, i.e. high density=poor snow and low density = good snow. The team evaluated using cryogenic liquids as a means to cool a chamber to provide an environment for the water droplets to cool and eventually freeze to form snow. The costs of various cooling

methods were evaluated and it was determined that liquid nitrogen was the most economical choice. From a nozzle stand point, several options were evaluated and the chosen nozzle atomized the water by collision. Three streams of water equally spaced were directed to the apex of the triangle. The collisions atomized the water and provided for the water droplets to form snow. The snow was extremely dense (500-700 kg/m³)[31.2-43.7 lb/ft³]. To help aid in the atomization of the water, compressed air was mixed with the water, which pressurized the water for a more explosive collision. The limitations of this setup were that achieving a perfect collision was very hard and therefore, not all the water was atomized, which then resulted in the dense snow due to unfrozen liquid water. However, if a better atomization process could be found, then the setup would provide for a means to make relatively low density laboratory scale snow. A description of one solution is provided in Chapter III.

2.3 Snow/Ice Physical Properties

To accurately describe snow melting in a numerical sense, several mathematical models need to be developed that describe physical properties. Because snow is an ever changing material the physical properties are not constant, but functions of the primary characteristics, such as density, grain shape, temperature, etc. These primary characteristics will be described below and other physical properties will be discussed thereafter.

Colbeck (1986) argued for the necessity of a new all inclusive snow classification scheme. As a result, a new classification scheme was created and is explained by Colbeck, et al. (1990) in the *International Classification for Seasonal Snow on the Ground*. The classification scheme classifies snow by 8 primary physical characteristics:

density, grain shape, grain size, liquid water content, impurities, strength, hardness index, snow temperature. Each of the characteristics are self-explanatory except for grain shape. The grain shape is dependent upon the conditions of the snow and the past history. For instance, if the snow was subject to a freeze-thaw cycle the crystal shape will be much different than, say, new fallen snow. For this reason the grain shape classification is divided into 9 subclasses with differing characteristics of crystal shape. To accurately describe snow, each of the primary characteristics should be addressed.

Past snow research did not use a classification scheme and, in fact, most of the correlations only deal with one of the variables. For example, snow thermal conductivity, as will be discussed later, has been measured and correlated to density by many researchers. Other characteristics besides density may also affect the thermal conductivity. If correlations were developed that accounted for grain shape, it might be possible to more accurately estimate the thermal conductivity.

Yen (1981) reviews the reported data on the various thermal properties of snow and ice. The following properties were reviewed:

- Ice Density as a function of inverse temperature
- Coefficient of linear expansion of ice as a function of temperature
- Compressibility of ice as a function of temperature
- Compaction (change of density over time) of snow as a function of density and temperature
- The change in equilibrium melting temperature of snow as a function of hydrostatic pressure (regelation)

- Constant pressure heat capacity as a function of temperature and a correlation to determine constant volume heat capacity from the data
- Latent heat of fusion as a function of temperature
- Thermal conductivity of ice as a function of temperature
- Effective thermal conductivity of snow as a function of density

The following chart presents representative data from Yen (1981) at a reference temperature of 0°C and atmospheric pressure. The reference snow density was set as 200 kg/m³.

Physical Property	Reference Value	Range	Equation Form
Density (Ice)	0.9167 Mg/m ³	0.916-0.918	
Coefficient of Linear Expansion (Ice)	54.41x10 ⁻⁶ (K ⁻¹)		$\gamma=A+B*T$
Compressibility	0.03x10 ⁻⁶ (bar ⁻¹)		$\omega=C*\exp(D*T)$
Regelation (Ice)	0.00738 (°C/bar)		
Constant Pressure Heat Capacity (Snow & Ice)	37.74 (J/mol K)		$c_p=E+F*T$
Latent Heat of Fusion	335 (kJ/kg)		$L_f=G+H*T$
Thermal Conductivity (Ice)	2.07 (W/mK)	2.0-2.1	$\lambda_i=I*\exp(J*T)$
Thermal Conductivity (Snow)	0.107 (W/mK)	0.03-0.6	$\lambda_{sc}=K*\rho_s^L$

Table 2.3-1: Representative Physical Property Data, Yen (1981)

Yen, et al. (1991) provide a slightly updated and expanded review of several thermo-physical properties of snow and ice. Eleven different correlations are presented that present thermal conductivity as a function of snow density. The authors also provide several equations for the specific heat of snow and ice (determined to be the same) as a function of temperature. Several other physical properties of ice are also presented including: thermal expansion coefficient, compressibility, latent heat, and thermal diffusivity.

2.4 Heat Transfer / Heat Balance

Heat gain and loss for the snow-melting model are evaluated using the heat balance method. This method will be discussed in detail in Chapter III. Heat balance equations are applied at the top surface of the snow, the snow/slush interface, and the slush/slab boundary. Each of the major heat transfer mechanisms that affect the heat balance are discussed below.

The numerical model used the recommended snow melting load calculation procedures adopted by ASHRAE, which can be found in the paper by Ramsey, et al. (1999) entitled *Updated Design Guidelines for Snow Melting Systems*. These guidelines provide for recommended convection correlations, radiation correlations, etc. They do not cover any snow-specific problems such as snow metamorphism. These guidelines will be discussed individually in the following subsections.

2.4.1 Surface Convection

Convection is defined as the transport of energy or mass to or from a surface by both molecular conduction processes and gross fluid movement (Kays and Crawford 1993). Convection is numerically calculated using the following equation, sometimes called Newton's Law of Cooling:

$$q_{conv} = h_c A (T_s - T_\infty) \quad (2-1)$$

Where:

q_{conv} = Heat loss from surface due to convection (W)

h_c = Convection coefficient (W/m²K)

A = Surface area (m²)

T_∞ = Free stream temperature (K)

T_s = Surface temperature (K)

To use this equation the convection coefficient must be found either using empirical or correlated values. The rest of this section will summarize the different convection correlations found in literature.

Kays and Crawford (1993) provide an empirical solution for an external turbulent flow over a flat plate with no unheated starting length and with the following restrictions:

$$h_c = 0.0287 \frac{k}{L} \text{Re}_x^{0.8} \text{Pr}^{0.6} \quad (2-2)$$

$$0.5 < \text{Pr} < 1.0 : 5 \times 10^5 < \text{Re}_x < 5 \times 10^6$$

Where:

k = Thermal conductivity of air (W/mK)

L =Length of plate (m)

Re_x = Reynolds number based on a characteristic length ($=xv\rho/\mu$)

x = Characteristic length (m)

v = Velocity of the free stream (m/s)

This equation is valid for fluids with Prandtl numbers between 0.5 and 1.0 and a length defined Reynolds number between 5×10^5 and 5×10^6 . Air, at standard conditions, has a Prandtl number of approximately 0.7 and therefore meets the first restriction. The second restriction is to ensure fully turbulent flow. The kinematic viscosity of air at standard conditions is approximately $13.30 \times 10^{-6} \text{ m}^2/\text{s}$. If we then set the definition of Reynolds number equal to the acceptable range defined by equation 2-2 the acceptable product of characteristic length and velocity:

$$13.3 \times 10^{-6} * 5 \times 10^5 = xv = 6.65 \dots \frac{\text{m}^2}{\text{s}} \quad (2-3)$$

$$13.3 \times 10^{-6} * 5 \times 10^6 = xv = 66.5 \dots \frac{\text{m}^2}{\text{s}}$$

For purposes of demonstrating the lower boundary condition we will assume a wind velocity of 2.23 m/s (5 mph), therefore the convection correlation is valid for lengths greater than 3 meters. When evaluating the upper limit, we will assume a wind velocity was 9 m/s (20 mph), which makes the convection correlation is valid for lengths less than 7.4 meters. Potentially there could be many cases in which the correlation is not valid especially for snow melting systems. This limitation may not significantly affect the end result and possibly could still be utilized with some modification.

Yazdanian and Klems (1994) provide another model that was experimentally determined from convection film coefficient over the exterior surface of a window. The convection coefficient correlated as a function of wind speed (both windward and leeward) and the temperature difference:

$$h_c = \sqrt{\left(C_t(\Delta T)^{\frac{1}{3}}\right)^2 + (aV_o^b)^2} \quad (2-4)$$

Where:

C_t = Turbulent natural convection constant (0.84 W/m²K^{4/3})

a, b = Constants [$a=2.38$ W/m²K(m/s), $b=0.89$]

V_o = Wind speed at standard condition (m/s)

This temperature difference changes Newton's law of cooling into a non-linear equation, which increases the computational time necessary to solve the equations.

Kustas, et al. (1994); Jordan, et al. (1999a); Kondo and Yamazaki (1990); and Tarboton and Luce (1996) use the simplified Thornthwaite-Holzman bulk transfer approach for parameterizing the turbulent transfer of heat and water vapor, which is based on the bulk Richardson number (Ri):

$$Ri = gz(T_a - T_s)(T_a V_o^2)^{-1} \quad (2-5)$$

Where:

g =Acceleration due to gravity (m/s^2)

T_a = Temperature of the air at z (K)

T_s =Temperature of the surface (K)

z = Reference elevation (for air temperature and wind speed) above the surface (m)

V_o = Wind speed at elevation z (m/s)

This method splits the convection heat gain/loss into a sensible and latent heat gain/loss as can be seen in the following equations:

$$Q_s = \rho c_p C_h k^2 \left[\ln \left(\frac{z}{z_o} \right) \right]^{-2} V_o (T_a - T_s) \quad (2-6)$$

$$Q_L = \rho L C_e k^2 \left[\ln \left(\frac{z}{z_o} \right) \right]^{-2} V_o (\phi_a - \phi_s) \quad (2-7)$$

Where:

ρ = Density of air at z (kg/m^3)

c_p = Specific heat of air (kJ/kgK)

L = Latent heat of vaporization (kJ/kg)

k = von Karman's constant ($=0.4$)

z_o = Roughness length for momentum (m), [$z_o=1$ mm]

ϕ_a = Specific humidity of air at z

ϕ_s = Specific humidity of air near the surface

C_h, C_e = Bulk transfer coefficients

The specific humidity, wind speed, and free stream air temperature are measured at a reference height, z . The bulk transfer coefficients are calculated as follows:

$$C_h = (1 - 58 Ri)^{\frac{1}{4}}; Ri < 0 \quad (2-8)$$

$$C_h = (1 + 7 Ri)^{-0.1}; Ri > 0 \quad (2-9)$$

$$C_e = 0.5 C_h \quad (2-10)$$

This method could be compared to the Lewis analogy. If we start with Fick's law we can define the heat gain/loss by the following:

$$Q_L = \dot{m}L = h_m A (C_w - C_\infty) \quad (2-11)$$

Where:

Q_L = Heat loss/gain due to latent heat (kJ/s)

\dot{m} = Liquid loss due to evaporation (kg/s)

h_m = Mass transfer coefficient (m/s)

A = Area (m²)

C_w = Wetted concentration (kg/m³)

C_∞ = Free-stream concentration (kg/m³)

Typically the concentration is reported as humidity ratio and therefore equation 2-11 can be changed to reflect that change:

$$Q_L = h_m A \rho (w_w - w_\infty) \quad (2-12)$$

Where:

w_∞ = Humidity ratio of free stream air

w_w = Humidity ratio of air near the surface

This can be compared directly with equation 2-7, with a more defined mass transfer coefficient.

2.4.2 Natural Internal Convection

Internal convection, as defined by Powers, et al. (1985), occurs due to a density gradient; this buoyancy force can be thought of as warm air rising and cold air assuming the space caused by the warm air void. Powers, et al. (1985) describe how, in low density snows, conduction through air is not negligible; however, in high density snows, which tend to have lower porosity and thus smaller air pockets, conduction through the ice lattice dominates. To determine the occurrence of this buoyancy force convection, the dimensionless Rayleigh number was utilized and is defined below.

$$Ra = Gr Pr = \frac{\rho_o g \beta \Delta T H K}{\mu \kappa} \quad (2-13)$$

Where:

Ra = Rayleigh number (dimensionless)

Gr = Grashof number (dimensionless)

Pr = Prandtl number (dimensionless)

ρ_o = Density of fluid at reference temperature (kg/m^3)

H = Depth of porous layer (m)

K = Intrinsic permeability (cm^2)

g = Gravitational acceleration (m/s^2)

ΔT = Temperature difference ($^{\circ}\text{C}$)

μ = Dynamic viscosity ($\text{mPa}\cdot\text{s}$)

κ = Thermal diffusivity ($k/\rho c$) (m^2/s)

β = Volumetric coefficient of thermal expansion (for ideal gas $\beta=1/T_{\infty}$)($1/\text{K}$)

Natural convection occurs when the Rayleigh number is greater than the critical Rayleigh number. The critical Rayleigh number is a function of boundary conditions and is defined as the onset of convection. The Boussinesq approximation is made, which states that the density changes due to temperature are considered for buoyancy calculations but ignored everywhere else. For a constant flux, impermeable bottom boundary condition and a constant temperature permeable top boundary condition the critical Rayleigh number was determined to be 17.7.

The Nusselt number is commonly defined as:

$$Nu = \frac{hx}{k} \quad (2-14)$$

Where:

h = Convection coefficient (W/mK)

x = Length (m)

k = Thermal conductivity (W/m²K)

Customarily when applying the Nusselt number to porous media is redefined (Powers, et al. 1985):

$$Nu = \frac{k_{eff}}{k_m} \quad (2-15)$$

Where:

k_{eff} = Effective thermal conductivity (W/mK)

k_m = Thermal conductivity of the media (W/mK)

The effective thermal conductivity accounts for both conduction and convection heat transfer. The thermal conductivity of the media accounts for the heat conduction through both the fluid and the solid.

The Nusselt number is a ratio of convection effects to conduction. If the Nusselt number is less than unity, conduction effects outweigh the convection effects, and thus, if the Nusselt number is exactly equal to 1.0, convection has an equal effect on heat transfer. Powers, et al. (1985) present a chart for critical Rayleigh numbers and the corresponding experimentally determined Nusselt. For the case described above, if the top boundary condition is permeable constant temperature and the bottom boundary condition is impermeable and constant flux, and the Rayleigh number is 200, the corresponding Nusselt number is 3.1.

A numerical model was developed and starts with the equation of motion developed by Darcy. It was shown that the Reynolds number for airflow in snow was sufficiently low that Darcy's Law should be valid. The energy equations took into account the effect of latent heat from vapor transport. Only steady state results were found because it was assumed that snow was at least quasi-steady due to the slow changes. The investigators then utilized a Taylor series expansion to discretize the PDEs and a numerical finite difference code to solve the equations. The numerical modeling was used with a constant flux thermal boundary condition to develop the following correlation:

$$Nu = 1 + 0.365 \left(\frac{Ra}{Ra_c} - 1 \right) \quad (2-16)$$

The effect of slope on the Nusselt number was also found. After the numerical model was compared to older experimental data, the investigators prepared several new experiments to compare with the numerical model. The data appeared to match the numerical model fairly well. Using the validated model the investigators back calculated

to find the critical temperature difference for the onset of convection. If we start with the definition of the Rayleigh number and replace Ra with Ra_{cr} and ΔT with ΔT_{cr} they obtain the following equation:

$$\Delta T_{cr} = \frac{\mu \kappa}{\rho_o \beta g K} \frac{1}{H} Ra_{cr} \quad (2-17)$$

An alpine snow pack was used as the example with a grain size of 1mm and a density of 0.25 g/cm^3 . The air temperature was assumed to be -20°C and pressure of 10^5 Pa . With an alpine depth of 100 cm the equation was reduced to:

$$\Delta T_{cr} = 1.73 Ra_{cr} \quad (2-18)$$

The critical Rayleigh number was found to be only a function of the boundary conditions from earlier work. With the boundary conditions stated earlier the critical Rayleigh number was found to be 17.7 and therefore the critical temperature difference for the onset of convection was found to be 30.6°C . The investigators stated that this temperature difference is not commonly reached in typical alpine snow packs.

The investigators provide the following conclusions from the work completed:

- Thermal convection in snow may be described as creeping flow.
- Convection was found to have a substantial effect on the transfer of vapor through the snow cover.
- Convection may not substantially increase the rate of metamorphism.

If the analogy described by Powers, et al. (1985) is used in our simple snowmelt case, the onset of thermal convection could be determined. At first we will assume there is a 10 cm snow already on the ground, and that the new fallen snow has a diameter of 0.2 mm and a density of 0.1 g/cm^3 . The air is at 0°C and standard atmospheric pressure. Equation 2-17 can then be solved for the new conditions:

$$\Delta T_{cr} = 0.197 Ra_{cr} \quad (2-19)$$

With the set boundary conditions the Rayleigh number was determined earlier to be 17.7 and therefore the temperature difference necessary for the onset of convection is 3.5°C. This temperature difference could be possible within the snow pack. If we assume a 5°C temperature difference and using equation 2-16 the Nusselt number was determined to be 1.17, which would seem to indicate that the convection would increase the heat transfer by 17% a substantial number but it must be kept in mind that this assumes a 5°C temperature difference which could occur; however, probably not. This melting case where initially there is 10 cm of snow on the “slab” and then melted usually does not occur except for extreme blizzard conditions. Usually the snow is melted as it falls and therefore the height does not reach our 10 cm, and would rarely reach 1cm. If we rework the earlier example replacing the 10 cm with 1 cm, the critical temperature difference can quickly be determined to be 35°C, which under normal circumstance would seem improbable and therefore internal convection is ignored.

2.4.3 Radiation

Thermal radiation is defined as the rate at which energy is emitted by matter as a result of its finite temperature (Incropera and DeWitt, 1996). The wavelength range that is defined as thermal radiation occurs between 0.01- 100 μm. Typically, when discussing environmental radiation, this thermal radiation is split into two categories, short wave and long wave radiation. Short wave radiation (0.2-2.2 μm) or solar radiation is that radiation given off by the sun. Long wave environmental radiation (2.2 –100 μm) includes emissions from the earth’s surface, clouds, sky, as well as other objects such as trees, buildings and people.

2.4.3.1 Solar Radiation (Short wave)

Solar radiation is transient in nature. Solar radiation is zero during the night and varies during the day, depending on the position of the sun in the sky and atmospheric conditions. The rate of irradiation (rate at which radiation is incident on a surface from all directions per unit area) from the sun normal to the mean earth-sun distance is constant at 1367 W/m^2 (McQuiston, et al. 2000), outside the earth's atmosphere. This does not account for absorption and scattering due to the atmosphere. A part of the solar radiation entering the earth's atmosphere is scattered by gases, water vapor molecules, dust and smog. The part of the radiation that is not scattered is called direct beam radiation and the scattered portion is called diffuse radiation.

Solar radiation for both clear and cloudy sky conditions is commonly modeled in building simulation programs. See Spitler (1996) for an annotated guide. What follows below is a discussion of solar radiation models applied to snow modeling applications. In addition, penetration of the snow by solar radiation is also discussed.

Anderson (1976) provides a numerical model for snow melting; however, the numerical model does not numerically calculate the solar radiation values. The investigator measured values and used the experimental data as the input for the numerical model. The investigator did provide a method for predicting the penetration of solar radiation in the snow layer. Snow was assumed to behave like a homogeneous diffusing medium and the following equations were used to model this behavior:

$$G_x = G_{ND} \exp(-\alpha x) \quad (2-20)$$

Where:

G_x = Solar radiation at depth x (W/m^2)

v = Extinction coefficient (cm)

The extinction coefficient for snow ranges from 0.035 to 0.54 cm^{-1} . For a given grain size the extinction coefficient increases with increasing density until reaching a maximum, after which the extinction coefficient decreases. The extinction coefficient for both limits (air, and ice) is near zero. The following equation provides a means to estimate the coefficient depending on the snow type.

$$v = 0.84 \left(\frac{v_i}{d_s} \right)^2 \frac{\rho_s}{\rho_i} \quad (2-21)$$

Where:

v_i = Extinction coefficient for clear ice (mm^{-1}): Mantis (1951)

d_s =Grain diameter (mm)

ρ_s =Density of snow (g/cm^3)

ρ_i =Density of ice (g/cm^3)

0.84 Has units of mm/cm

There are many numerical models that have included solar radiation in the literature. Each of these models have different ways to account for the solar radiation. Several of these models will be briefly discussed below.

Kustas, et al. (1994) describe a method in which the outer atmosphere solar radiation level is reduced due to different scattering and absorption terms. These values are then modified by a cloud cover factor. The snow albedo (surface reflectance) is calculated as a function of snow grain diameter. These equations can be seen below:

$$G_{ND} = G_o [(1 - A_o) t_R - A_w] \downarrow_{ad} t_{sd} \quad (2-22)$$

$$G_d = G_o \{0.5(1 - A_o)(1 - t_r) + 0.8[(1 - A_o)t_R - A_w]t_{ad}(1 - t_{sd})\} \quad (2-23)$$

$$G_{ND} = G_{ND}(1 - m_c) \quad (2-24)$$

$$\alpha_{ND} = \alpha_{ND,i} - \left(0.083 + 0.23r^{\frac{1}{2}}\right) \cos^{\frac{1}{2}} \alpha_s \quad (2-25)$$

Where:

G_o = Outer atmosphere solar radiation (W/m²)

$\alpha_{ND,i}$ = Direct surface reflectance at sunset and sunrise (0.965)

r = Mean grain radius (mm)

α_s = Solar zenith angle (radians)

m_c = Fractional cloud cover

A_o = Absorption by ozone

t_{ad} =Transmission after absorption by dust

t_{sd} = Transmission after scattering of dust

t_R = Transmission after Rayleigh scattering

A_w = Absorption by water vapor

Jordan, et al. (1999) use measured direct normal solar radiation terms in the numerical model. The short wave radiation is again split into two groups high and low energy bands 0.4-1.12 μm and 1.12-2.4 μm respectively. Visible light ranges from 0.4-0.7 μm and therefore the two bands can loosely be thought of as visible light and infrared radiation. The low energy band is assumed to be totally absorbed by the top layer of the snow. For low-to-medium density snow (snow porosity >0.38), the high-energy band is assumed to decay according to Beer's law, where the extinction coefficient is given by

$$\beta = \frac{0.003795\rho_t}{\sqrt{d}} \quad (2-26)$$

Where:

β = Bulk extinction coefficient (1/m)

ρ_t = Density (kg/m³)

d = Grain size (m)

For high-density snow, the extinction coefficient is linearly interpolated between equation 2-26 and the extinction coefficient for white ice under cloudy skies (1.5 m⁻¹). The effect of cloud cover in the high-energy band is accounted in the equation shown below:

$$f_{high} = f_{high,o}(1 - N) + (f_{high,o} + 0.17)N \quad (2-27)$$

Where:

f_{high} = Fraction of high energy solar radiation under cloudy skys

$f_{high,o}$ = Fraction of high energy solar radiation under clear skys (=0.41)

N = Cloud fraction (clear sky $N=0$, totally cloudy sky $N=1$)

Kondo and Yamazaki (1990) and USA CoE (1998) also utilize measured values of solar radiation to calculate the energy balance. This model considers the absorbed solar radiation in the following equation:

$$G_t = (1 - \alpha)G_{th} \quad (2-28)$$

Where:

α = Snow albedo = Snow reflectance

G_{th} = Total horizontal solar radiation (direct and diffuse) (W/m²)

Tarboton and Luce (1996) also utilize measured incident solar radiation. The measured value is then multiplied by (1- α) to arrive at the net solar radiation. The albedo is calculated as a function of snow surface age and solar illumination angle. Again the

solar radiation is split into two energy bands, visible and near infrared. The following equations illustrate how the albedo is calculated:

$$\alpha_v = (1 - C_v F_{age}) \alpha_{v,o} \quad (2-29)$$

$$F_{age} = \frac{\tau}{1 + \tau} \quad (2-30)$$

$$\Delta \tau = \frac{r_1 + r_2 + r_3}{\tau_o} \Delta t \quad (2-31)$$

Where:

α_v = Snow albedo in the visible range

$\alpha_{v,o}$ = Fresh snow albedo: $\alpha_{v,o}=0.85$, $\alpha_{ir,o}=0.65$

C_v = Sensitivity parameter to snow aging: $C_v=0.2$, $C_{ir}= 0.5$

F_{age} = Function to account for aging of the snow surface

τ = Non-dimensional snow surface age

τ_o = 10^6 seconds

Δt = Time step (seconds)

r_1 = Parameter dependent on snow surface temperature

r_2 = Additional effect near and at freezing point due to melt and refreeze

r_3 = Effect of dirt and soot (=0.03)

2.4.3.2 Radiation exchange (Long wave)

Long wave environmental radiation (2.2 –100 μm) includes emissions from the earth's surface, clouds, sky, as well as other earth objects such as trees, buildings and people. When applied to the snowmelt scenario, there is one major long wave radiation

component atmospheric radiation between the snow surface and the atmosphere (Anderson, 1976). Anderson (1976) also describes snow as a nearly perfect blackbody with regards to long wave radiation. A blackbody is an ideal surface having the following properties (Incropera and DeWitt, 1996)

- A blackbody absorbs all incident radiation regardless of wavelength and direction
- For a prescribed temperature and wavelength, no surface can emit more energy than a blackbody
- Although the radiation emitted by a blackbody is a function of wavelength and temperature, it is independent of direction. That is, the blackbody, is a diffuse emitter.

In the following paragraphs, numerical models found in the literature will be described with respect to how they account for long wave radiation. Most long wave radiation models calculate either an effective emissivity or an effective sky temperature.

Tarboton and Luce (1996) account for the long wave radiation using the Stefan-Boltzman equation as seen below:

$$G_{L,t} = G_{L,i} - G_{L,o} \quad (2-32)$$

$$G_{L,i} = \varepsilon_a \sigma T_a^4 \quad (2-33)$$

$$G_{L,o} = \varepsilon_s \sigma T_s^4 \quad (2-34)$$

Where:

$G_{L,t}$ = Total absorbed long wave radiation (W/m^2)

$G_{L,i}$ = Incoming long wave radiation (W/m^2)

$G_{L,o}$ = Outgoing long wave radiation (W/m^2)

σ = Stefan Boltzman constant ($2.07 \times 10^{-7} \text{ kJ}/(m^2 \text{ hrK}^4)$)

T_a = Air temperature (K)

T_s = Snow temperature (K)

ϵ_a = Air emissivity

ϵ_s = Snow emissivity (0.97)

The air emissivity is a function of the air vapor pressure and cloud cover and is calculated using the following equations:

$$\epsilon_{acls} = 1.08 \left[1 - \exp \left(- \left(\frac{e_a}{100} \right)^{\frac{T_a}{2016}} \right) \right] \quad (2-35)$$

$$CF = 1 - \frac{T_f}{a} \quad (2-36)$$

$$\epsilon_a = CF + (1 - CF)\epsilon_{acls} \quad (2-37)$$

Where:

ϵ_{acls} = Emissivity for clear sky condition adjusted for vapor pressure

ϵ_a = Emissivity of the sky

e_a = Air vapor pressure (Pa)

CF = Cloud cover fraction

T_f = Transmission factor

a = Maximum transmission factor

Kondo and Yamazaki (1990) and USACoE (1998) both utilize measured values of long wave radiation.

Jordan, et al. (1999) uses a modified Stefan Boltzman equation to calculate the long wave radiation:

$$G_L = \varepsilon_s \sigma (\varepsilon_* T_a^4 - T_x^4) \quad (2-38)$$

$$\varepsilon_* = 0.765 + 0.22N^3 \quad (2-39)$$

Where:

ε_* = Modified sky emissivity

N = Cloud cover fraction

Kustas, et al. (1994) use still another modified Stefan Boltzman equation to calculate the long wave radiation:

$$G_L = \varepsilon_s \sigma (\varepsilon_{sky} (1 + cN^2) T_a^4 - T_s^4) \quad (2-40)$$

$$\varepsilon_{sky} = 0.642 \left(\frac{e_a}{T_a} \right)^{\frac{1}{7}} \quad (2-41)$$

Where:

ε_{sky} = Modified sky emissivity

c = Empirical coefficient dependent on cloud type (mean value=0.22)

Ramsey, et al. (1999) modify the Stefan Boltzman equation in yet another manner to evaluate the long wave radiation.

$$G_L = \varepsilon_s \sigma (T_s^4 - T_{MR}^4) \quad (2-42)$$

Where

T_{MR} = Mean radiant temperature (K)

Instead of modifying the air emissivity like the earlier examples, the apparent sky temperature is modified. A mean radiant temperature (MRT) is defined below:

$$T_{MR} = [T_{cloud}^4 N + T_{skyclear}^4 (1 - N)]^{\frac{1}{4}} \quad (2-43)$$

Where:

T_{cloud} = Temperature of the cloud (K)

$T_{skyclear}$ = Temperature of the clear sky (K)

The clear sky temperature includes a modification for the water content of the atmosphere and is approximated using the following equation (Ramsey, et al. 1982):

$$T_{skyclear} = T_a - \left(\frac{1.1058 \times 10^3 - 7.562 T_a + 1.333 \times 10^{-2} (T_a)^2}{-31.292 \phi + 14.58 \phi^2} \right) \quad (2-44)$$

Where:

ϕ = Relative humidity of the air

The clouds were assumed to be at a constant height of 3,048m and the cloud temperature can be estimated using the following equation:

$$T_{cloud} = T_a - 19.4 \quad (2-45)$$

This equation is valid except when the atmosphere contains very high water content, in which case, the cloud temperature is set equal to the air temperature.

2.5 Water Flow

In this sub section two types of water flow will be discussed. The first and most important for purposes of this experiment is described as capillary flow. Capillary flow arises when the attraction between the fluid and a solid (in our case the ice particles) is great enough to overcome the mutual attraction (cohesion) of the molecules (Munson et al. 1994) due to the surface tension of the fluid and the pore diameter. Capillary flow could then be simplified as the flow of water due to the porous nature of snow. The

second type of water flow described involves the flow of water due to either rainfall or the melting of the top layer and the water percolating through the snow. This type of water flow is important for the prediction of flood events.

Coleou, et al. (1999) focus on developing a model to relate capillary rise with snow characteristics. To develop a model, several experiments were run using a controlled batch of natural snow. The snow was pre-wetted to reduce the changes in grain type and texture. The snow was packed in a parallelepiped and then brought into contact with water at 0°C. The authors report that the water reached its final height at a time of ten seconds, and that there was no evidence of capillary hysteresis when comparing imbibition and drainage experiments. The authors then developed an experimental relationship between the capillary height and the snow porosity and grain size. To start to model the capillary rise the authors made several assumptions:

- The cross section of the capillary is circular
- The radius is small enough (i.e. less than the capillary length, which for water is 3mm)
- The liquid wets the solid (the contact angle is null). The contact angle is defined as the angle between the solid and the liquid-gas interface. If the contact angle is $< 90^\circ$, the liquid is said to be the wetting fluid (Bear, 1972).

The authors then utilize the Laplace equation to determine the capillary pressure as a function of the radius and the surface tension of water. The Laplace equation was developed for a group of parallelepiped (straws) (Bear, 1972). The capillary pressure can then be set equivalent to the hydrostatic pressure of the column of water. This is then coupled with a cubic link network or lattice modeling. The results of the modeling were

mixed. In the real world, as the water is drawn up to the maximum saturation height, there is a rapid drop off of the water content, i.e. a sharp interface. The model was accurate in modeling the point of the drop-off. However, instead of showing a sharp interface, the model predicted a gentle drop off in water saturation.

Jordan, et al. (1999) investigated the relationship between snow permeability and capillary height both experimentally and theoretically. Historically, capillary pressure has been related to pore structure through fitting parameters for the pressure-saturation curve; however, these curves are hard to measure. This is due to the fact that snow has very low tension and is very friable, and therefore capillary height was chosen as the measurement variable. It was stated that most porous media equations do not work with snow because snow is not dynamically stable, i.e. grain size and shape change rapidly as the snow is exposed to water flow. Jordan, et al. (1999) start with Darcy's law and then work toward a relationship between the estimated permeability as a function of porosity and saturation height. Darcy's law was chosen as the starting point due to the low Reynolds number. The following relationship was proposed:

$$K_{est} = \frac{1}{5} \left(\frac{\sigma_{al} \cos \theta}{\rho_l g} \right)^2 \frac{\phi}{h^2} \quad (2-46)$$

Where:

K_{est} = Permeability estimate (m^2)

θ = Contact angle (radians)

ρ_l = Density of the liquid (kg/m^3)

h = Saturation height (m)

ϕ = Porosity

σ_{al} = Surface tension of water (N/m)

$g = \text{Gravity (m/s}^2\text{)}$

Jordan, et al. (1999) also used a correlation developed by Shimiz (1970) that gives permeability of snow as a function of the density of the snow and the grain diameter:

$$K = 0.077 \exp(-0.0078\rho_s)D^2 \quad (2-47)$$

Where:

$K = \text{Permeability of snow (m}^2\text{)}$

$\rho_s = \text{Density of snow (kg/m}^3\text{)}$

$D = \text{Snow grain diameter (m)}$

These two functions were then combined to form a single equation for grain diameter as a function of saturation height and porosity. This equation was then compared to experimental data that was collected in New Hampshire. The results were plotted and it was determined there was significant scatter that was hypothesized as being due to structural differences and measurement error. As a conclusion the authors recommended using the combined equation, while suggesting further research to provided better results.

Colbeck (1972a) describes the theory behind water percolation in snow. General Darcian flow of two fluids is applied to the gravity drainage problem in snow. Interstitial air was considered because it substantially affected the character of the flow. To reduce the complexity of the problem the snow was considered isothermal; however, variation in porosity of the snow was considered. One major assumption made that capillary effects of the snow were ignored. It was shown that the capillary effects are more than three orders of magnitude smaller than gravitational effects and therefore can be ignored. This assumption is only true when the water saturation was greater than the irreducible water saturation. Irreducible water saturation is defined as the lowest water saturation reached

when the porous media is drained. The results of the theory were then compared to water drainage data collected in Sharp (1952). After comparison it was determined the theory could predict the water flow in the snow pack.

Colbeck (1972b) investigates the capillary effects on water percolation in homogenous snow. This paper gives a detailed explanation as to why capillary effects may usually be ignored. Colbeck performed a capillary-pressure experiment to provide a chart for the water saturation curve; however, because snow and water are the same fluid, water was replaced with kerosene to differentiate the two. One important result of the experiment was that the irreducible liquid saturation was found to be 7%. It was also found that water saturation in snow generally exists within the range of 10%-20% for water drainage. After some analytical modeling of the capillary behavior, two conclusions were drawn:

- All flow rates are dominated by gravity except in cases where the water velocity is near 10^{-8} m/s in which case capillary effects must be included.
- Capillary behavior is important at the wave front; however, there are other simpler models that can approximate the effects.

Colbeck (1974a) develops a time-dependent model of water flow through a two-dimensional snow pack over an impermeable boundary. Colbeck split the snow pack into two zones: saturated and unsaturated. In the unsaturated zone, the water flow was considered vertical percolation which was described in Colbeck (1972b). The saturated zone was the zone of interest. The water could collect above the boundary and then flow down the gradient. As the water moved further down the gradient the saturated zone increased and it is this phenomenon that was modeled. In the end, a height of the

saturated layer was found with time and the total flux of water was derived. This paper also describes the water flow in the saturated zone from rainwater and from surface melt water.

Colbeck (1975) continues the research of water flow through a snow pack. Snow in this research is classified as anisotropic. In this research, snow is defined as a layer of homogenous snow with layers of impermeable ice scattered throughout. This effect causes channeling and horizontal water movement.

Colbeck (1976) developed a model to predict the water flow through a snow pack. This is important for predicting potential flood events. Colbeck explains as the water moves down through the snow the liquid water provides a source of thermal energy which will raise the snow to the melting temperature and cause significant metamorphism of the snow. Colbeck developed a set of equations to predict this phenomenon and subsequently ran four test cases to illustrate the results (rain-on-snow, ripe snow, refrozen snow, and fresh snow). The larger diameter snow showed almost immediate water leakage through the snow, whereas the fresh snow ($\rho_s = 0.3 \text{ Mg/m}^3$, $d = 0.2 \text{ mm}$, $h = 1 \text{ m}$) had a significant "lag" time (almost 16000 seconds).

Tseng, et al. (1994) develop a 2-D Galerkin finite element method to solve a water infiltration problem. As the water trickles through snow, the water will locally melt the snow until the infiltrated water refreezes in the snow layer, which has been defined as a "Stefan" boundary condition. Along with this coupled freeze-thaw complication, the authors added a moving surface boundary, which occurs during melting. This article emphasized the numerical results of the FEM and only gave very limited experimental results.

2.6 Snow Metamorphism

Colbeck (1982a) describes how snow crystals grow and change shape. There are three major avenues by which snow crystals change shape. The first is when the snow comes into contact with water. The water will quickly round the particles, although how quickly is not stated. This has been termed wet metamorphism. The second major growth pattern is caused by low temperature gradients. The result of this low temperature gradient is that the snow crystals also round off; however, it occurs over a much longer period of time. The last effect is when a large temperature gradient is imposed on the snow (e.g. due to weather conditions) and the result is large multi-faceted crystalline structure. The faceted crystal structure has been linked to avalanches and the crystalline structure responsible for avalanches has been given the name "depth hoar". The process by which the snow changes shape has been called snow metamorphism. Colbeck explains that the vapor flux arising from the temperature gradient is the most significant contributor to snow metamorphism and has been determined to be the rate-determining step. Snow metamorphism can simply be thought of as transformation of the crystal size and shape.

Colbeck (1982b) gives a summary of the crystalline structure of snow from the time it falls until metamorphism occurs. Colbeck explains that new fallen snow is generally faceted (has a complex structure like a new snow flake rather than being rounded). After the snow collects on the ground, the snow crystals lose their angularity and assume the fully rounded equilibrium form. The snow crystals, now rounded and bonded to other snow crystals, can re-crystallize back into a faceted form under large temperature gradients (metamorphism) and, in the most severe cases, the crystals become large and faceted, taking on depth hoar crystalline structure, which lacks cohesion and

thus causes avalanches. Faceted snow crystals prevail during rapid crystal growth (and thus are also termed the kinetic growth form) whereas the fully rounded, well-bonded crystals prevail during slow growth (and thus are termed the equilibrium form).

Colbeck (1983) describes the theory and effect of metamorphism on dry snow. Metamorphism is generally a result of a temperature gradient imposed on the snow cover by the environment. If no temperature gradients were imposed on the snow cover, small chemical potential differences due to difference in curvature and stress would cause small temperature and vapor pressure differences among the grains, which would cause slow grain and neck growth by vapor diffusion and heat flow. These self-imposed gradients are small in comparison to the imposed temperature gradients. The imposed temperature gradient causes a gradient in the vapor density, which then diffuses upwards which has been labeled the "Soret effect". The number of crystals effected per unit volume has been found to be inversely related to the third power of the mean crystal size. An indirect effect of the fact that most of the original crystals disappear is that, their bonds also disappear, thus the recrystallized snow will lose strength unless the new crystals sinter. Colbeck developed a set of equations to calculate reasonable crystal growth rates, distinguish between the growth of rounded and faceted crystals, explain the rapid growth of depth hoar in the lower warmer part of the snow cover and explain the rapid growth of depth hoar below buried crusts.

In Colbeck (1973) the thermodynamics of wet snow are used to describe the processes of grain growth, bond growth and densification. The saturation regimes have been categorized depending on water saturation as either pendular or funicular. Pendular water saturation can be visualized as isolated water phase (e.g. pockets of water are

formed within the crystalline structure). Funicular water saturation can be described as a continuous water phase (e.g. the water is continuous throughout the crystalline structure). Water saturation during normal gravity drainage is low and thus described as pendular; however, large saturations can occur over impermeable boundaries and thus the funicular regime is also important. The funicular regime is characterized by rapid metamorphism of snow, which produce three major phenomena: rapid grain growth, loss of mechanical strength, and rapid densification. One experimental result presented in Colbeck (1973) was that in the funicular regime all grains smaller than 0.1mm in radius disappeared within three days (after the water was introduced to the snow). Therefore, it was concluded that metamorphism produces large changes during the first three days but much smaller changes in the succeeding days. The pendular regime is characterized by the small amount of water present and thus most grains are in contact with the vapor phase. Fundamentally, as the addition of liquid water reduces the capillary pressure and increases the effective heat transfer area, metamorphism is increased. Several conclusions were drawn in this paper:

- Metamorphism, strength, and densification of wet snow are determined by the occurrence of small temperature gradients around the particles
- The equilibrium temperature of the snow matrix is controlled by the size of the air bubbles and the size of the ice particles
- The smaller particles exist at a lower equilibrium temperature causing heat flow from the large particles to the smaller particles.
- The rate of metamorphism decreases with time after the small particles disappear.

- In the funicular regime the equilibrium temperature at a contact between the grains is decreased by the compressive stress between the grains.
- The temperature depression (depression of the melting temperature) is increased by overburden pressure causing melting of the inter-grain contacts and removing any bond-to-bond strength which explains the loss of strength that causes wet snow slide over impermeable layers.

Colbeck (1986a) investigates the effect of wet metamorphism in snow by measuring the particle size distribution. The growth of a population of particles in a liquid is usually referred to as the LSW theory. Colbeck describes a simple experiment run in which distilled water was introduced to a snow sample and the ice particles were measured with the use of photography. The growth process is said to depend on the inverse relationship between particle radius and melting temperature (for instance, large particles grow by losing heat to the small particles which melt). As a result of the experiments, the mean diameter of the particle was then represented in the following equation

$$\bar{D} = \bar{D}_o + 0.132 * t^{0.362} \quad (2-48)$$

$$D_g = D_{g,o} + 0.117 * t^{0.369} \quad (2-49)$$

Where:

D_g = geometric mean diameter (mm)

$D_{g,o}$ = Initial geometric mean diameter (mm)

\bar{D} = Average mean diameter (mm)

\bar{D}_o = Initial average mean diameter (mm)

t = Time (hours)

The particle was then assumed to be spherical and thus the mean volume of the particles could be found. After this assumption was challenged, the experimental results were reexamined to measure two characteristic shape factors: The PE ($4\pi\text{area}/\text{perimeter}^2$) and the AR ($4\text{area}/\pi*\text{maximum diameter}*\text{minimum diameter}$). The PE is a measure of circularity and AR is a measure of ellipticity of the particles. It was found the particles have a mean axial ratio of 1.4 to 1 and it was suggested by the author that the shape was not spherical but prolated spheroids. The other main conclusion of the paper was that the particle size distribution was lognormal.

Colbeck (1987) builds on Colbeck (1986a) and derives a crystal growth rate as a function of particle size. Particle growth was described as controlled by diffusion, which in the case of snow is controlled by the diffusion of heat through the liquid filled pores. Diffusion to or from the particle was determined by the size difference between the particle and its neighbors. The model that was developed was based on an electrostatic capacitance analogy along with the particle size distribution found in Colbeck (1986). Conclusions that were drawn from this model include that the particle shrinkage rate accelerates below a size of 70-80% of the mean size. The growth rate vanishes at a size just above the mean size. The particle growth rate increases linearly above 1.5 times the average diameter.

2.7 Snow Melting from the Bottom

The melting of snow is complex process. The problem is transient, and the medium has three phases. It is complicated by the fact that the solid and liquid phases are the same compound, water, and the gas phase is a mixture of air and water. This section

only covers one snow melting geometry due to the intended usage of the numerical model. The model is being developed to model snow melting on a bridge deck or other heated pavements, which is horizontal or nearly horizontal. There are three papers written by the same authors that describe snow melting from the bottom surface (Aoki, et al. 1982, 1986, 1987). The investigators (Aoki, et al. 1982) describe a method in which snow is removed from a horizontal surface by the introduction of a constant heat flux from the bottom. The analytical model made several assumptions:

- 1) Melting is one-dimensional
- 2) Porous materials are homogenous
- 3) Throughout the melting process, each layer is continuous and air gaps due to the change in volumes are absent.
- 4) The density difference between ice and water can be neglected
- 5) Natural convection in the water layer can be neglected

Together, these assumptions simplify the process down to a 1-D transient porous medium conduction problem with phase change. Another melting scenario without porous media effects is called the Stefan problem. The Stefan problem, in brief, entails the melting of solid homogenous material. The Stefan problem is characterized by a distinct moving phase change boundary at which a heat balance condition is met (Minkowycz and Sparrow, 1997). After the investigators (Aoki, et al. 1986) developed an analytical model and experimentally validated it, they show that snow melting should not be simplified as a classical Stefan problem. Snow, by definition, is a porous material. When a liquid comes in contact with the snow, it is transported into the snow by capillary action.

Capillary effects are commonly associated with surface tension effects. Surface tension is defined as the intensity of the molecular attraction per unit length. A conceptual analogy commonly associated with surface tension effects, is that the surface tension forces cause a “skin” or “membrane” that covers the liquid (Munson, et al. 1994). This “skin” can be visualized with water droplets. The curvature of the water droplet can be calculated by the following equation (Munson, et al. 1994):

$$\Delta p = \frac{2\sigma}{R} \quad (2-50)$$

Where:

Δp = Pressure difference between internal pressure and surface pressure(N/m²)

σ = Surface tension (N/m)

R = Radius of droplet (m)

When applying this to porous media, the void space provides a pressure difference due to the curvature, which is balanced by hydrostatic pressure. This is the fundamental definition of capillary rise. The curvature causes a capillary pressure in porous media, which, in the case of snow, is balanced by the hydrostatic pressure of the melt water. As the snow near to the heated surface melts, the resulting water is then wicked away by the snow due to the capillary effects. The water will not drain off the heated surface until the water content in the snow is above the saturation point, or the snow is melted faster than it can be wicked away. Ohtani and Maeda (1964) developed and experimentally validated a model of this capillary effect, which Aoki, et al. (1986) used in his snowmelt model. This model assumes that snow is a conglomeration of ideally connected parallel tubes of various sizes.

With these assumptions in mind, Aoki, et al. (1987) then proceeded to describe the physical nature of snow melting from beneath. After observing the snowmelt process, Aoki, et al. (1986) divide snow melting into three main types of snowmelt phenomenon, labeling them A, B and C. The differences between the A, B, and C melt patterns are the surrounding temperature and initial snow height. For example, if the surrounding temperature is above freezing the melt pattern is classified as “A”.

“A” type snowmelt

Physically this type of snowmelt only occurs when the air temperature is near 0°C (the freezing point of water). The following steps are common steps found in “A” type snowmelt:

- 1) Introduction of a heat source.
- 2) The snow at the lower surface begins to melt, and as the snow melts the water permeates into the porous layer by capillary action.
- 3) The water content in the porous media begins to rise and the water permeation front begins to move upward through the snow.
- 4) Water drainage will occur when the instantaneous volume of snowmelt is greater than that of the capillary suction volume. In other words, if the rate of snowmelt is greater than the permeation rate water drainage occurs.

Aoki, et al. (1987) then subdivides the “A” type snowmelt into two subcategories type “A1” and type “A2”. The only difference between the two is when in time the drainage occurs. If drainage occurs when the water permeation front reaches the top surface then it is classified as type “A2”, and conversely, if drainage occurs before the permeation front reaches the top surface it is labeled type “A1”.

“B” type snowmelt

Type “B” snowmelt occurs only when the temperature of the surroundings falls below freezing. This will allow for the re-freezing of a layer of liquid water, known as an ice lens. The steps that describe type “B” snowmelt are as follows:

- 1) Introduction of heat source.
- 2) The snow at the surface begins to melt, and as the snow melts the water permeates into the porous layer by capillary action.
- 3) The water content in the porous media begins to rise and the water permeation front begins to move through the snow.
- 4) As the water permeation front moves through the snow layer, a portion of the layer refreezes. If the water permeation front has not reached the surface then the water permeation rate is greater than the refreezing rate. It is important to note that the refreezing does decrease the water permeation front, and was modeled as an added resistance.
- 5) When the water permeation layer reaches the top surface and stops an ice lens is formed.

Aoki, et al. (1987) then subdivides the “B” type snowmelt into two subcategories type “B1” and type “B2”. The only difference between the two is when in time the drainage occurs. If drainage occurs when the water permeation front reaches the top surface then it is classified as type “B2”, and conversely, if drainage occurs before the permeation front reaches the top surface it is labeled type “B1”.

“C” type snowmelt

Type “C” snowmelt can be described as type “B” snowmelt except that the ice lens forms in within the snow layer. As the water permeation front moves through the snow, the rate of refreezing increases until the water permeation front become lower than that of the refreezing rate. At this point, the snow melts as a type “B” snowmelt problem. After the ice lens has been melted the remaining snow melts as either type “B” or “C”, and the process continues until all the snow has melted.

The analysis portion of the paper covers one particular melt pattern step. The paper describes a type “C” melt pattern, and specifically describes what happens after the ice lens has formed within the snow layer. Aoki, et al. (1987) first describes the capillary suction pressure equations that were derived by Ohtani and Maeda (1964). The equation he proposes is in the form of water permeation flux and is described below:

$$m = \frac{-\varepsilon^2}{12 * (1 - \varepsilon)} * \frac{\sigma d}{\mu} * \rho_w * \alpha \left\{ \frac{\varepsilon}{6(1 - \varepsilon)} * \frac{\rho_w d}{\sigma} - \frac{dP^+}{dx} \right\} \quad (2-51)$$

Where:

m = Water permeation flux (kg/m²hr)

ε = Porosity

μ = Viscosity (Pa*s)

ρ_w = Density of water (kg/m³)

σ = Surface tension of water (N/m)

α = Non-dimensional parameter, solved numerically

P^+ = Non-dimensional pressure driving force

x = Height (m)

The governing equations for each region (water permeation layer, ice layer, and porous layer) are detailed below.

Water Permeation Layer:

In the water permeation layer the temperature is assumed to be constant at 0°C. Equation 2-52 is a transient mass balance. The left side of the equation can be described as the change in water content with respect to time. The right side can be described as the change in water permeation rate with respect to location and the change in the water content ratio with respect to location.

$$\epsilon \rho_w \frac{dS_{wp}}{dt} = -\frac{dm}{dx} - u_x \epsilon \rho_w \frac{dS_{wp}}{dx} \quad (2-52)$$

Where:

S_{wp} = Water content ratio

u_x = Velocity due to the reduction in volume (m/hr)

ρ_w = Density of water (kg/m³)

Ice Layer:

In the ice layer the temperature may vary with time and is described in equation 2-53. The left side is defined as the change in temperature with respect to time. The right side includes conduction effects in the first term and convective effects in the second term.

$$\frac{dT_i}{dt} = a_i \frac{d^2T_i}{dx^2} - u_x \frac{dT_i}{dx} \quad (2-53)$$

Where:

a_i = Thermal diffusivity of ice(m²/s)

T_i = Ice temperature (°C)

Porous (virgin snow) layer:

In the porous layer, the temperature may vary with time and is described in equation 2-54. The left side is defined as the change in temperature with respect to time. The right side includes conduction effects then the convective effects.

$$\frac{dT_p}{dt} = a_p \frac{d^2T_p}{dx^2} - u_x \frac{dT_p}{dx} \quad (2-54)$$

Where:

a_p = Thermal diffusivity of the porous layer(m²/s)

T_p = Porous temperature (°C)

These equations coupled with the following boundary conditions were then solved using a finite difference method (Crank-Nicholson) using a variable space network method for moving boundary conditions:

- At the top boundary only convection is included
- At the bottom boundary, constant flux and 100% water saturation

The following conclusions were formed from results of the experiments:

- The rate of water drainage and time change of each layer from experimental results agreed with the one-dimensional model.
- The heat loss from the top of the body varies with melting patterns.
- The melting time and melting efficiency are affected by water permeation and its refreezing.

- The results calculated assuming the classical Stefan problem by neglecting water permeation predicts a higher melting efficiency.

2.8 Road Effects

Colbeck, (n.d.) discusses the effects of water and traffic induced compaction of snow with an emphasis on snow removal on highways. Colbeck describes the following phenomena important to snow removal:

- Dry snow compresses very slowly by wet snow can be compressed to ice quickly.
- Compressibility of wet snow decreases with decreasing water content but increases with decreasing salinity
- The tendency for snow to splash on highways increases with increasing water content but increases with decreasing salinity.

Colbeck, (n.d.) goes onto explain that when water is first introduced, snow undergoes rapid changes (grain rounding, grain growth, and densification). The first being grain rounding and, as a result, there is very little bonding between the ice particles. This destruction of inter-particle adhesion partly accounts for the densification. If wet snow is confined and stressed it can compact to densities of approximately 500 kg/m^3 under normal efficient packing manner. To increase the density any more the particles would have to change shape. Wet snow is unique in that pressure melting is the dominant mechanism responsible for deformation of particles, which occurs at the stressed particle contacts. The pressure melting occurs because the ice-liquid temperature is depressed by 0.0074°C per 10^5 Pa . This rate of pressure melting and rate of densification has a very complicated dependence on the density, particle size, applied load, salt content, and liquid water content.

CHAPTER 3

NUMERICAL MODEL

3.1 Overview

A numerical model was created by Spitler, et al. (2001) to predict the melting of snow on a heated bridge deck or other paved surfaces. The intended application of the numerical model is to aid in the design of pavement embedded with hydronic tubing. This thesis deals partly with providing some inputs for the snow melting part of the numerical model and partly with experimental verification of the model. The model is described in this chapter.

3.2 Model

The two-dimensional transient snow melting system model consists of four principal elements. These are the grid generation code, the finite volume solver, the boundary condition model and the user interface. The grid generation code creates an appropriate grid for the bridge deck with embedded pipes. An example is shown in Figure 3.2-1. The finite volume solver models conduction heat transfer from the inside pipe wall to the surface of the pavement and into the surrounding ground. The boundary conditions model is where snow accumulation, snow melting, and all heat transfer to the environment is modeled. A user interface was developed which provides a convenient

method for input data to be entered and transferred to the numerical model, execution of the program, and post processing of the results.

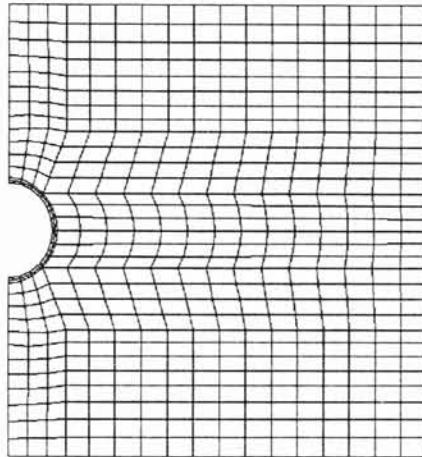


Figure 3.2-1: Grid generated of the bridge deck and embedded pipes (Spitler, et al. 2001)

3.3 Boundary condition model

In order to determine how the slab will respond to a range of weather conditions, it is necessary to be able to model a number of other conditions in addition to snow melting. The simplest is when the slab is dry, which in most circumstances is the initial condition during the real time simulations. The slab surface may also be wet, either due to rain or melting of snow or ice. In order to deal with the whole snow storm event – from onset of snow to drying of the slab – it is also necessary to model the snow when it is saturated with liquid, i.e. when only slush remains towards the end of melting. Furthermore, additional combinations of conditions are possible involving the formation and melting of solid ice.

The management of the selection of the appropriate model at each time step (depending on past conditions and current temperatures and precipitation) must be somewhat sophisticated. A summary of the possible current conditions, and the possible conditions at the end of the time step, are given in Table 3.3-1.

Initial Surface Condition	Precipitation Condition		
	None	Rain	Snow
1. Dry	1	2,6	1, 3, 4, 5, (2)
2. Wet	1, 2, 6	2, 6, (1)	2, 4, 6
3. Dry snow layer	3, 4, 5, (2)	4, 5	3, 4, 5, (2)
4. Slush layer	2, 4, 6, (1)	2, 4, 6, (1)	2, 4, 5, 7
5. Snow & Slush	4, 5, (6, 7)	4, 5, (6, 7)	4, 5, (6, 7)
6. Solid ice layer	2, 4, 6	2, 4, 6	5, 7, (4)
7. Solid ice & snow layers	5, 7, (4)	4, 5, (2, 7)	5, 7, (2, 4)

Table 3.3-1: Possible Boundary Conditions at the end of the time step vs. Current Environmental Conditions (Spitler, et al. 2001)

Note: unlikely conditions are indicated in parenthesis.

3.4 Model Detail Considerations

With the different modes of heat and mass transfer in mind, a model was created to accurately predict the melting of snow in certain circumstances, more specifically thin snow layers on a heated pavement. As can be seen in the literature review section, there are many snow-specific problems that arise when addressing snow melting such as metamorphism. These arise due to the porous nature of the snow, but also are due to the fact that snow is formed from crystalline water. Interdependencies between the snow

properties complicate the problem, e.g. the heat transfer imposed on the snow will cause the crystal to facet and grow, affecting the density and thus the porosity, which affects the mass transport in the snow, which causes metamorphism, which in turn affects the thermal properties and heat transfer. These problems were considered when developing the snow model. If the initial crystal size of snow is not known (and for this application it is not typically known), then it is very difficult to predict any features of the snow, and therefore would not be appropriate to create a model that is detailed down to the level of crystal size and crystalline affects. Therefore, with the limited snow information that is reported by weather stations and forecasters, a model with a more suitable level of detail was created.

3.5 Geometry

In this subsection, the overall geometry of the numerical model will be discussed. Because of the complex nature of the snowmelt scenario, the model was divided into two distinct layers. These layers will be defined and the major differences will be defined as they relate to the snowmelt problem.

Several simplifications are used within the numerical model. The first simplification is that snow is treated as either dry snow or a wet, saturated snow that is called slush. Typical conditions during snow melting, where there might be a layer of dry snow covering a layer of slush are visually represented in Figure 3.5-1. The “slush” layer is shaded to indicate the presence of water. It is also possible that there may be a slush layer without a dry snow layer, or a dry snow layer with a slush layer.

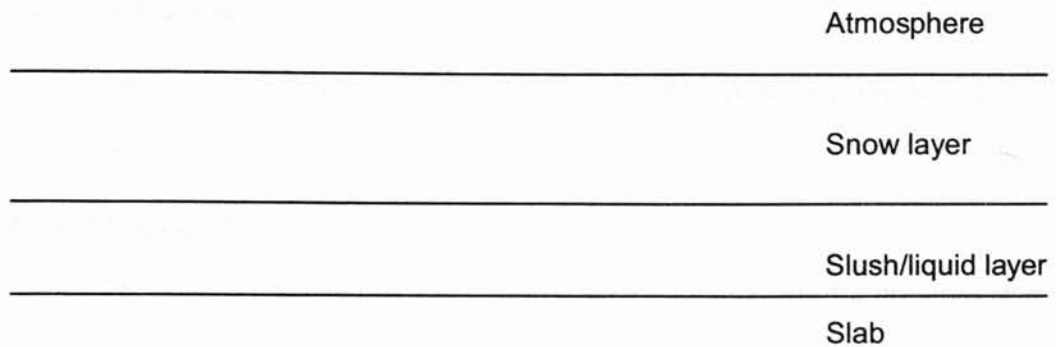


Figure 3.5-1: Snow/Slush Layer Diagram

Both the snow layer and the saturated (slush) layer may be considered as porous media. The two-layer simplification assumes the layers are homogeneous. The snow layer has air in the void space between the snow crystals, and the slush/liquid layer has water in the void space between the snow crystals. Because the snow layer is porous, air may flow through the snow layer and evaporation may occur from the slush layer. The amount of evaporation was considered negligible when there was snow was void of liquid water (dry snow), however was considered when water was present (slush layer).

In real life there could be different geometries. As mentioned in the literature review, an ice lens could form if the air temperature is below freezing. This ice lens could significantly affect the geometry, and heat and mass transfer. The ice lens is assumed to be impermeable and therefore any melting occurring above the lens would percolate through the snow and collect above the ice lens. This would, in effect, cause the geometry to include two separate slush/liquid layers. Melting occurring at the top layer (caused by the sun, or a rising air temperature) would percolate through the snow and collect in the slush/liquid layer; however, as the water percolates through the snow, the snow grain size and shape will change.

3.6 Mass Transfer

The mass transfer section will discuss the possible mass transfer mechanism by layer starting from the top and moving down.

Snow Layer Inputs

- The primary mass transfer mechanism is snowfall; this is how the dry snow layer thickness is created and increased as snowfall continues.
- Rain is a very difficult input to consider. When it rains, the water first contacts the dry snow layer. The liquid water that comes into contact with the dry snow will cause wet metamorphism to occur and will percolate through the dry snow layer due to gravity. In the model, however, it is assumed that the water does not affect the dry snow layer and is transmitted directly to the slush layer.
- It is likely that sublimation of the dry snow is significantly small over the time scale studied that it can be eliminated from the mass transfer equation. It is neglected in the model.

Snow Layer Outputs/Slush Layer Inputs

- Any rainfall is assumed to percolate through the dry snow and is added to the slush layer.
- As the slush layer melts and runs off the slab, snow from the snow layer is added to retain the maximum saturated layer height. (This is actually due to the water diffusing upward into the snow layer.)

Slush Layer Outputs

- The main mass transfer mechanism of the slush layer is the liquid water run-off, which is a direct effect of snow melting mechanisms and any excess rainfall.

Water will runoff the slab if the maximum saturated layer height has been reached, i.e. the slush layer can not hold any more water in the pores.

- When the thickness of the dry snow layer has decreased to zero, evaporation from the slush layer is also taken into account.
- Because the solid snow particles are totally immersed in water, the likelihood of sublimation is very small and therefore it is also ignored.

These mass transfer effects across the control volume are illustrated in Figure 3.6-1.

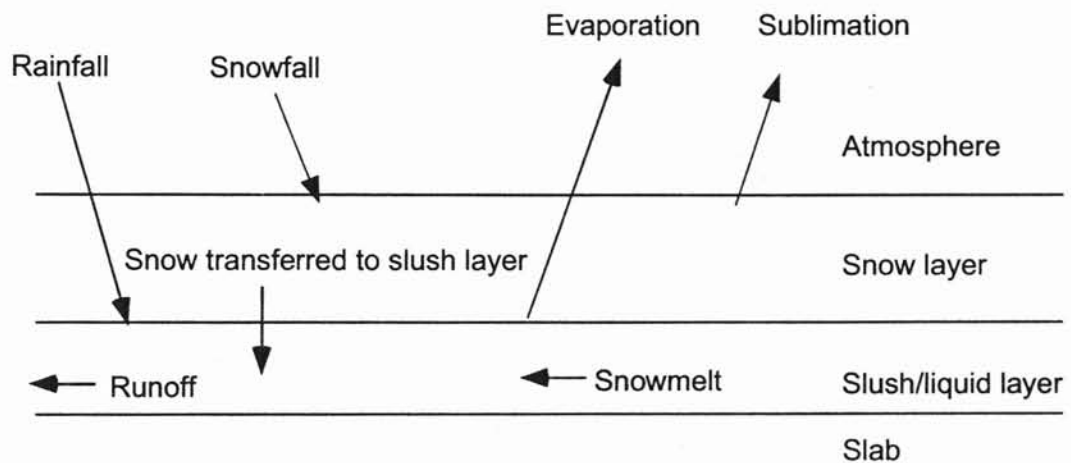


Figure 3.6-1: Mass Balance

3.7 Heat Transfer

Now that we have addressed the mass transfer, we can evaluate the heat transfer that melted the snow. The heat transfer mechanisms are summarized as follows.

- The most important heat transfer mechanism is the conduction that is imposed on the snow layer from the slab. The conduction through the slab is the parameter that is controlled by the user to keep the slab clear of snow and ice. Therefore the

effective time scale for conduction heat transfer is much smaller than the remaining heat transfer mechanisms.

- Because solar radiation data were not available and for purposes of snow melting system design, it is desirable to obtain a conservative answer, solar radiation was ignored.
- While solar radiation is ignored, long wave (or atmospheric) radiation is not ignored. This radiation occurs to temperature differences between the snow and the atmosphere.
- Convection, caused by wind, will affect the upper surface of the snow and will be accounted for in the model. Forced convection effects within the snow layer, sometimes called wind pumping, will not be accounted for, nor will the natural convection due to buoyancy through the porous snow layer. Likewise, convection from the slush layer will be neglected.
- The dry snow layer is absent of liquid water and therefore evaporation from the dry snow layer will not occur, however evaporation from the slush layer will be included when the dry snow layer thickness has decreased to zero.
- The last remaining heat transfer mechanism that has not been described are the sensible gain/loss from mass transfer. For example, if the temperature of the water runoff from the slab is greater than 0°C then there was heat added to raise the temperature and must be accounted for in the program. By the same manner there could be sensible gains from both snowfall and from rainfall and these will be included.

The heat transfer effects can be seen in the following Figure 3.7-1.

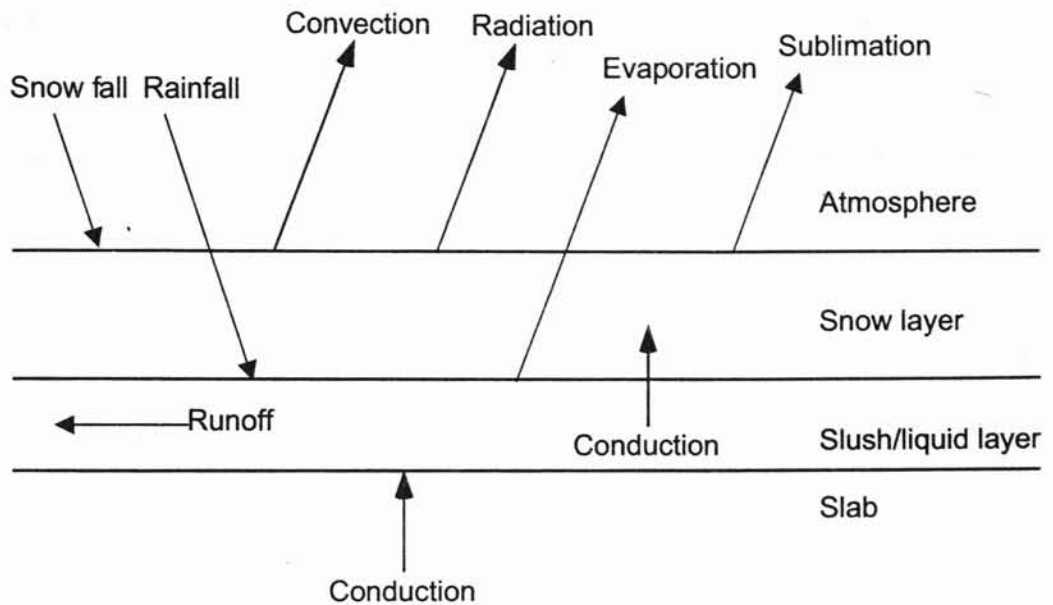


Figure 3.7-1: Overall Heat Transfer Balance

3.8 Mathematical Model

The mathematical model will take the issues presented in the above subsections and formulate a model to find a mathematical solution. The main part of the problem is how to organize the heat transfer model so that an appropriate accuracy is achieved. One possible solution technique would discretize the two layers into a number of finite volume cells. With this scheme, the actual positions of the top of the snow layer and the snow/slush interface would be tracked with one of several methods. This scheme would be extremely detailed and would take a considerable amount of computational time. Given the limited amount of detail available with regards to snow density and other characteristics, and given the level of detail utilized in the other models, this approach is not warranted.

A much simpler approach would be to simply treat the snow and slush/liquid layers with a single node. If implemented carefully, this may be a potential solution. However, it severely limits possibility of adequately accounting for the insulating effect of the snow. It would also limit the ways in which evaporation might be treated when there is a thin snow layer over the slush layer.

Therefore, a model with a level of detail intermediate between the detailed finite volume approach and the single node approach was developed. This model involves the use of three nodes – one at the upper surface of the snow layer, one in the center of the snow layer and one at the saturated (slush) layer. This preserves the possibility of adequately accounting for the insulating effect of the snow, while otherwise maintaining the simplicity of the original model. This model is represented schematically in Figure 3.8-1.

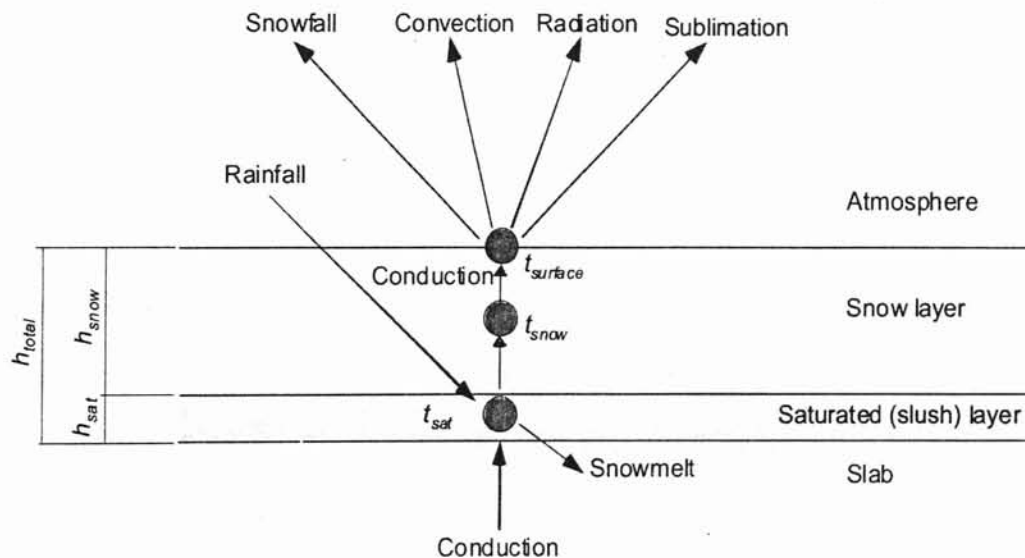


Figure 3.8-1: Schematic representation of heat transfer in the two-node snowmelt model (Spitler, et al. 2001)

A number of assumptions are made with this model. These include:

- The slush/liquid layer was considered to be at a uniform temperature.
- Melting of snow occurs at the lower node only, either at the interface between the snow and slush layers, or in the slush layer.
- Transfer of solid snow from the snow layer to the slush layer will be explicitly accounted for in the mass balance. However, from a heat transfer standpoint, it may be neglected. Because the lower node covers both the slush layer and the bottom of the snow layer, it makes no difference whether the snow melts at the interface or in the slush layer. Therefore, no heat transfer path accounting for the transfer of solid snow from the snow layer to the slush layer is shown in Figure 3.8-1.
- While convection from the upper surface of the snow is accounted for, convection due to airflow through the porous snow layer will be neglected. The model could account for this natural convection and may be included if further research indicates that it is important.
- Likewise, convection from the slush layer is neglected. At the present time evaporation from the saturated layer is also neglected when a dry snow layer is present. The model does not necessitate neglecting this evaporation, so it may be included if further research indicates that it is important.
- If any rainfall occurs after a snow layer has formed, it will be accounted for only at the saturated layer and has no affect on the dry snow layer.
- The snow melting process is treated as a quasi-one-dimensional process.
- Sublimation of dry snow is ignored.

The model is formed by five primary equations – a mass balance for the solid ice, a mass balance for liquid water, an equation for the mass of the ice in the dry snow layer and similarly for the slush layer, and a heat balance on each node. Each equation is given below.

Mass balance on the ice

$$\frac{dm_{ice}}{d\theta} = \dot{m}_{snowfall} - \dot{m}_{melt} \quad (3-1)$$

Where:

m_{ice} = Mass of snow per unit area in the snow layer, kg/m²

θ = Time, s

$\dot{m}_{snowfall}$ = Snowfall rate in mass per unit area, kg/(s-m²)

\dot{m}_{melt} = Rate of snow that is transferred to the slush in solid form, kg/(s-m²)

The mass flow rate of snowfall is given by the weather data file in terms of equivalent precipitation of water. The rate of snow that is transferred to the slush layer in solid form is determined based on the heat balance for the slush layer, computed as shown below.

Mass balance on liquid water

$$\frac{dm_l}{d\theta} = \dot{m}_{melt}'' + \dot{m}_{rain}'' - \dot{m}_{runoff}'' \quad (3-2)$$

Where:

m_l = Mass of liquid water per unit area in the slush layer, kg/m²

θ = Time, s

\dot{m}_{rain}'' = Rainfall rate in mass per unit area, kg/(s-m²)

\dot{m}_{melt}'' = Snowmelt rate in mass per unit area, kg/(s-m²)

\dot{m}_{runoff}'' = Rate of runoff in mass per unit area, kg/(s-m²)

The water runoff was calculated in two different manners due to the physical aspect of the snow melt problem. During the first part of the snowmelt problem when there is dry snow above the slush layer, the run off was determined as the excess water due to melting. As mentioned beforehand, the slush layer has a maximum height, this value was also determined experimentally. The slush layer then has a maximum amount of water that can be stored within its pores and therefore any excess water was deemed as runoff water. The second part of the runoff was defined as when the only remaining snow was the slush layer and thus absent of any dry snow. During this time the saturated layer is being melted off, and being already saturated, the runoff was determined directly from the amount of water melted by the plate.

Mass of the saturated and snow layers

In order to calculate the heat balances on the snow and saturated layers it is necessary to work out the total mass of these two layers. To accomplish this, the height of the dry snow and slush layer must be calculated. The total height of the dry snow and slush layers can be found by:

$$h_{total} = \frac{m_{ice}}{\rho_{ice}(1 - n_{eff})} \quad (3-3)$$

Where:

h_{total} = Total thickness of the snow and saturated layers, m

m_{ice} = Mass of snow or ice per unit area in the slush layer, kg/m²

n_{eff} = Effective porosity of the ice matrix, dimensionless

ρ_{ice} = Density of ice, kg/m³.

The liquid water in the slush layer can be found in the pores of the snow, and thus the height of the slush layer can be found by:

$$h_{sat} = \frac{m_l}{\rho_l n_{eff}} \quad (3-4)$$

The height of the snow layer can then be found by subtracting, $h_{snow} = h_{total} - h_{sat}$. The mass of the snow in the dry snow layer can be found by:

$$m_{snow} = \rho_{ice} h_{snow} (1 - n_{eff}) \quad (3-5)$$

Energy balance on the snow layer

The energy balance on the snow layer is given as:

$$m_{snow} c_p \frac{dt_{snow}}{d\theta} = q_{conduction\ snow} - q_{snowfall} - q_{convection} - q_{radiation} - q_{sublimation} - q_{evaporation} \quad (3-6)$$

Each of the various terms will be defined in additional detail. The conduction heat flux from the slush layer to the snow layer is given by:

$$q''_{conduction, snow} = \frac{k_{snow}}{0.5h_{snow}} (t_{slush} - t_{snow}) \quad (3-7)$$

Where:

k_{snow} = Effective thermal conductivity of the snow, W/(m-K)

t_{sat} = Temperature of the slush layer, C

t_{snow} = Temperature of the snow node, C

The heat flux due to snowfall is given as:

$$q''_{snowfall} = \dot{m}''_{snowfall} c_{p,ice} (t_{snow} - t_a) \quad (3-8)$$

The convective heat flux is given by:

$$q''_{convection} = h_c (t_{surface} - t_a) \quad (3-9)$$

The convection coefficient used to calculate the heat transfer from the slab was calculated using the following equation (Incropera and Dewitt, 1996). This coefficient was used with the recommendation of an ASHRAE research project on snow melting calculations (Ramsey, et al. 1999).

$$h_c = 0.037 \left(\frac{k_{air}}{L} \right) Re_L^{0.8} Pr^{\frac{1}{3}} \quad (3-10)$$

Where

h_c = Convection coefficient, W/m²C

k_{air} = Thermal conductivity of the air at t_a , W/mC

L = Characteristic length of the surface measured in the direction of the wind, m

Pr = Prandtl number of the air, taken as $Pr = 0.7$

Re_L = Reynolds number based on the characteristic length L

And

$$\text{Re}_L = \frac{VL}{\nu_{air}} \quad (3-11)$$

Where:

V = Design wind speed, m/s

ν_{air} = Kinematic viscosity of air, m^2/s

The radiative heat flux is given by:

$$q_{radiation}^* = \sigma \epsilon_s (T_{surface}^4 - T_{MR}^4) \quad (3-12)$$

The mean radiant temperature (MRT), T_{MR} , is equivalent blackbody temperature of the surrounding of the slab. When snow is falling the surroundings are approximately at ambient air conditions and thus the MRT is equal to the ambient air temperature, and under no snow conditions the MRT can be calculated using the following equations

$$T_{MR} = [T_{cloud}^4 F_{sc} + T_{skyclear}^4 (1 - F_{sc})]^{1/4} \quad (3-13)$$

Where:

T_{cloud} = Temperature of the clouds, K

$T_{skyclear}$ = Temperature of the clear sky, K

F_{sc} = Fraction of the sky that is free of clouds.

For more information on the clear sky temperature and the cloud temperature can be found the literature review section.

The sublimation and evaporation heat fluxes have been neglected in the model for the snow layer. The snow surface temperature is found from a heat balance on the surface node:

$$t_{surface} = t_{snow} - \frac{k_{snow}}{0.5h_{snow}} (q_{convection}'' + q_{radiation}'' + q_{sublimation}'' + q_{evaporation}'') \quad (3-14)$$

Because the surface temperature also appears in equations 3-9 and 3-12 the surface temperature must be determined iteratively.

Energy balance at slush node

The energy balance at the slush node presumes that the liquid/ice mixture is in thermodynamic equilibrium and therefore the temperature is uniform at 0°C. (This can be altitude adjusted as necessary.) Then, the energy balance is given by:

$$\dot{m}_{melt}'' h_{if} = q_{conduction,slab}'' + q_{rainfall}'' - q_{evaporation}'' - q_{conduction,snow}'' \quad (3-12)$$

The conduction heat flux from the slab is determined by a finite volume program.

Assuming rainwater will be at the air temperature, the heat flux due to rainfall is given by:

$$q_{rainfall}'' = \dot{m}_{rainfall}'' c_{p,water} (t_a - t_{slush}) \quad (3-13)$$

The heat flux due to evaporation (for the slush layer only when the dry snow layer is absent) is given by:

$$q_{evaporation}'' = \dot{m}_{evaporation}'' h_{fg} \quad (3-14)$$

The heat flux due to conduction through the snow layer is given in equation 3-7.

3.9 Model Changes

To model the experiments several changes had to be made to the numerical model. These changes had to be made to ensure the numerical model accurately predicted the environmental conditions, i.e. temperature, radiation, and convection. Each of the changes to the numerical model will be discussed below.

The first change to the numerical model occurred due to the voltage drift in the power source. The supply voltage significantly affected the power supplied to the plate. To model the voltage drift, a fourth order polynomial (heat flux vs. time) was fit for each experiment. This polynomial then replaced the constant flux condition set in the numerical model.

The second change was to use the air temperature and a set convection coefficient to calculate the convection heat transfer. The numerical model uses an hourly weather file that includes such variables as temperature and humidity. A weather file was created for each of the heat flux cases with experimentally determined temperatures. The model predicts a convection coefficient as a function of the Reynolds number and air properties, however, in the experimental setup, only natural convection was present. The natural convection regime at the plate is described as “retarded” because buoyancy maintains the stratified, still air conditions. A typical value of the convection coefficient for retarded flow in an enclosure was found to be $1.25 \text{ W/m}^2\text{K}$ (ASHRAE, 1997). The convection coefficient calculation in the model was overridden with this constant value. From experimental measurements the relative humidity inside the chamber was near 90%, which was reflected in the weather file.

The next change to the model was to use the measured sky temperature (ceiling temperature) and a corresponding radiation coefficient. The model based on the air temperature and the cloud conditions given in the weather file would determine the sky temperature. Because the sky temperature was measured in the experiment, this calculation was overridden. A ceiling temperature data file was created and the data was

read into the model and used in place of the calculated value. To estimate the radiation coefficient the following equation was used:

$$h_r = \varepsilon_s F_{ij} \sigma \frac{(T_{sky}^4 - T_{snowsurface}^4)}{T_{sky} - T_{snowsurface}} \quad (3-15)$$

Where:

h_r = Estimated radiation coefficient (W/m²K)

ε_s = Snow emissivity = (0.84)

σ = Stefan Boltzman constant = (5.670x10⁻⁸ W/m²K⁴)

T_{sky} = Sky temperature (K)

$T_{snowsurface}$ = Snow surface temperature (K)

F_{ij} = View factor from plate (i) to the sky (j)

To determine the radiation coefficient, a three node radiation network, Figure 3.9-1, was set up. The Plexiglas cylinder in this setup would act like a reradiating surface.

Incropera and Dewitt (1985) describe a reradiating surface as a surface that has zero net radiation and is commonly used for surfaces that are well insulated on one side and where convection effects may be neglected.

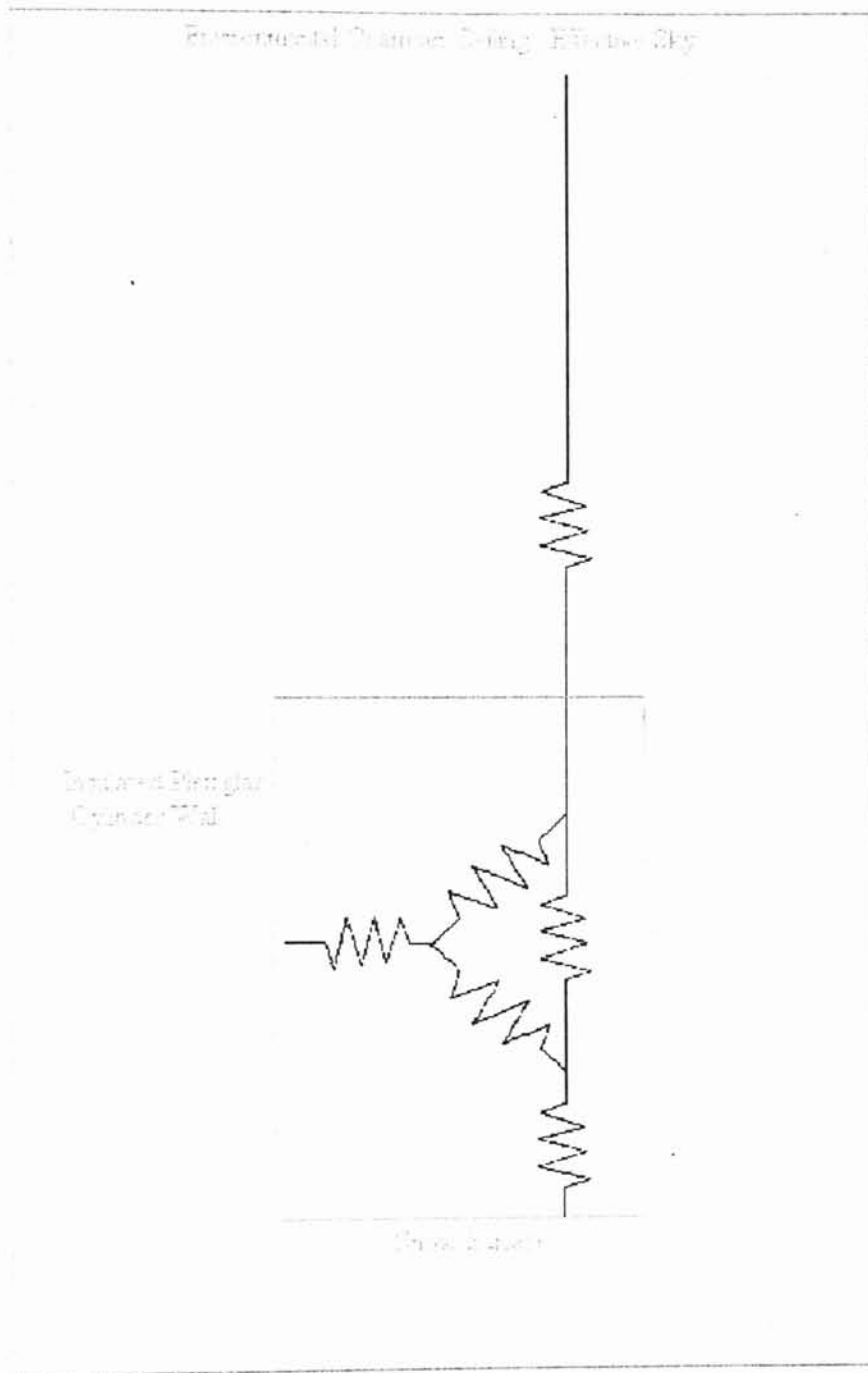


Figure 3.9-1: Reradiating Surface Node Diagram

The radiation coefficient is then given by.

$$h_r = \frac{1}{\frac{1-\epsilon_i}{\epsilon_i A_i} + \frac{1}{A_i F_{ij} + \left[\left(\frac{1}{A_i F_{iR}} \right) + \left(\frac{1}{A_j F_{jR}} \right) \right]^{-1}} + \frac{1-\epsilon_j}{\epsilon_j A_j} \frac{\sigma (T_{sky}^4 - T_{snowsurface}^4)}{A_i (T_{sky} - T_{snowsurface})} \quad (3-16)$$

Where:

F_{ij} = View factor from plate to sky (estimated in Equation 3-17)

$F_{iR}=F_{jR}$ = View factor from plate to reradiating surface = $(1-F_{ij})$

i = Plate

j = Sky

Initially to estimate the view factor of the plate to the sky a simple two surface radiation network was modeled. This resulted in the geometry of the coaxial parallel disks.

Incropera and Dewitt (1985) provide a view factor for this geometry:

$$F_{ij} = \frac{1}{2} \left\{ S - \left[S^2 - 4 \left(\frac{r_j}{r_i} \right)^2 \right]^{\frac{1}{2}} \right\} \quad (3-17)$$

$$S = 1 + \frac{1 + R_j^2}{R_i^2}; R_i = \frac{r_i}{L}; R_j = \frac{r_j}{L}$$

Where:

r_i = Radius of the plate (m)

r_j = Radius of the sky (m)

L = Distance from the plate to the sky (m)

The distance L varies from a maximum value at the beginning of the snowmelt experiment to a minimum value at the completion of the experiment. Because L is a function of snow height, F_{ij} is a function of height, therefore the radiation coefficient is a strong function of the ceiling temperature and the height of the snow.

Several constants were changed in the numerical model. The snow emissivity was changed from a value of 1.0 to a value 0.84. The snow thermal conductivity was changed from 0.8 W/mK to 0.39 W/mK. Yen, et al. (1991) provide several correlations for thermal conductivity as a function of snow density. An average value of the density (400 kg/m^3) was found and the corresponding thermal conductivity (0.39 W/mK) was used in the numerical model.

The last major change was how the model interfaced with a convection and radiation coefficient. The model assumed that the radiation and convection were absorbed by the top layer, however the model did not melt the snow with these heat fluxes. The model increased the temperature of the snow to balance the heat fluxes (The model was developed for conditions where it was assumed that the air temperature is below freezing). For our experimental conditions, the model typically predicted the snow layer temperature to be above 2°C , which is unrealistic. Therefore, the model was changed. If the snow temperature would be predicted to be greater than 0°C , it was fixed at 0°C and the net radiative and convective gains were added to the heat flux provided by the slab. This is equivalent to the melt water melted by convection and radiation at the top surface percolating through the snow with no other effect on the snow.

CHAPTER 4

EXPERIMENTAL APPARATUS

4.1 Introduction

Before snow melting can be observed and measured, snow must be available. Because the testing will occur throughout the year and snow is not readily available throughout the year at the current research facility, artificial snow must be utilized. Also, to simulate the weather conditions during freezing conditions an environmental chamber must be utilized to produce the necessary environmental conditions and will be described in the following section. In addition, the snow making apparatus and the heated horizontal surface used to validate the numerical model are described in the Sections 4.5 and 4.6.

4.2 Snow Making/ Environmental Chamber

The first main purpose of the environmental chamber is to provide a controllable environment in which snowmelt experiments can be conducted. To achieve this goal, the chamber needs to be enclosed, insulated to reduce/eliminate heat gain to the chamber environment, and outfitted with a mechanical refrigeration device to maintain a constant environment conditions. The second main purpose is to provide a space to make artificial snow. As mentioned before, snow is not available naturally year round and, in fact, can be rather scarce even during the winter months in Oklahoma.

In the early phases of the chamber design, one of the major design criteria was the future plan to allow a 0.91m x 0.91 m (3' x 3') concrete slab to be tested inside the chamber. This concrete test slab would contain embedded hydronic tubing. A circulating pump and electric heater are to be used to simulate an actual heated bridge deck. The concrete slab and circulating equipment would be placed on an insulated cart that could be wheeled in and out of the chamber for testing, see Figure 4.2-1.

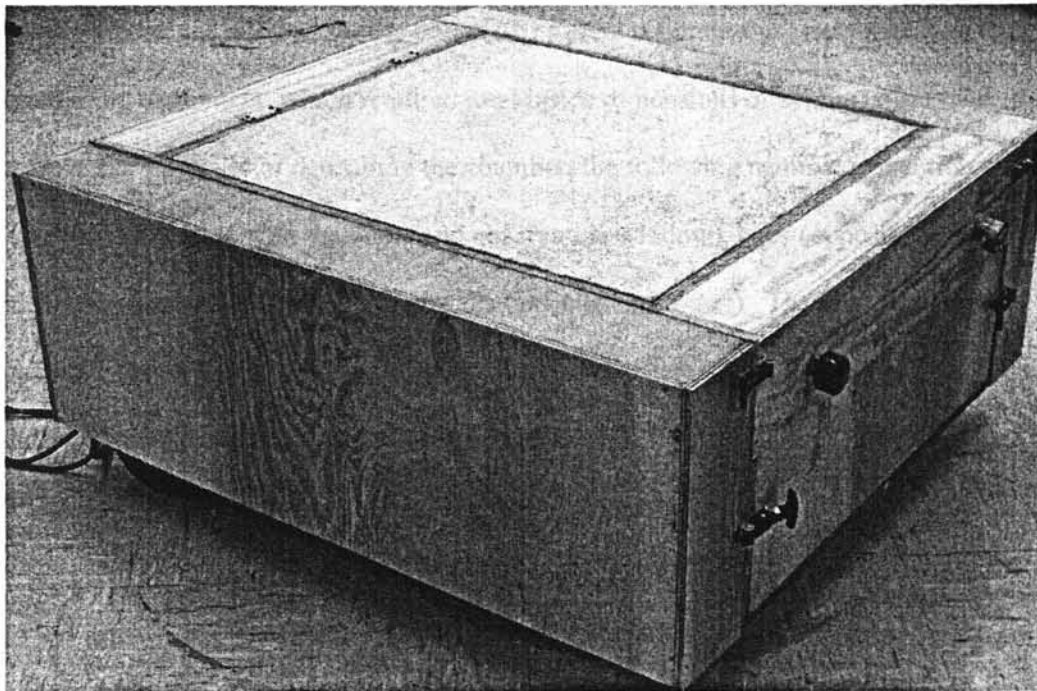


Figure 4.2-1 Concrete Test Slab

This main design criterion is what governed the shape of the chamber. The second main criterion was the size restrictions (i.e. the ceiling height, etc.), which controlled exterior dimension and the amount of insulation. From a construction standpoint, the major obstacle was to allow the chamber to be broken down and moved

from room to room, and therefore strict depth and width criterion were set by the door frame measurement. To facilitate meeting this requirement, the chamber was made into three sections which could be split when moving: the bottom chamber allowed the concrete slab to roll in and out, the middle chamber houses the snow making equipment, and the top section provided space for snow to be formed. The main physical difference between these chambers are the inside dimensions. The top and middle section have an inside dimension of 0.91m (3') square which will allow the snow that is formed in the chamber to fall directly on the 0.91m (3') square concrete slab. The bottom section inside dimensions allowed for the 0.91m (3') square concrete slab, slab insulation and circulating equipment, which required total inside dimensions of nearly 1.52m (5') square. For purposes of describing the chamber, the following naming convention will be adopted: front (side with the doors and observation window), back (opposite of front side) and side walls (two remaining walls opposite each other). The two sides are basically the same and therefore there is no need to differentiate between the two. The side view of the chamber can be seen in Figure 4.2-2.

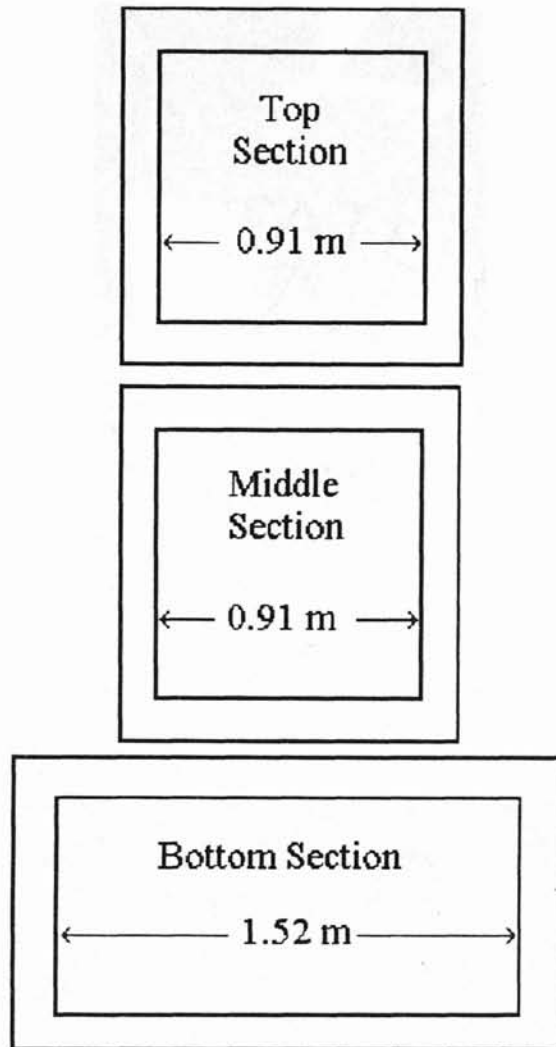


Figure 4.2-2: Side View of Chamber (inside dimensions are noted)

To facilitate the understanding the construction of the chamber, Figure 4.2-3 shows the chamber, with important features labeled. The observation windows, doors to allow the slab to enter, snowmaking equipment, and liquid nitrogen nozzle can all be seen in the Figure 4.2-3.

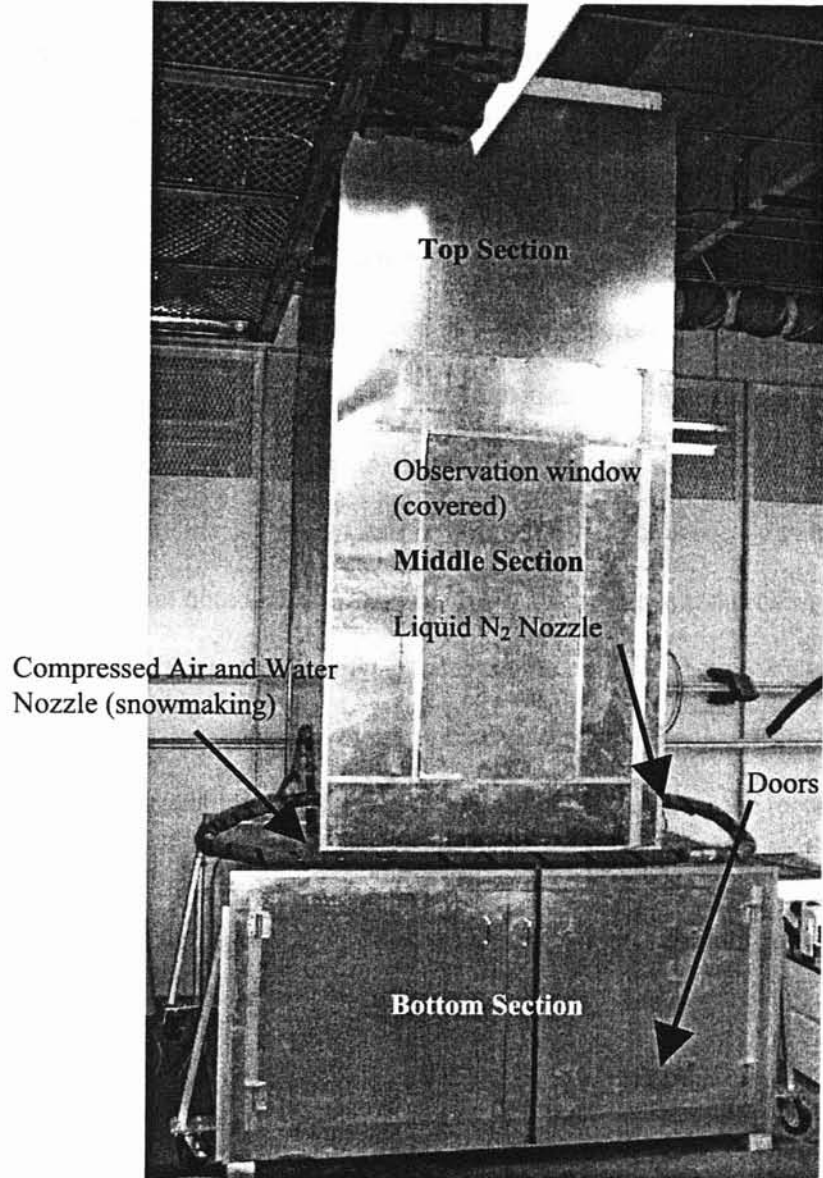


Figure 4.2-3: Environmental Chamber

4.2.1 Top Section

The top section of the chamber is basically a vertical extension of the chamber. The inside box dimension is 0.91m (3') square which will match with the middle section. The roof of the top section is removable and houses a fluorescent light. The walls were built with 5.08cm X 15.2cm (2"x6") pine wood construction (Note: wood dimensions are

measured on a pre-cured basis and therefore the given dimensions are nominal) on 0.4m (16") centers and filled with 13cm (5") thick Styrofoam insulation. The inside walls were covered with 1.6 mm (1/16") hard plastic sheets that were sealed with silicone caulking to the surface of the insulation, which provided for a waterproof wall. The exterior wall was covered with 0.8 mm (1/32") sheet metal, which enclosed the wall to prevent damage and reduced infiltration into the insulation.

As stated before, the roof was constructed to be removable, and due to the fact that the roof of the box saw no load, the top was constructed solely out of Styrofoam insulation. The inside of the roof was covered with a hard plastic sheet to prevent water damage. To aid in photographic documentation of the snowmelt process a standard 1.2m (4') fluorescent shop light was then installed in the roof. A 15cm x 20cm x 1.2m (6" x 8" x 4') rectangular slot was cut in the roof insulation so that the florescent light could be mounted in the insulation. A sheet of Plexiglas was placed over the rectangular slot from the inside to reduce the heat gain to the chamber and provide a translucent medium for the light to shine through. Figure 4.2-4 depicts the view of the roof from inside the chamber.

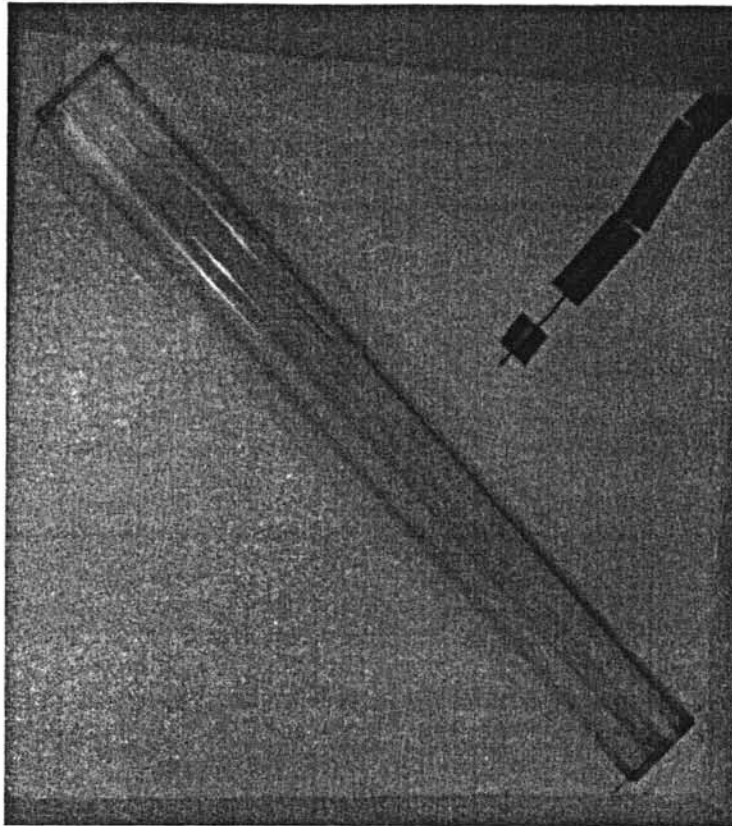


Figure 4.2-4: Chamber Roof viewed from the inside

At the top of one of the sidewalls, a permanent hole was cut through the wall. In the hole, a 12.7cm (5") diameter, 0.61m (2') long piece of polyvinyl chloride (PVC) pipe was inserted through the wall. This pipe functions as a connector for the air return duct for the mechanical refrigeration system. The air that exits through this pipe is passed through the duct and is then cooled by the heat exchanger box and enters through a similar type connector pipe in the bottom section of the chamber. If the mechanical refrigeration is not needed or during hazardous conditions (i.e. snowmaking) the air return duct can be blocked with PVC end caps. Figure 4.2-5 shows the air return pipe in the side wall of the top section.

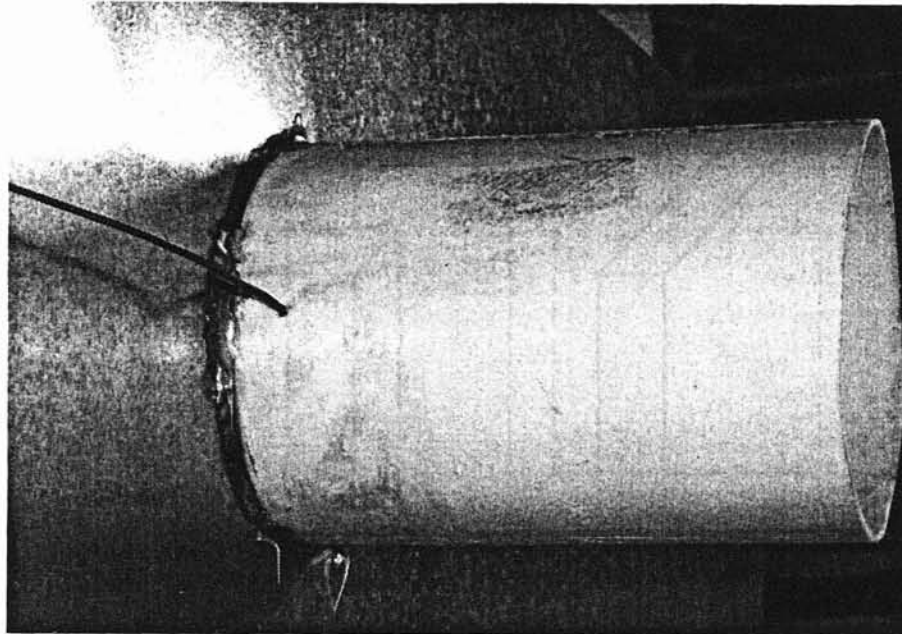


Figure 4.2-5: Air return in the sidewall of the top section

4.2.2 Middle Section

The middle section of the chamber houses the snow making equipment itself. The snow making equipment will be discussed in subsection 4.6. The inside box dimension is 0.91m (3') square which will match with the 0.91m (3') concrete test slab. The top section sits directly on the middle section. The top section can be removed from the middle section and the middle section can be removed from the bottom section to fit through the door frame. Also, the walls of the middle section were built such that they could be split apart to fit through the door. To accomplish this task, the walls were built as permanent "L" shapes and the two "L's" are butted together and fastened; see Figure 4.2-6.

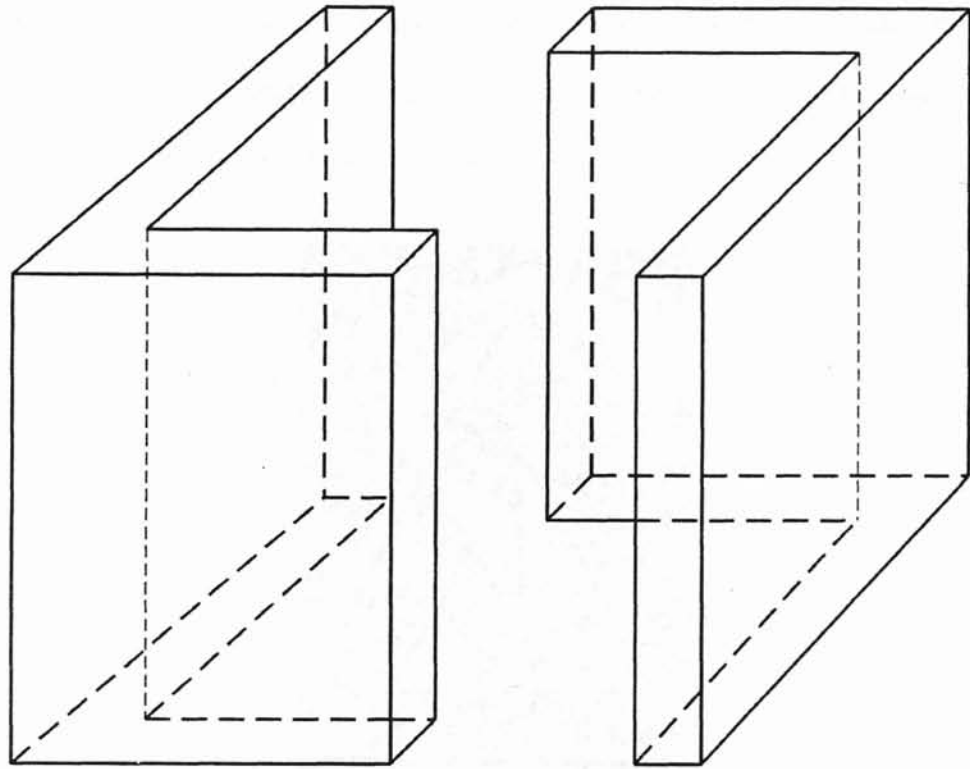


Figure 4.2-6: Middle Section Breakdown in two L's

The walls were built with 5.08cm X 15.2cm (2"x6") pine wood construction (Note: wood dimensions are measured on a pre-cured basis and therefore the given dimensions are nominal) on 0.4m (16") centers and filled with 13 cm (5") thick Styrofoam insulation. The inside walls were covered with 1.6 mm (1/16") hard plastic sheets that were sealed with silicone caulking to the surface of the insulation, which provided for a waterproof wall. The exterior wall was covered with 0.8 mm (1/32") sheet metal, which enclosed the wall to prevent damage and reduced infiltration into the insulation. The required height of the top and middle section was determined from prior experiments and will be discussed in the snow making section.

At the bottom of the side walls, holes are drilled through the walls to allow for the snow making equipment to enter the chamber. Hard plastic pipes were inserted through

the hole and sealed with silicone caulking to the chamber. This procedure sealed the wall preventing water from entering the wall and possibly damaging the wood or insulation.

Figure 4.2-7 shows the two snow making holes.

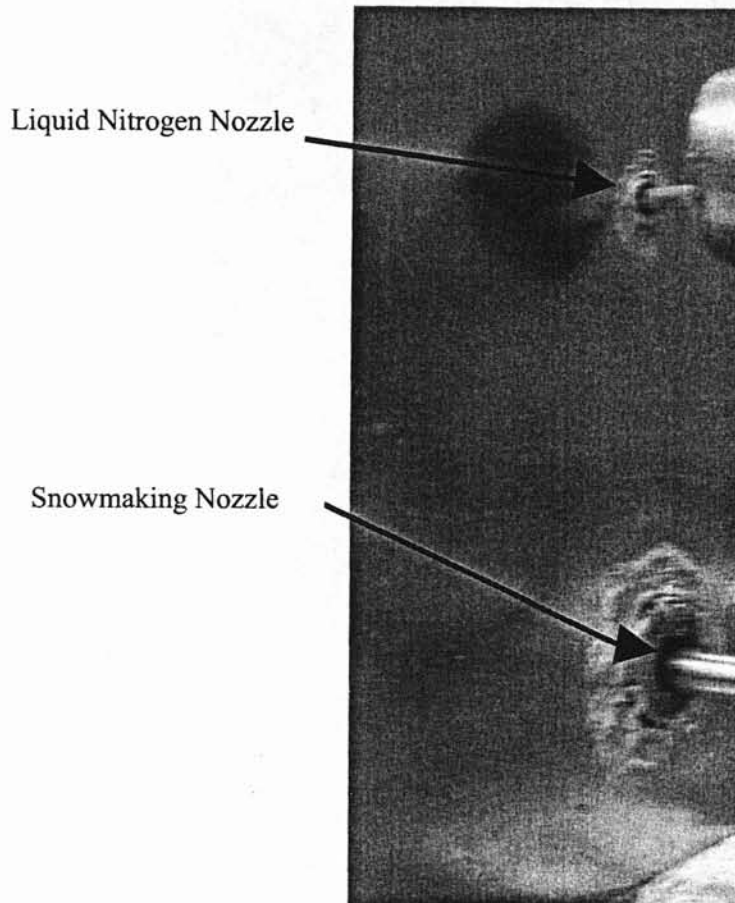


Figure 4.2-7: Snowmaking holes in side wall

The last main feature of the top section is the addition of a viewing window in the front wall. The window measures 0.61m X 1.22m (2' X 4'). Instead of the interior of the being covered with a hard plastic sheet, the inside is covered with a transparent Plexiglas sheet, which will allow viewing of the experiments. To insulate the window, an insulation "plug" was made to fit in the cutout of the window and covered on the exterior

with the sheet metal. Handles were attached on the exterior to allow the plug to be removed from the chamber wall for visual inspection. In Figure 4.2-8, the Plexiglas window and the insulating plug can be seen.

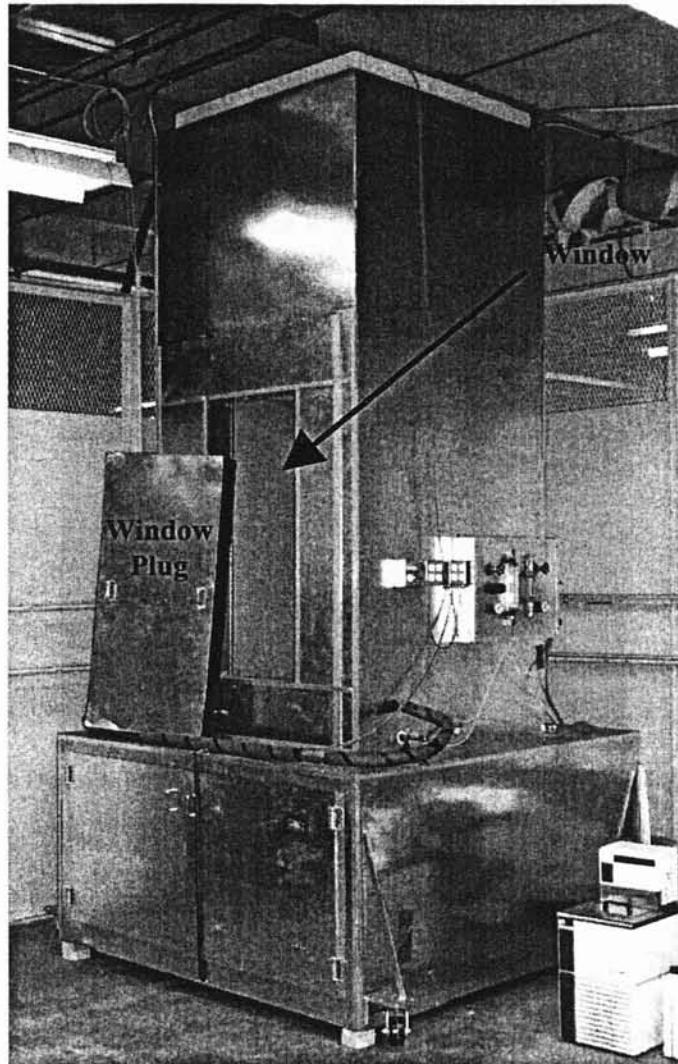


Figure 4.2-8: Window and Insulative Plug

In Figure 4.2-9 the middle section can be seen with the window plugged and the snowmaking equipment installed in the sidewall.

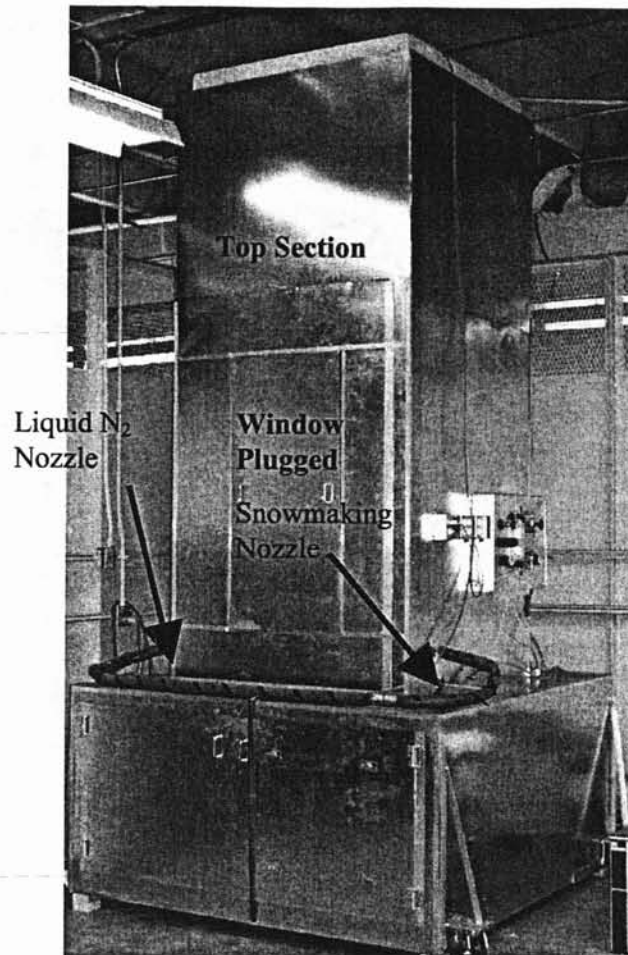


Figure 4.2-9: One side of the chamber (note the location of the snow making equipment)

4.2.3 Bottom Section

The bottom section of the chamber is fabricated as one piece. The exterior dimensions are just small enough to fit through the doorframe when the sections is turned on end. The bottom section of the chamber will house the 0.91m (3') square concrete test slab and therefore the inside dimensions are set to accommodate the slab and cart at near 1.52m (5') square. The front wall of the section is constructed with two 0.91m (3') doors to allow for the slab and cart to roll in and out of the chamber. The doors were

constructed of insulation covered with sheet metal on the outside and hard plastic on the inside; see Figure 4.2-10.

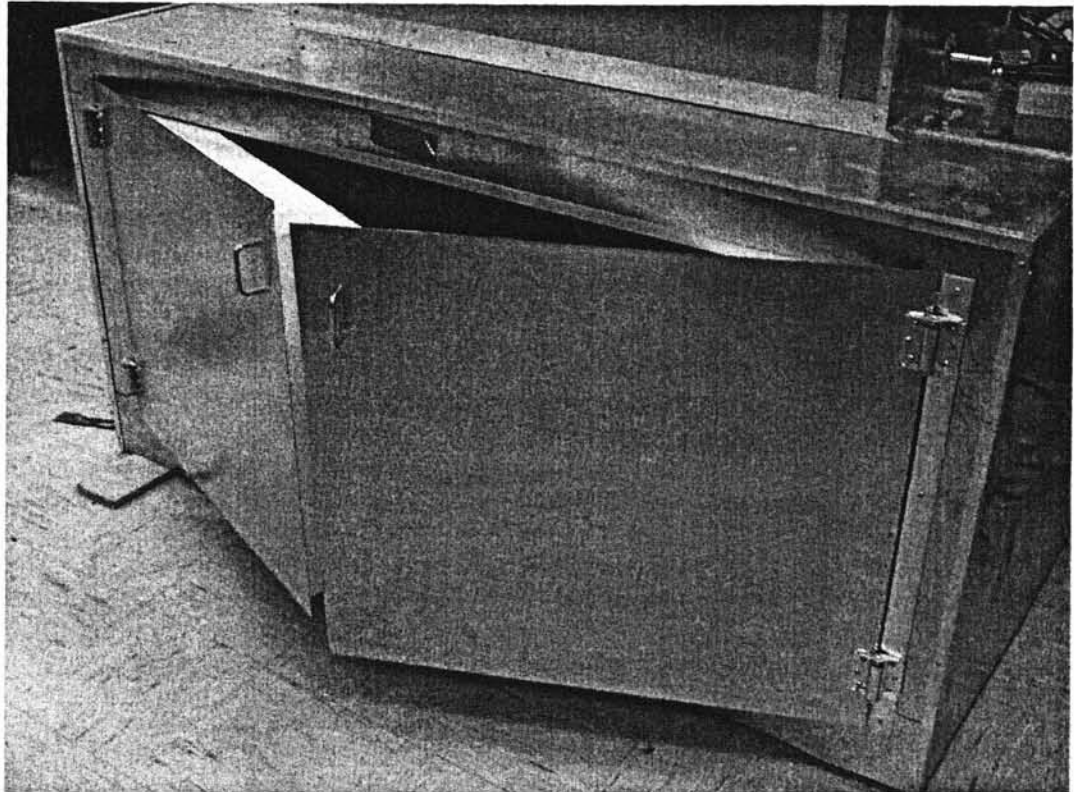


Figure 4.2-10: Bottom Section and doors

The back and sidewalls are built the same as the top section walls. They have 5.08cm X 15.2cm (2"x6") pine wood construction on 0.30m (12") centers with 13cm (5") thick Styrofoam insulation. Again they were covered with the hard plastic on the inside and sheet metal on the outside. The roof of the bottom section was built with the same construction as the walls except for the 0.91m (3') square hole in the center of the roof to allow access to the top section.

Special consideration was given to the floor due to the weight of the concrete slab. To ensure the floor did not deform under the weight of the slab the 5.08cm X 15.2cm (2"x6") pine wood construction were placed on 20.3cm (8") centers. Also the

second main concern was the water that would collect in the chamber after the snow making and melting experiments had been completed. For this reason a drainage channel was added. To achieve this affect a 2.5cm (1") deep by 12.7cm (5") wide section of the Styrofoam insulation was removed to provide for the channel and a hole was drilled in the floor near the sidewall. Standard 2.54 cm (1") PVC SCH 40 pipe was installed into the drainage hole to protect the floor from water damage. At the end of the drainage pipe, a valve was installed to seal the chamber from the exterior environment if water runoff will not be present. Figure 4.2-11 depicts the drainage channel.

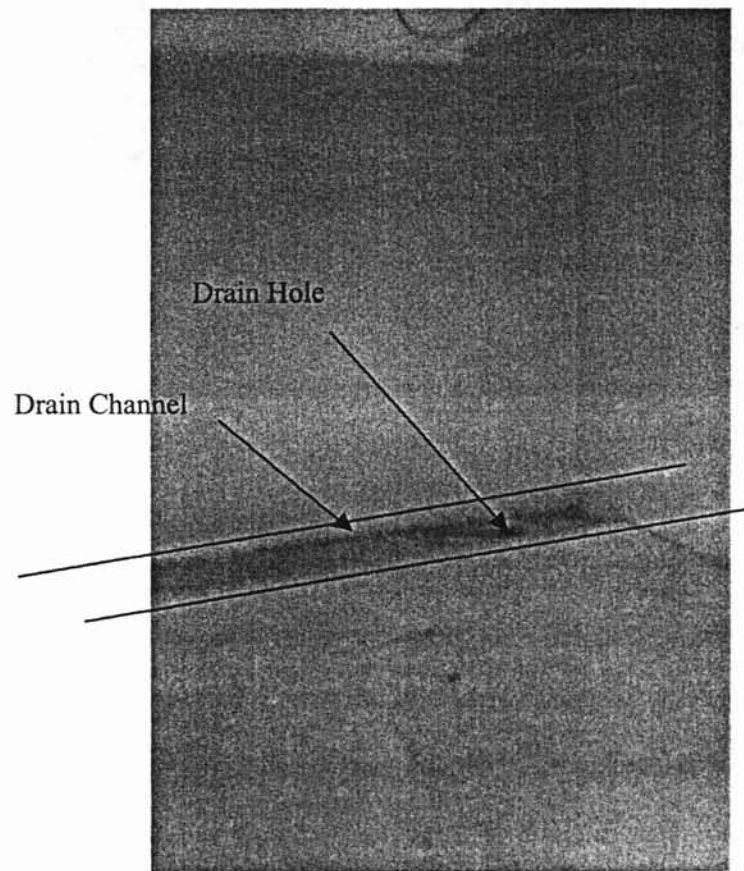


Figure 4.2-11: Drainage Channel

On the base of the back wall of the bottom section, a permanent hole was cut through the wall. In the hole, a 12.7cm (5") diameter, 0.61m (2') long piece of PVC pipe was inserted through the wall. This pipe then attached to a 'U' shaped air diffuser also made out of PVC pipe. 2.5cm (1") holes were drilled in the diffuser PVC pipe to distribute the airflow. This diffuser was made such that the air velocity in the chamber was kept to a low enough such that forced convection was kept to a minimum. Figure 4.2-12 shows the air diffuser inside the bottom section.

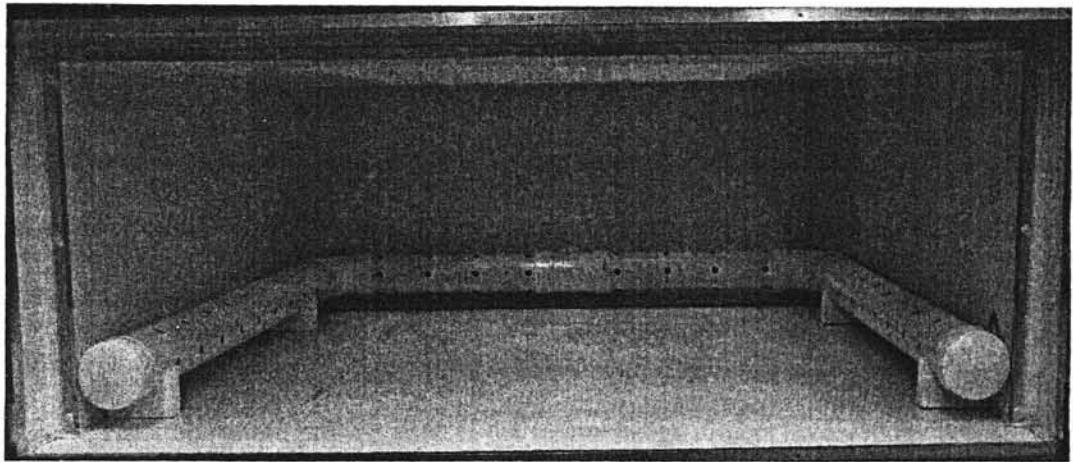


Figure 4.2-12: Air Diffuser

4.3 Snow Making Equipment

After the chamber had been built, the snow making equipment was added to the exterior of the chamber. A group of senior mechanical engineers were given the task to develop a simple method of making artificial snow (Longwill, et al. 1999). The results of their investigation were included in design of the environmental chamber. The actual snowmaking procedure is described in Chapter V. The first main result of the senior project was the required height of the chamber. Longwill, et al. (1999) found that a chamber height of 2.1 m (7') to be sufficient. The height of the middle and top sections currently is 2.6 m (8.5') which exceeds the requirement.

Real snow is formed by water particles in the cloud crystallizing as they fall to the earth. As they fall, the crystals grow in size. Presumably, the higher the chamber, the better the quality of the snow. To maximize the resonance time, the water droplets were jetted upward and then fall such that the maximum distance traveled is 5.2 m (16'). This approach increases the time the water droplets are in the air and thus will help each crystal grow. The jet is formed by mixing compressed air and liquid water in the upward directed nozzle. As the air/water mixture is shot up, it mixes with a liquid nitrogen stream, which cools the water droplets. As the water is cooled to freezing, it will form snow crystals. The smaller the water droplets, the faster they can be cooled and the less liquid water droplets will reach the snow (liquid water mixed in with the snow creates a wet, high density snow). If the nozzles do not effectively atomize the water droplets, the resulting snow will have a consistency more like that of slush than of snow, and therefore useless as an artificial snow in our snow melting apparatus.

The atomization process used in the senior design project involved the collision of 3 jet streams. While this could be made to work, the setup to correctly aim the streams for complete collision was quite difficult. In our apparatus, engine degreaser nozzles were selected, as shown in Figure 4.3-1. The engine degreaser nozzles used a venturi effect to draw fluid from a bucket, which is then sprayed over an engine. The nozzles were modified for use in the snow chamber. Instead of using the venturi effect to draw the water from a reservoir, pressurized water was sent to each nozzle and controlled with a trim valve.

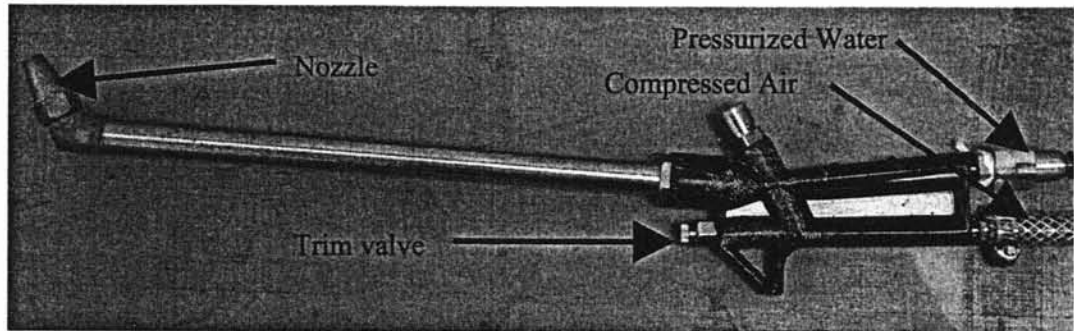


Figure 4.3-1: Snowmaking Nozzle

This modification allows the operator to control the amount of water that enters the chamber. Each nozzle is connected to a compressed air line and also a water line. Each nozzle supplies approximately 56.6 L/s (2 cfs) of compressed air and 0.00315 L/s (0.05 gpm) of water. This mixture can be modified depending on the density of the snow that is necessary. After consulting Jordan, et al. (1999), the average density of “real” snow ranges from 100kg/m^3 to 300 kg/m^3 . With the settings mentioned above the chamber will produce 250kg/m^3 artificial snow. The water/air pressures were controlled using ball valves that were installed in a control box with rotameters to measure the respective flowrates. The control box can be seen in Figure 4.3-2 and Figure 4.3-3. Again the nozzles were chosen because they atomized the water well enough that the density of the resulting snow was within the given range of “real” snow densities. Several other nozzles were investigated; however, these nozzles did not produce snow in the given range of densities.

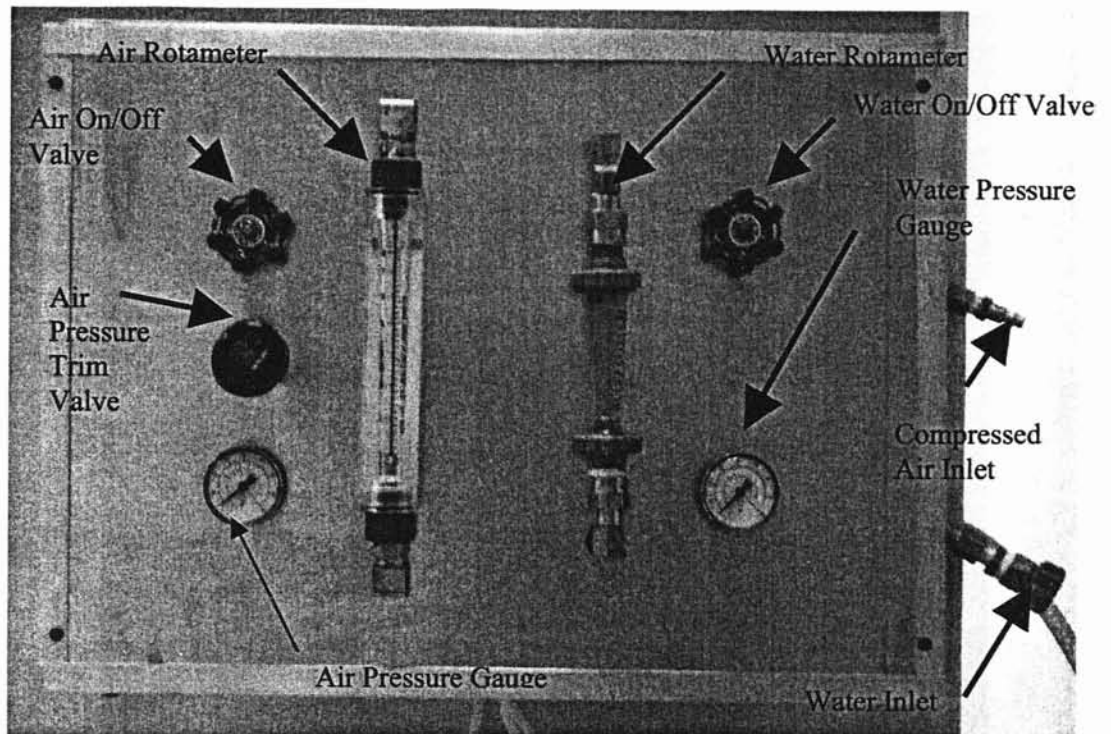


Figure 4.3-2: Snowmaking Control Box

Only the tips of the nozzles were inside the chamber, to reduce the risk of freezing. They were inserted in the 3.8cm (1 1/2") holes at the sides and back of the middle section. The hole diameter was required to insert the tip through the wall, and therefore insulation was added to reduce the infiltration rate. An additional 3.8cm (1 1/2") hole was drilled in the middle section to allow for a communication link between the chamber and the room. Communication cables and power cords were run from the outside of the chamber inside to the necessary equipment such as the balance, camera, and the snow melting plate. Thermocouples for measuring the plate temperature as well as the chamber environment were also passed through this hole.

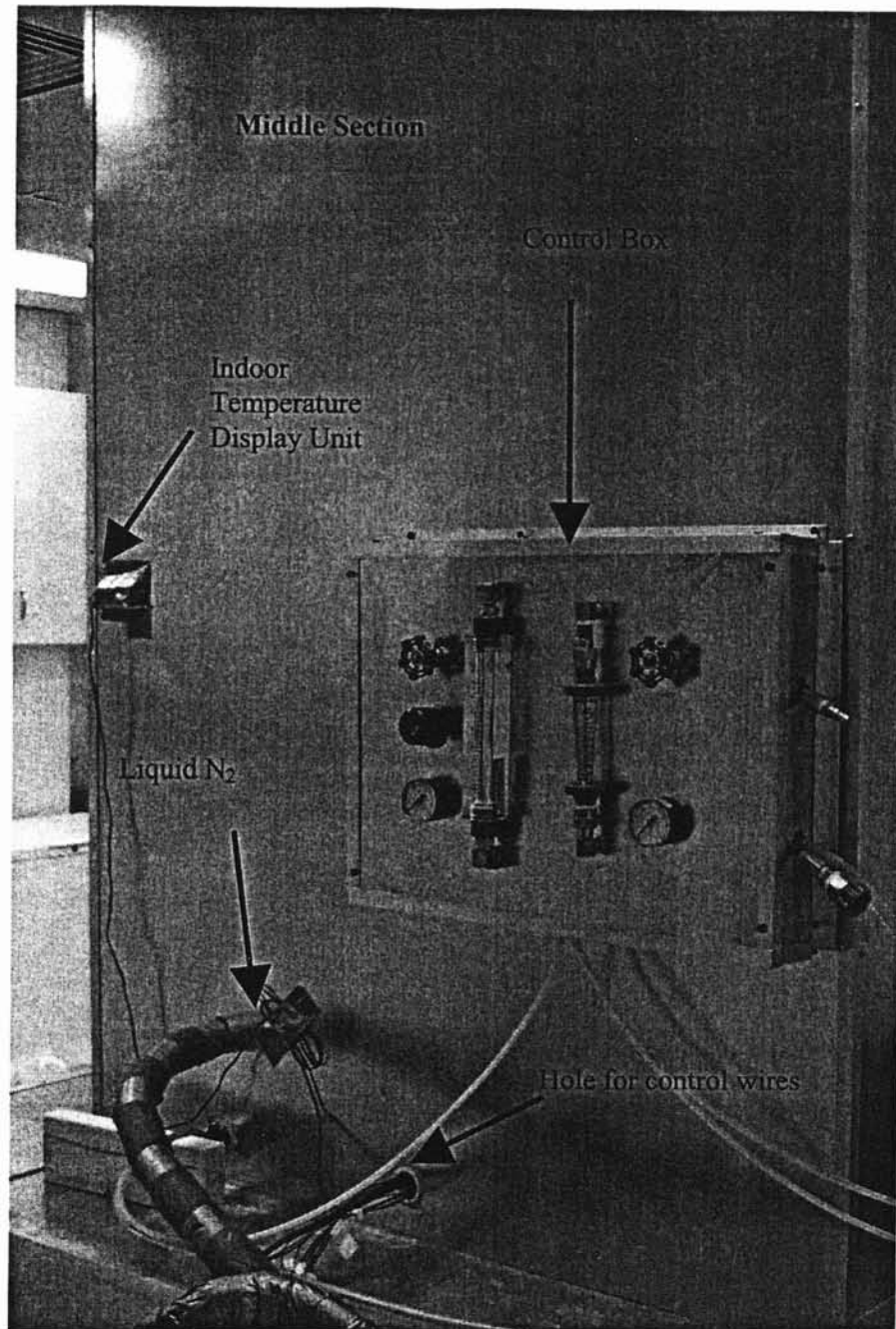


Figure 4.3-3: Snowmaking Setup

Above each of the snowmaking nozzles, a 1.27cm ($\frac{1}{2}$ ") hole was drilled and fitted with 1.27cm ($\frac{1}{2}$ ") PVC pipe. These holes allowed for liquid nitrogen lines to be plumbed into the chamber. 0.64cm ($\frac{1}{4}$ ") copper tubing was used to transport the liquid nitrogen

from the tank to the chamber. The tubing on the inside of the chamber was bent to direct the liquid nitrogen stream to collide with the water stream that was shot into the chamber using the snow making nozzles. This rapidly cooled the water in the stream to enhance the snow making performance of the chamber. This can be seen in Figure 4.3-4.

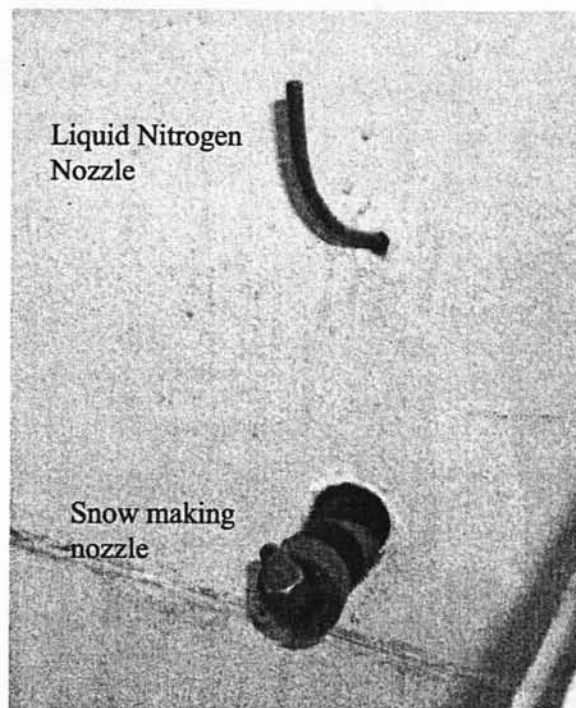


Figure 4.3-4: Liquid Nitrogen Nozzle and Snow Making Nozzle from the Inside of Chamber

4.4 Mechanical Refrigeration Setup

In the above sections the environmental chamber has been discussed. One of the goals of the chamber was to reduce the heat gain from the room environment so that a mechanical refrigeration device could keep the chamber environment constant near freezing conditions. The chamber was outfitted with an air return pipe and an air diffuser, which have been discussed in the sections above. The mechanical refrigeration apparatus is attached to the pipes and supplies the chamber with chilled air. Figure 4.4-1

shows the setup of the chamber and mechanical refrigeration setup. Each of these portions will be discussed more in detail in the following paragraphs.

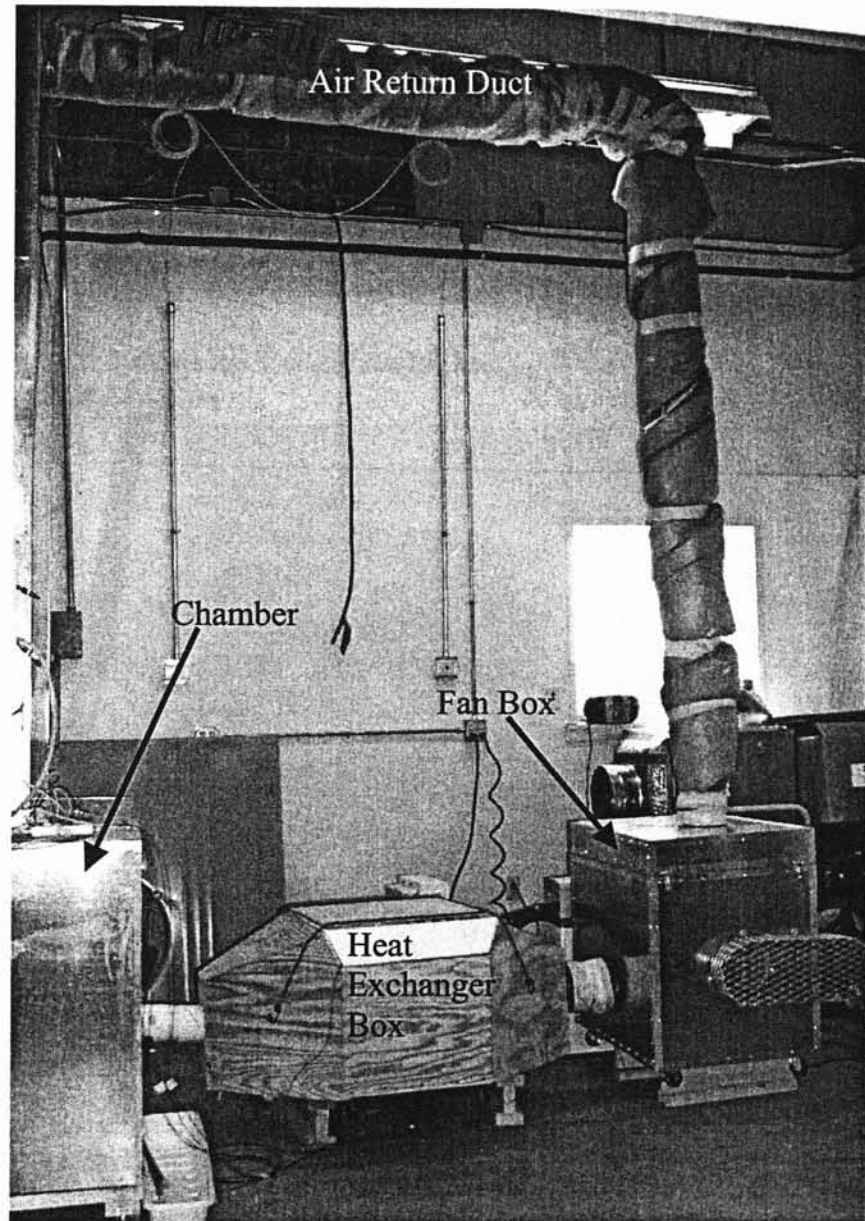


Figure 4.4-1: Mechanical Refrigeration Setup

The air return duct was constructed of 10cm (4") inside diameter PVC pipe. The duct was connected to the air return pipe mounted near the roof of the chamber. The duct

then was connected to the inlet of the fan box. The overall length of the duct is 4.6 m (15'). The air return duct was insulated with R-25 fiberglass bat insulation.

The fan box was used to supply air to the chamber. The fan box was made out of 13cm (5") Styrofoam insulation. The outside was covered with 6mm (1/4") plywood on the outside. This provided a form for the box. The plywood was then covered with 0.8mm (1/32") sheet metal. The inside of the fan box was covered with 1.6mm (1/16") hard plastic. The edges were sealed with Silicone. The fan was then installed inside the box. Figure 4.4-2 shows the inside of the fan box.

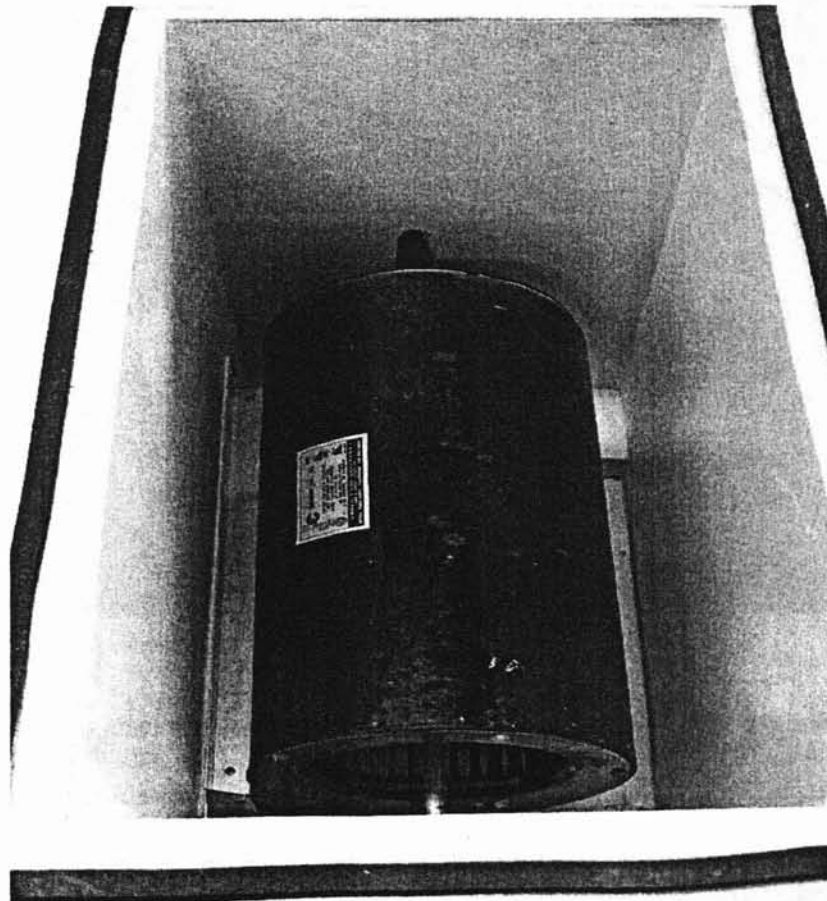


Figure 4.4-2: Inside of Fan Box

The fan drive shaft to was mounted through the wall of the fan box so that the motor could be placed outside the box. This would remove the heat created by the motor from the system and reduce the overall heat gain by the system dramatically. The motor is a 1/6 hp 120V/60Hz AC motor which will produce approximately 125W of heat. When installed in the system the fan provides a volumetric flow rate of 0.08 m³/s. Figure 4.4-3 shows the fan box.

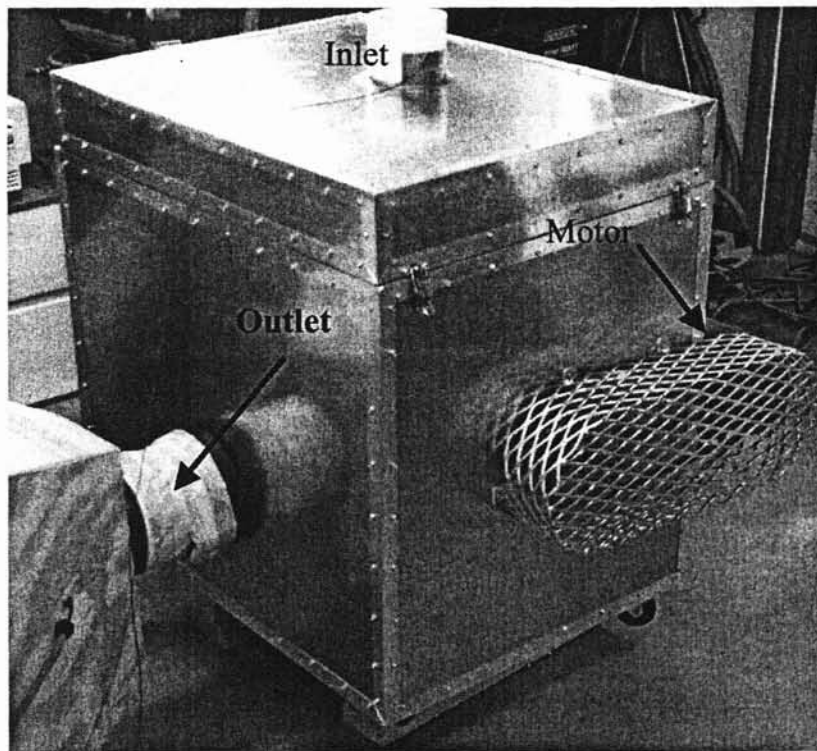


Figure 4.4-3: Fan Box

The fan outlet was then hooked to the heat exchanger box. The fan inlet and outlet pipe was insulated with R-4 foam rubber insulation. The heat exchanger box housed four air-to-water heat exchanger coils. Figure 4.4-4 shows the heat exchanger box without the coils installed.

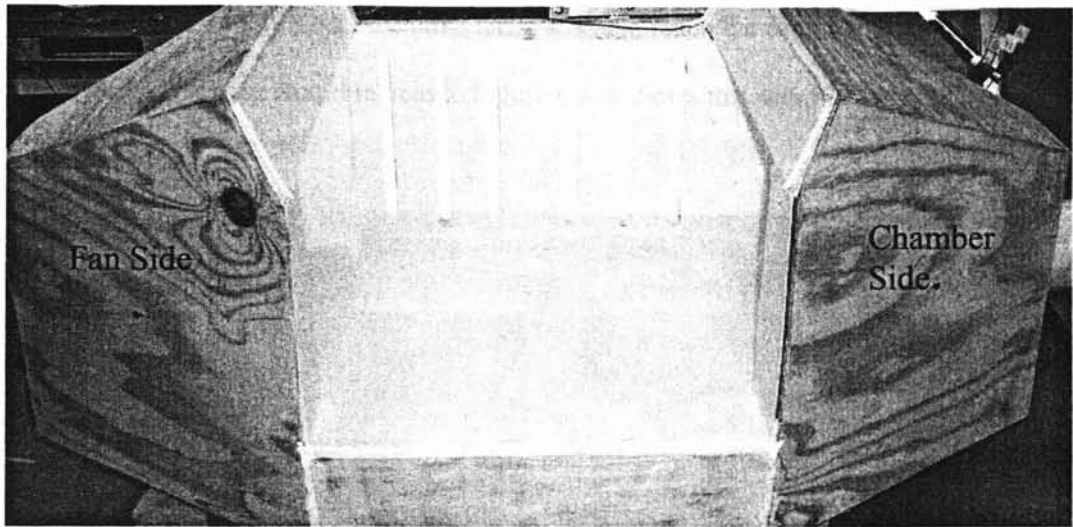


Figure 4.4-4: Empty Heat Exchanger Box

The coils are a six tube pass fin type heat exchanger. The fin spacing is 4 mm. The tube inside diameter is 9.5mm (3/8 "). The tubes and fins were constructed out of Stainless Steel. Figure 4.4-5 shows one of the air-to-water heat exchanger coils.

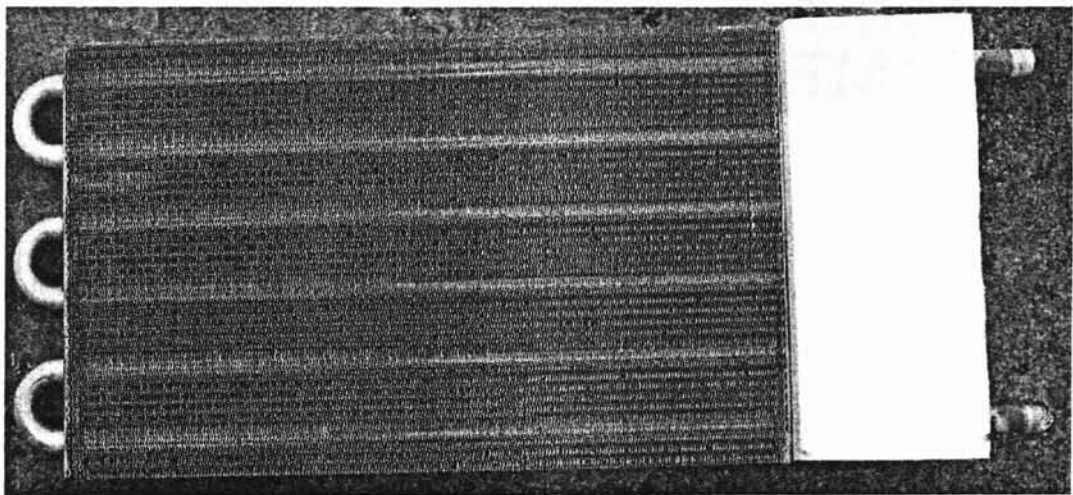


Figure 4.4-5: Heat Exchanger Coil

These coils were the installed in the heat exchanger box along with a 1.6mm (5/8") copper tubing 7.6m (25') long. This tubing provided for a place for frost to develop without plugging the coil and therefore reducing the coil effectiveness. If a coil was

completely blocked by frost no chilled airflow would reach the chamber and thus the chamber temperature would increase. Figure 4.4-6 shows this setup of the heat exchanger box.

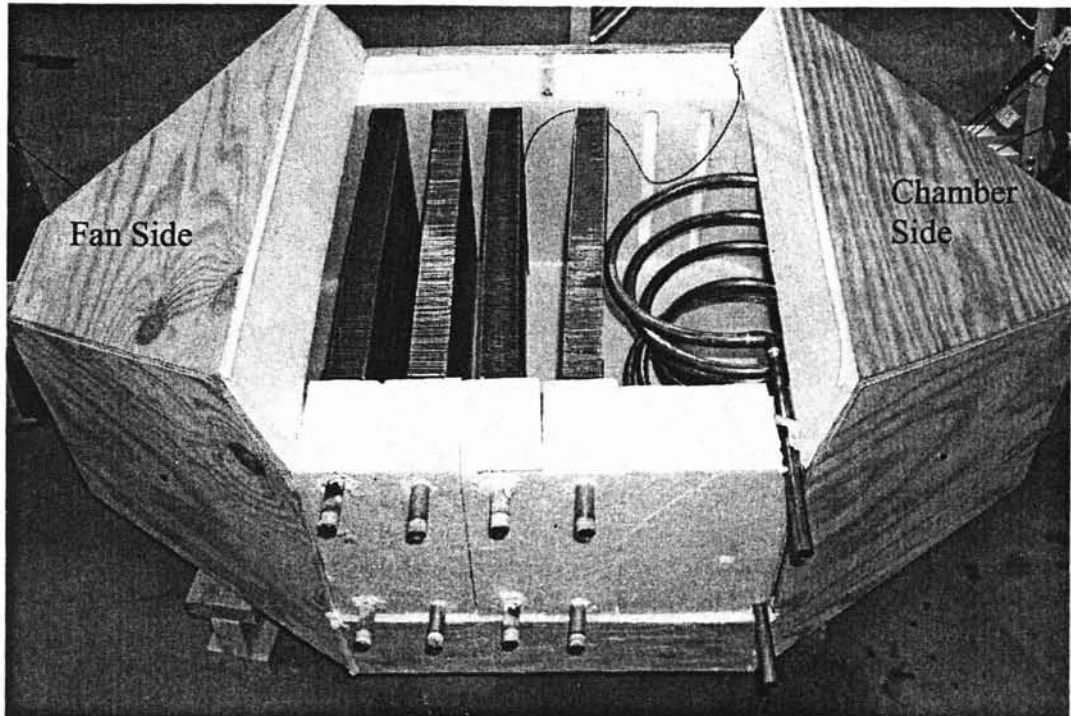


Figure 4.4-6: Heat Exchanger Box

The heat exchanger box was made in the same manner as the fan box. The outside was constructed of 6mm (1/4") plywood. The inside was covered with 13cm of Styrofoam insulation. The inside was covered with 1.6mm (1/16") of hard plastic. This step is very important for this unit because of the condensate runoff. Future plans include covering the box in sheet metal.

The heat exchanger coils are then attached to mechanical chillers. These chillers have small circulation pumps and an approximately a 7L bath. The fluid is circulated from the coils back to the chiller. The fluid chosen was a 50%/50% (by volume) solution

of ethylene glycol and distilled water. Figure 4.4-7 shows the heat exchanger box hooked up to the chillers.

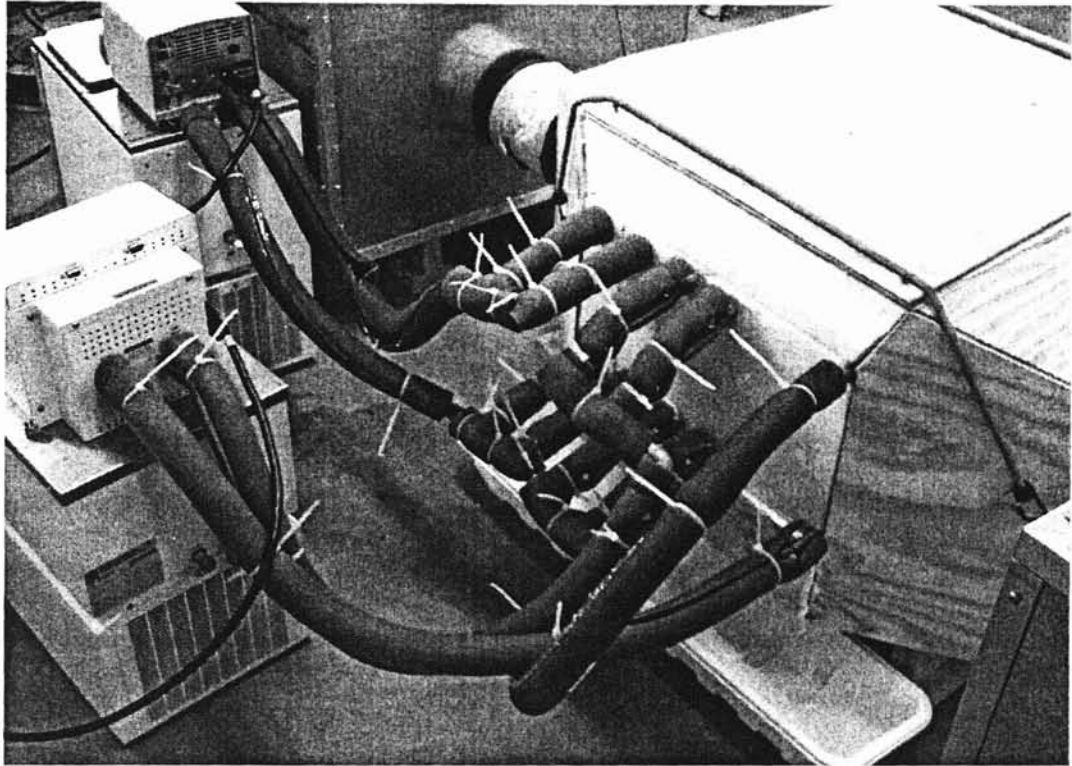


Figure 4.4-7: Heat Exchanger Box with Chillers

The chillers were produced by ThermoNeslab (www.thermoneslab.com). The larger of the two chillers (RTE-740) has a cooling capacity of 750 W at 0°C. The smaller chiller (RTE-140) has a cooling capacity of 500W at 0°C. These chillers operate with 120V/60Hz AC electricity. The pumping capacity of both chillers is 15 lpm at 0m head and 0 lpm at 4.9m head.

4.5 Chamber Thermocouple Placement

The chamber and mechanical refrigeration devices were outfitted with thermocouples to measure the air temperatures. The placement of the thermocouples is detailed below:

- The center of the chamber outlet pipe.
- The center of the inlet pipe to the fan box.
- The center of the inlet pipe to the heat exchanger box.
- The first heat exchanger coil.
- The center of the outlet pipe from the heat exchanger box.
- Taped to the ceiling of the chamber.
- Taped to the bottom of the chamber.
- Mounted 30 cm, 60 cm, 90 cm and 120 cm from the bottom of the chamber.

The inlet and outlet chamber air temperature measurements along with the chamber airflow rate could be used to determine the heat gain by the chamber, air return duct, and the fan box. The chamber's heat gain calculated to be 470 Watts. The air return duct had a heat gain of 94 Watts and the fan box had a heat gain of 190 Watts.

4.6 Snow-melting apparatus

The snow melting process is investigated with a heated plate mounted inside a Plexiglas tube. The tube has an inside diameter of 17.8cm (7"), 0.64cm (¼") thick walls and a total length of 71.1cm (28"). The plate was mounted 20.3cm (8") from the top of the tube, as shown in Figure 4.6-1. The plate was constructed of two 4.76mm (3/16") aluminum plates. A 4.76mm (3/16") hole was then drilled in the center of the plate to allow for the melted water to drain off the plate. The bottom of the plate was covered with a thin layer of epoxy to insulate the resistive wire from the aluminum plate. A 1.8m (6') length of 0.76mm (0.030") diameter Nichrome wire was then coiled on the back of the aluminum plate.

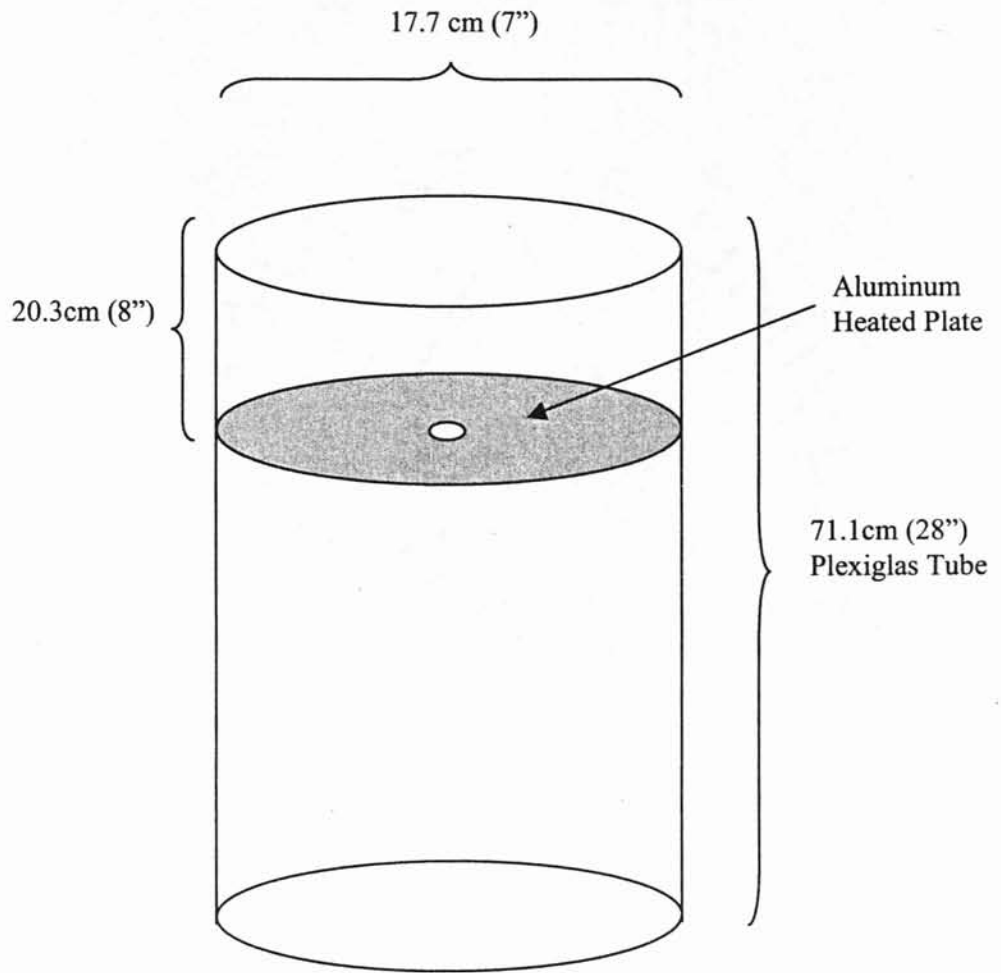


Figure 4.6-1: Plexiglas Tube Fitted with Aluminum Plate

Figure 4.6-2 shows a photograph of the Nichrome wire epoxied to the plate.

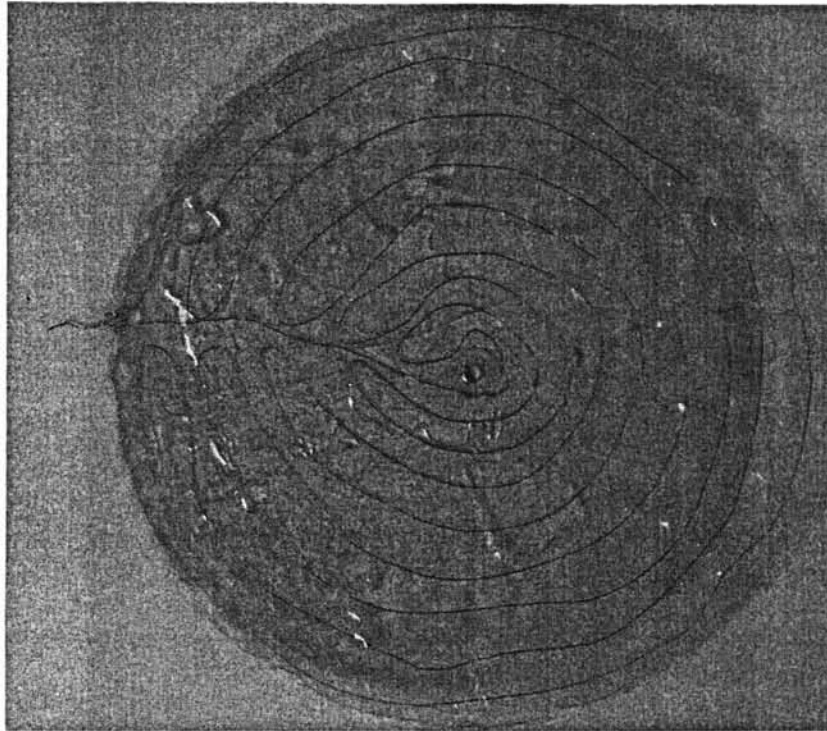


Figure 4.6-2: Nichrome wire coiled and epoxied to the plate

Figure 4.6-3 shows a photograph of the actual snow melting apparatus setup up with the heated plate and the Plexiglas tube.

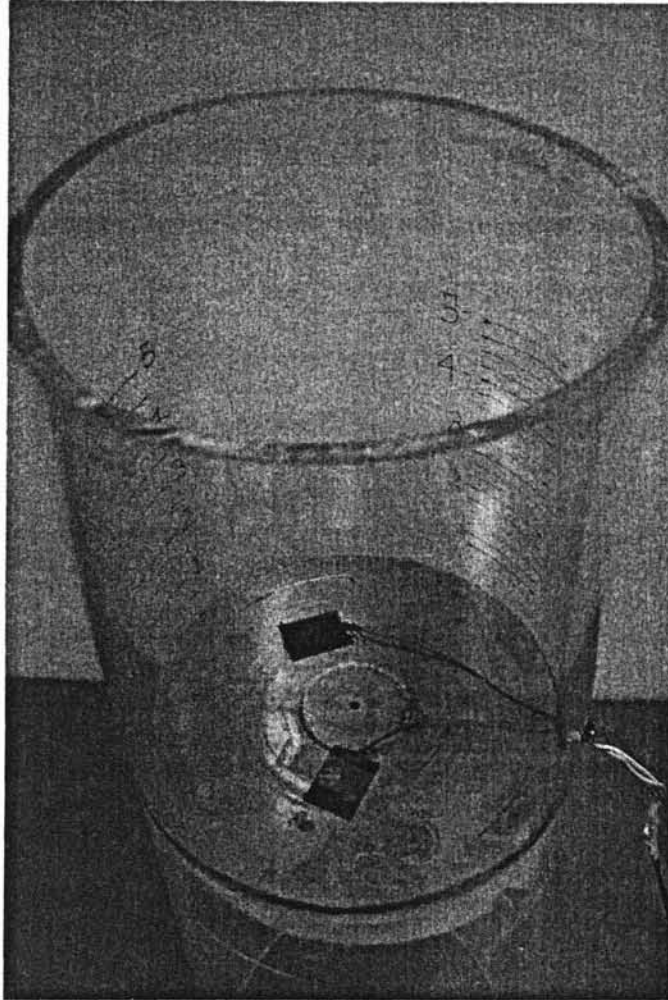


Figure 4.6-3: Heated Plate Setup

The length of Nichrome wire necessary was calculated to replicate the heated bridge deck, which was designed to produce a heat flux around 433 W/m^2 (150 Btu/hr ft^2) (Spitler, et al. 2001). The Nichrome wire used (Nichrome 30, 0.462mm diameter) had an electrical resistance of 27.78 Ohms/m (8.47 Ohms/ft). To reduce the overall length of wire, 24 volts were used, which allowed the length of wire to be a mere 2.05 meters. After the wire was evenly spaced along the bottom of the plate, a second coat of epoxy was applied over the wire. Special care was taken while mixing the epoxy to reduce the number of air pockets that formed within the epoxy, which could reduce the

heat transfer. After the epoxy had cured over night, the plate was connected with to a 24V DC source and the plate was tested for shorts and continuity.

Before the plate was installed in the Plexiglas tube, two 6.3mm ($\frac{1}{4}$ ") holes were drilled in the Plexiglas tube to allow for the electrical wires, that heat the plate, to pass through the Plexiglas wall. The plate was then sealed to the tube using silicone sealant. Three T-type thermocouples were then attached to the plate using medical tape. The thermocouples were connected to a Fluke Hydralogger, which recorded the plate temperature at a specified interval. The plate was then filled with snow and the voltage source was turned on supplying the plate with a current, which was also measured using the Fluke Hydralogger. After time passed it became obvious that the plate was melting the snow unevenly. This was evident not only by physical observation but also by analyzing the plate thermocouple data. To rectify the problem, a second 4.76mm ($\frac{3}{16}$ ") plate was added on top of the existing plate. This required the use of a thermally conductive paste to ensure contact between the two plates. This paste was made with copper powder and aircraft grease. The thermal paste was spread over the existing plate and the additional plate was placed over the existing paste and the two plates were compressed to ensure contact and limit the spacing between the two plates. Two thermocouples were then reattached to the plate and a second snowmelt experiment was run, this time the results pointed to a more even melting pattern. The layer-by-layer construction is shown schematically in Figure 4.6-4.

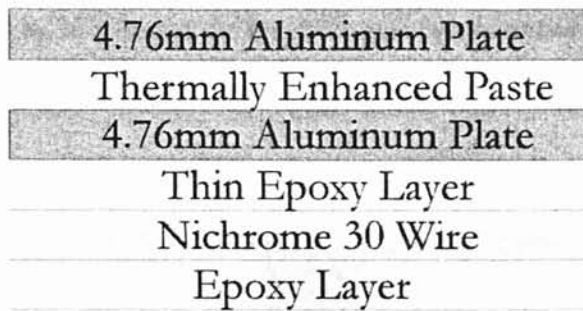


Figure 4.6-4: Layer profile of heated plate

The final construction of the heated plate can be seen in Figure 4.6-5.

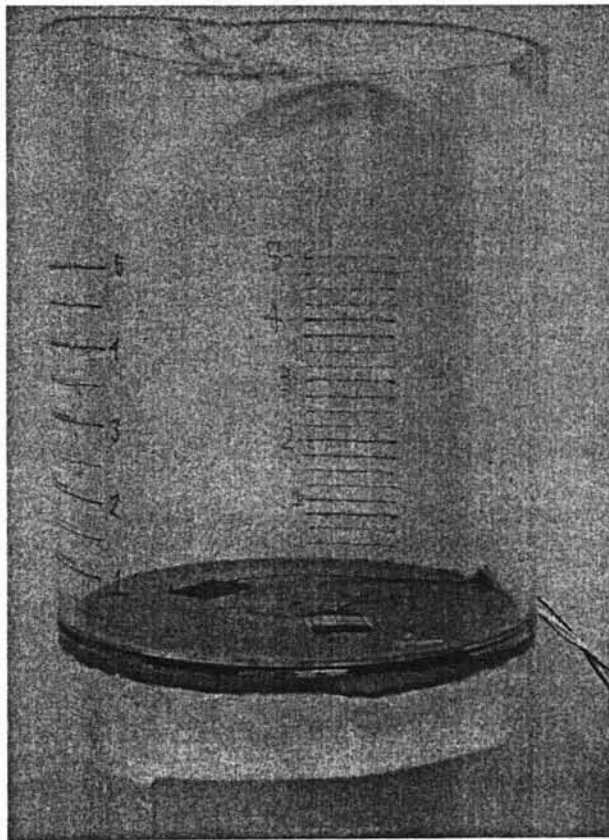


Figure 4.6-5: Final Heated Plate Setup

After the plate was completed, the top part of the tube was then surrounded with Styrofoam insulation, as seen in Figure 4.6-6. The insulation has an outer dimension of

66 cm X 66 cm (26" by 26") so that the Plexiglas tube is surrounded by at least 20.3cm (8") of insulation. The Styrofoam insulation has an insulation value of 0.14 mK/W (R-value of 2 per inch).

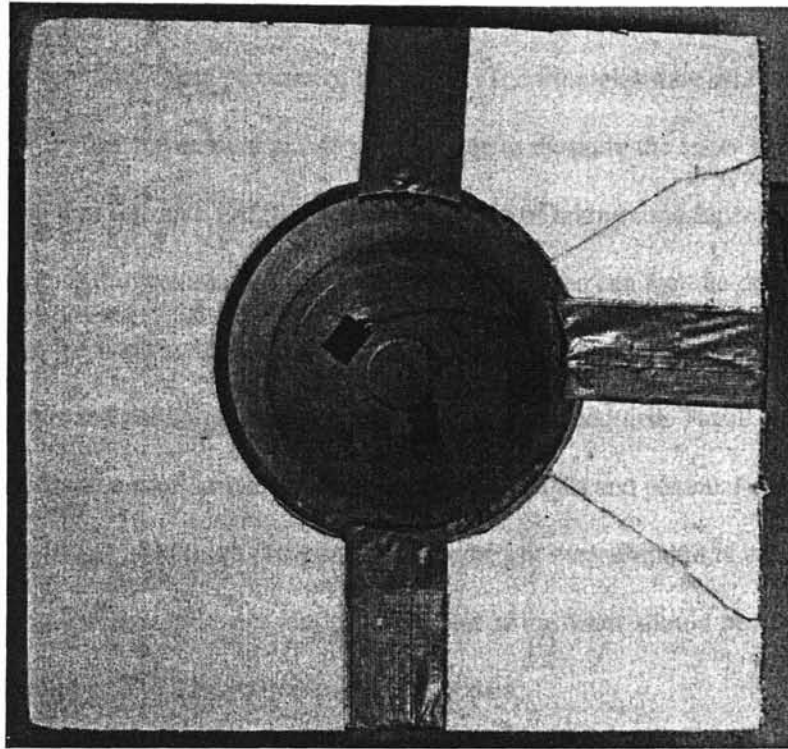


Figure 4.6-6: Insulation Around Plexiglas Tube

4.7 Weight Measurement

As the snow melts in the Plexiglas tube, part of the water is “wicked” upwards through the snow due to the capillary pressure, which then forms a “slush” layer. After the “slush” layer becomes saturated, the water will drain off the plate through the 4.76mm (3/16”) hole in the center of the heated plate. The water then collects in a 1L plastic graduated cylinder. The graduated cylinder rested on an Acculab VIR-1200 balance. This balance has a maximum capacity of 1200mg with an accuracy of $\pm 0.1g$. The balance has the capability to be connected to a computer using a RS-232 serial port.

A simple terminal program will interface with the balance, making data taking fairly convenient.

4.8 Height Measurement

To facilitate the measurement of the transient snow as it melted, a camera was positioned to take time-lapse pictures of the snow. The Plexiglas tube was marked on the wall every $\frac{1}{4}$ " so that the camera would have a scale to measure the snow against. The camera chosen was a Kodak DC290, which is capable of taking time-lapse pictures, and capable of storing the pictures on a photo card. The pictures can then be downloaded to a computer after the snowmelt experiment was completed. The pictures were then viewed on the computer and the height of the snow was manually recorded. These pictures also provided information such as maximum "slush" layer height and physical changes that the snow underwent. Although this procedure for height measurement is not as accurate as the water run-off measurement, the general trend of the snow should be comparable with numerical results and literature experimental data.

4.9 Instrument Calibration

See Appendix A for instrument calibration information.

CHAPTER 5

RESULTS AND DISCUSSION

5.1 Experimental Procedure

To perform the snow melting experiments, the environmental chamber must be cooled and kept cool for the experiments. To reduce the amount of heat added to the chamber, the doors of the chamber should remain closed. A description of the procedure that was adopted to minimize the heat input into the environmental chamber can be found in this subsection.

The experimental apparatus was set-up prior to the experiment inside the environmental chamber. The balance was set up and connected to the communication port, which exported the data to a computer via a terminal program. The melting apparatus was mounted on a platform raised above the chamber floor four inches to allow the balance to slide under the melting apparatus.

After the apparatus and balanced were positioned in the chamber, the height measurement devices were installed. The camera was mounted above the snow melting apparatus and set to take pictures every 10 minutes. The camera stored the pictures electronically in an internal memory device so that they could be downloaded to a PC after the snowmelt experiment was complete. The fluorescent light mounted in the chamber ceiling was manually switched on for the picture and then turned off, to minimize the heat gain to the chamber.

The FLUKE hydra data logger was then connected to the thermocouples, power supply, and humidity sensor and set to record the chamber and plate temperature, the plate voltage, and the chamber humidity.

After the chamber and the apparatus were setup, the chamber window was shut and the insulating plug was installed. The mechanical refrigeration system was then turned on. The chillers were set at a set point of -1.0°C . This resulted in a chamber air temperature of 2°C . A chiller set point of -1.0°C was chosen because this resulted in a coil temperature of 0.1°C . If the coil temperature dropped below 0.0°C , the coils would begin to frost over and eventually the whole coil would be frozen solid and no airflow would pass over the coil. This frost over condition basically eliminated the mechanical refrigeration and thus the chamber temperature would increase rapidly. The chamber air temperature was allowed to stabilize before the experiments were completed.

After the chamber air temperature reached the desired value, the door was quickly opened and snow (taken from the freezer) was added to the apparatus and the time-lapse pictures were started. The plate was not started until 40 minutes after the snow was added. This allowed the plate temperature to stabilize. At the start of the experiment, the power to the voltage supply was turned on and the weight measurement log was started. The balance sent the electronic weight every 0.2 seconds and a log of the data was started to collect the data.

After the experiment was completed, the data were then downloaded to the PC for processing and evaluation.

5.1.1 Snow-Making Procedure

The artificial snow was made days prior to the snowmelt experiment. The nozzles were adjusted to the preset values, and the chamber was closed and plugged. The liquid nitrogen was turned on, to cool the chamber down below freezing. After the chamber temperature was satisfactorily below freezing, the compressed air/water mixture was turned on, which caused snow to be formed. The water/air mixture was kept on for approximately 30 minutes, which in turn produced about 6 kg of usable snow. The water/air mixture was shut off first, and then the liquid nitrogen. The doors were opened and the snow was collected in a plastic bag, and then placed inside a chest type freezer, which kept the temperature at -18°C .

5.2 Preliminary Experiments

Preliminary experiments were made to evaluate the overall system operation. When modeling the chamber, there were several unknowns that needed to be evaluated before an accurate numerical model could be created.

There were several unknowns that needed to be estimated prior to the model validation. The first significant unknown parameter was maximum saturated layer height (MSLH) that could also be described as the saturated layer height or the capillary height. Another unknown parameter was the snow crystal size. Although the crystal size was not input into the numerical model, the crystal size was necessary to describe the type of snow used in the experiments. The second major unknown dealt with the possible uneven heating on the plate. The last unknown was a direct result of the water runoff experiments. It was found that after the experiment was completed a certain fraction of water remained on the plate. It was hypothesized that the size of the hole was not

sufficiently large which combined with the surface tension of the water resulted in skewed data.

5.2.1 Uneven melting/Hot spots on the plate

The preliminary snowmelt experiments had several signs of uneven melting. From visual inspection it appeared that the snow was “pulling” away from the Plexiglas wall. As a possible result, the half of the plate seemed to melt the snow faster than the other half. The cause of this uneven melting was attributed to heat gain from the wall due to the lack of insulation. It was for this reason that the Plexiglas tube was surrounded with insulation. As a result, the snow stopped “pulling” away from the sides, however the plate still seemed to melt at an uneven rate.

One half of the plate still seemed to melt faster than the other half. Several thermocouples were added to the surface of the plate in order to “measure” the hot spots. This was done to confirm the existence of a hot spot without visual inspection. From Figure 5.2-1, it can be seen that all the thermocouples do not exactly match. Specifically, the temperature, t_3 , measured near the edge of the plate, was 1°C higher than t_5 or t_6 during the first 2:00 hours. The three thermocouples were placed approximately $2\pi/3$ radians apart. The thermocouple labeled t_5 was placed approximately 2cm from the center of the plate, t_6 was placed 4.5 cm from the center and t_3 was placed 7 cm from the center of the plate.

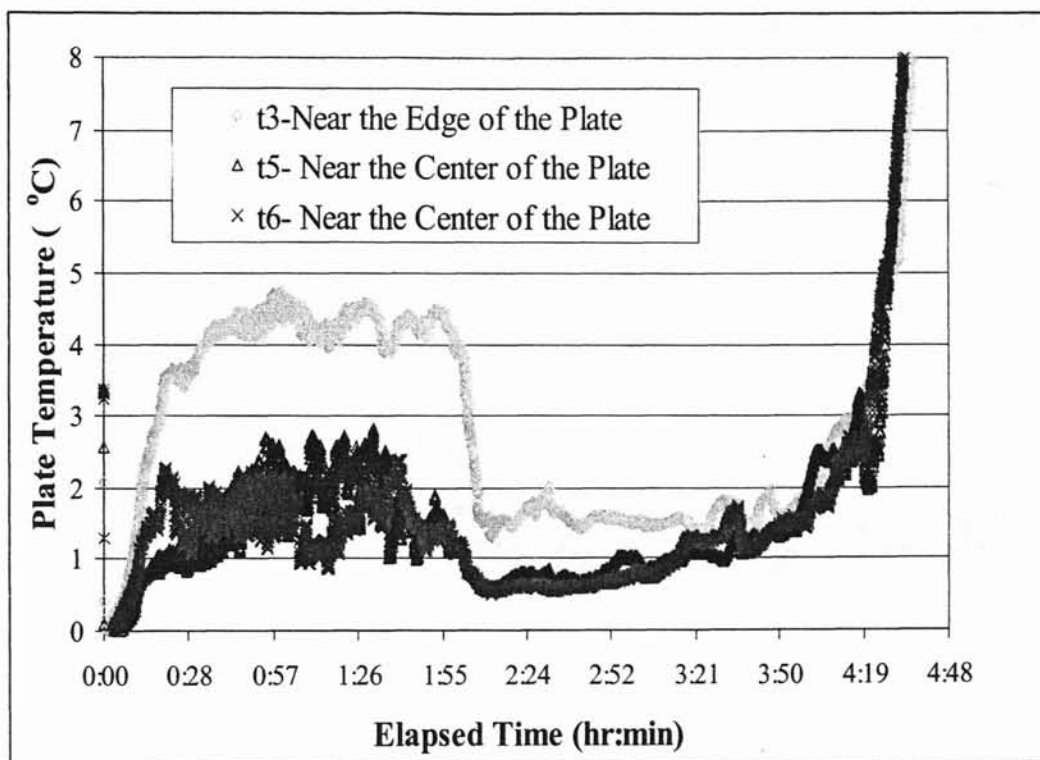


Figure 5.2-1: Hot Spot Temperature Profile

Figure 5.2-1 is of an actual snowmelt scenario. Each of the lines depicts a different spot on the plate. From visual inspection, it was confirmed that there was an unequal melting over the half of the plate with the higher temperature.

In order to eliminate these hot spots, it was decided to increase the thickness of the plate. Increasing the thickness of the plate allowed increased transverse conduction. In order to make use of the existing plate, a second plate was added on top of the current plate to make a sandwich. A thermally enhanced paste was placed between the two aluminum plates to reduce the contact resistance. The old thermocouples were removed, and only two thermocouples were replaced one on each side of the old hot spot. Thermocouple t2 was placed 4.5cm from the center and t9 was placed 3.2cm from the center. From Figure 5.2-2 it can be seen that the temperatures are much more uniform:

From a visual inspection the snow appeared to melt evenly and therefore it was decided to continue the experiments.

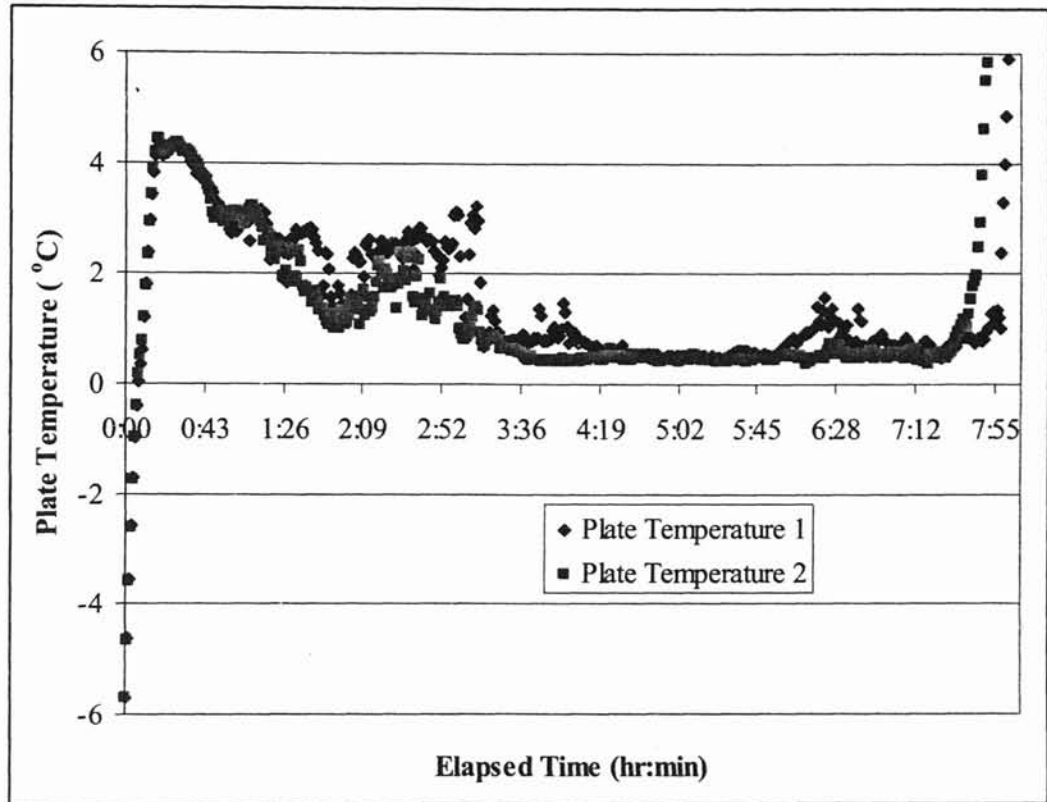


Figure 5.2-2: Plate Temperature Profile after Thickening

5.2.2 Water drainage experiment

After several preliminary experiments were completed it was noticed that the last 20 ml of water seemed to “cling” to the runoff plate. The surface tension seemed to keep the water from draining through the hole in the plate. Note: the plate was leveled to ensure a homogeneous “slush” layer thickness. This level plate seemed to keep the remaining 20 ml of water from running off the plate. It was this residual water that

top of the capillary fringe. This method described by Jordan, et al. (1999) was then utilized to measure the saturated height of the artificial snow utilized in the snowmelt experiments. A 3.8 cm diameter clear plastic tube was filled with snow, and then inserted into a red dyed ice-bath. From the experiments it was noticed that the maximum height was reached in approximately 10 seconds; however, the fringe height continued to rise for up to two minutes. This may have been due to the surface tension effect with the cylindrical wall. This procedure was completed for two snow densities, 250 kg/m^3 and 340 kg/m^3 . These densities were representative of the type of snow made and eventually used in the snowmelt experiments. The lower density snow had a higher capillary height of 3.1 cm and the higher density snow had a capillary height of 2.5 cm. A picture of the 250 kg/m^3 experiment, with red dye, can be seen in the following Figure 5.2-3.

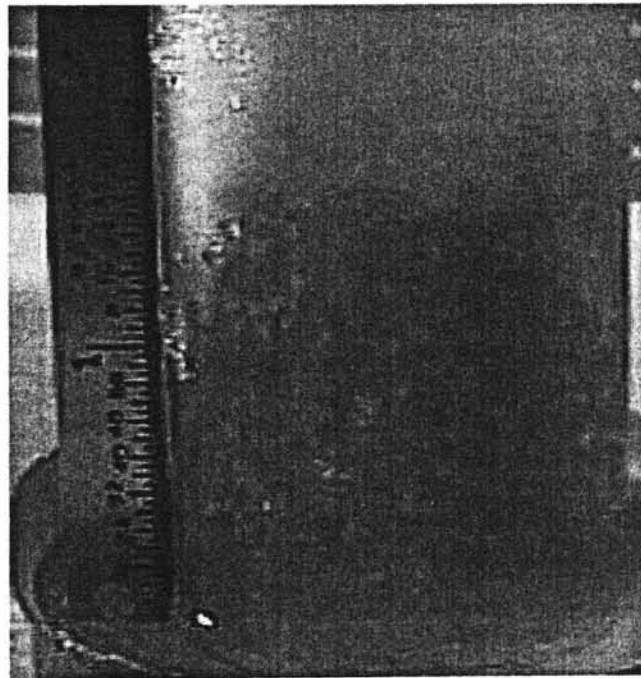


Figure 5.2-3: Capillary height measurement (density= 250 kg/m^3)

From these capillary height experiments it was found that the maximum saturated height was about 3.0 ± 0.7 cm. With the given uncertainty, this value correlates to the average value of 2.5 cm given by Colbeck (2000). A representative picture of a snowmelt experiment can be seen in Figure 5.2-4. This photograph was taken right when the overall snow height dropped such that the saturated layer could be seen. Notice the discoloration of the snow due to the appearance of water and then the corresponding height on the wall, 1" [2.5cm], of the Plexiglas container. This value correlates well with the value determined in Figure 5.2-3.

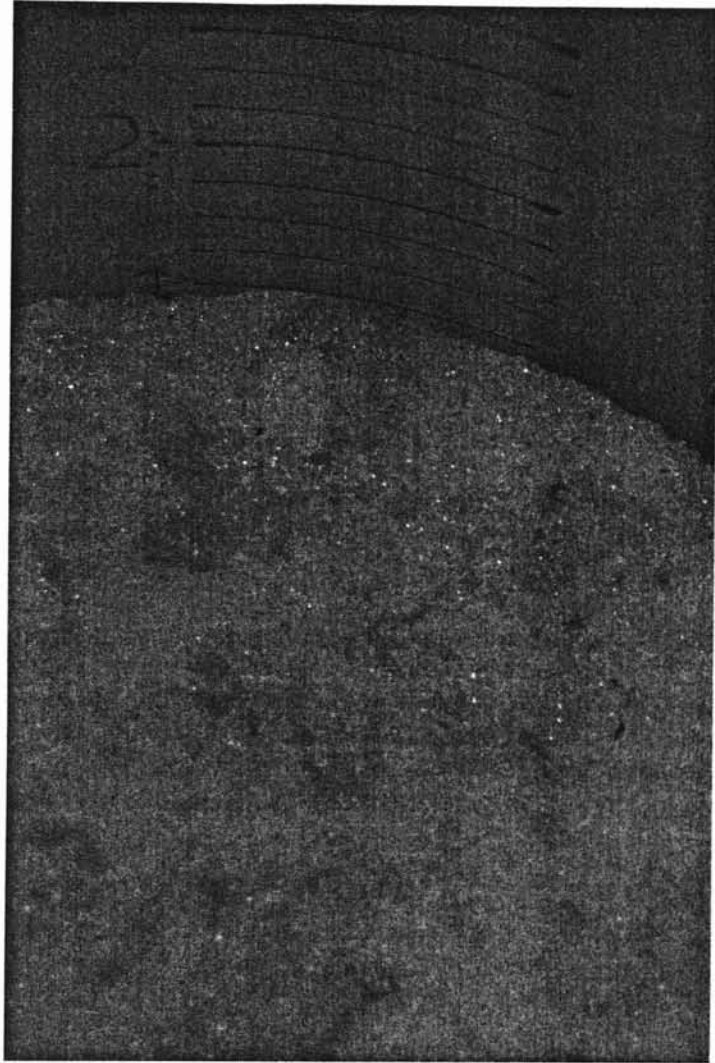


Figure 5.2-4: Experimental Saturated Height

5.2.4 Plate Temperature – Qualitative Analysis

In Appendix A, the thermocouple calibration is addressed. For part of the calibration, the thermocouples were placed in a large ice-water bath. The thermocouples recorded a temperature of $0^{\circ}\text{C} \pm 0.2^{\circ}\text{C}$. It was initially hypothesized that the plate temperature after the slush layer had formed would be near 0°C . After running a few snowmelt experiments, this hypothesis was proven partially correct. The plate

temperature reached 0°C at the beginning of the experiment before the heater was turned on. After the heater was turned on, the plate temperature usually hovered around 1°C after the slush layer was fully developed. A general temperature profile can be seen in Figure 5.2-5.

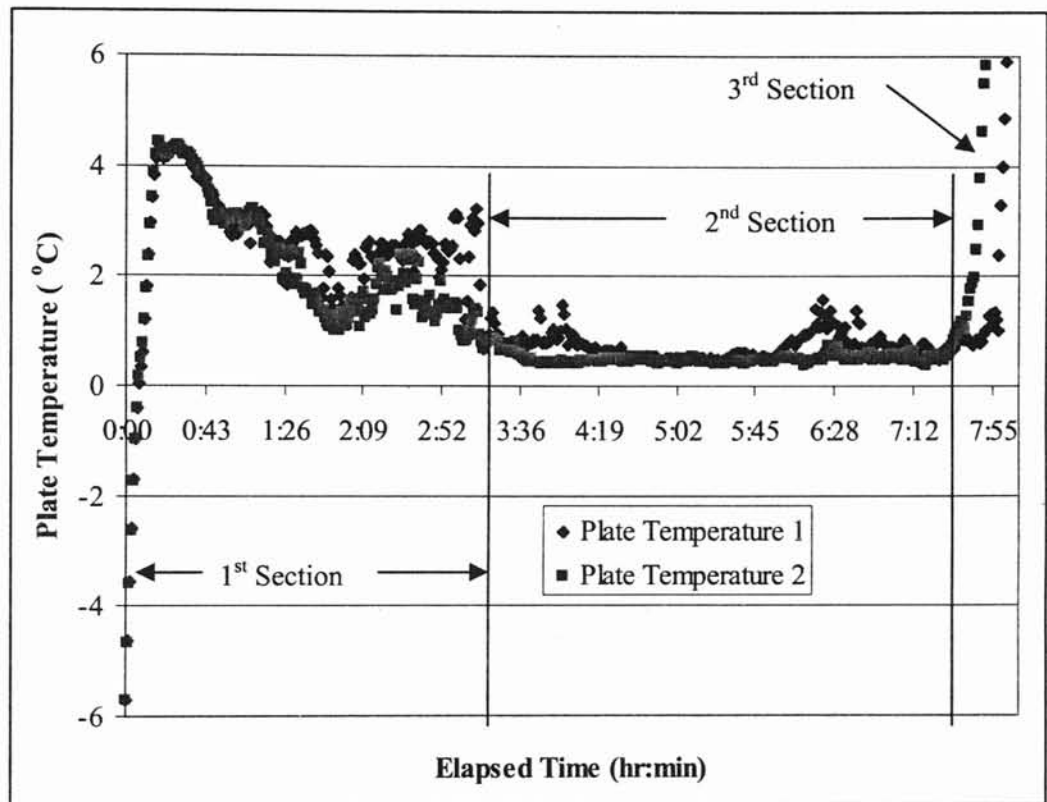


Figure 5.2-5: General Temperature Profile with Water Run-off

During the first three hours, the slush layer was being built up (i.e. water was diffusing up through the snow) and the temperature fluctuated around 3°C (depending on the plate heat flux) and will be discussed further below. After the slush layer was completely built up, the experiment was similar to the calibration experiment where the thermocouple measured an ice-water bath. However, the plate temperature was recorded near 0.5°C instead of 0°C which was expected. This difference is hypothesized to be due to the

presence of a small layer of water (or during the first few hours there could be a small layer of air) on the plate, which caused a conductive resistance between the snow and the thermocouple. The heater provided a constant flux of heat to the snow/slush. The thermocouples were pre-made from the factory installed in a special “patch” which had glue on one side to allow the patch to attach to the plate. This introduced two contact resistances: one between the plate and the thermocouple, and the second from the thermocouple through the patch to the slush layer.

Figure 5.2-5 has three main sections or three separate regimes of interest. The first section (time 0:00-3:00) is characterized by a fluctuating, temperature profile averaging between 2 and 4°C. During the second section (time 3:00-7:20) the temperature profile is flat near 0.5°C with very minor infrequent fluctuations. The third section (time 7:20-8:00) temperature profile is continuously increasing until the experiment has completed. Each of these sections will be discussed further in the following paragraphs.

The first section, characterized by the slightly higher average temperature and the fluctuating temperature profile, occurs while the saturated zone is growing. During the first hours of the experiment the melt water is wicked through the porous snow and held until a maximum height has been reached. During this time, there is no runoff water and air pockets could form between the plate and the snow/slush layer as the snow is melted away. Because air has a lower thermal conductivity than water/ice, the plate temperature begins to rise until the air pocket collapses and the temperature of the plate drops accordingly. This cycle is repeated until the maximum saturated layer height has been reached.

In Figure 5.2-5, the temperature profile of the plate is plotted with the water run-off. The temperature profile seems to level off around 3:00, at which time the large temperature fluctuations cease and a constant temperature is arrived at (0.5°C); this correlates to the onset of water run-off at 3:15. This time delay could be a function of the surface tension of the water on the plate.

The second section of the temperature profile is characterized by the relatively constant temperature profile at near freezing conditions. It is assumed that during this time the maximum saturated height has been reached. As discussed in subsection 5.2.3, the maximum saturated height was found to be near 3.2 cm. The maximum saturated height was also discussed by several researchers, including Jordan, et al. (1999), which also reported the maximum height was reached in seconds after introduced with water. With this in mind, it is assumed that any melted water present on the plate is immediately wicked up into the snow, until the snow cannot hold any more water i.e. the maximum saturated height has been reached. Therefore, the plate during this time is in contact with a water/snow layer or the so called “slush” layer. This layer is fairly homogenous and due to the excess water held in the snow good thermal contact is maintained between the plate, the thermocouples, and the slush. This profile will then continue until the point in time in which the plate temperature starts to rise. At the point in time the temperature profile starts to rise the third section starts.

The third section of the temperature profile starts when the temperature begins to increase above freezing. Physically, the snow layer has reduced to only the saturated layer or the so-called slush layer. During this time, the plate did not see a homogenous slush layer. In fact the plate may see in some areas a pocket of water in which snow has

already melted near the plate. It was expected that if the plate temperature increased above 1°C that the melting would be complete; however, from visual inspection all the snow had not melted. If slush or ice is not present near some parts of the plate, the heat flux from the heater will, in fact, heat the water, and the water temp will rise above 0°C. As this heated water comes in contact with ice, it will melt the ice.

5.2.5 Plate Temperature - Quantitative Analysis

In the above section the plate temperature does not match what would be expected. When the snow is melting the plate temperature was hypothesized to be near freezing (i.e. 0°C). The plate temperature in fact deviated several degrees from this value. As defined above during the first section of melting, the plate melts the snow and the resultant water is wicked up into the snow to form a slush layer, however the maximum saturated layer height has not been reached. When the snow melts, it is hypothesized that this causes a void in the snow, which is immediately filled with air. This air will cause a conductive resistance between the snow and the thermocouple.

If we assume an air thermal conductivity of 0.0263 W/mK, a 2°C temperature difference could be caused by a 0.2mm thick air gap (assuming a 236W/m² heat flux). In Appendix D, the complete temperature data is provided. In the appendix it can be seen that during the 789 W/m² case the plate temperature reached 13°C. Again if we assume the snow temperature is 0°C and the stated thermal conductivity of air, the resulting air gap thickness would be 0.4mm. This is a very reasonable value. The snow crystal size was determined to be 0.2mm, which means the necessary air gap to explain this temperature difference, would be two crystals thick.

In section 2 of the snowmelt experiment where the temperature stabilizes near 0.5°C , we again would hypothesize that the slush layer would be equivalent to a water bath, which would have a temperature of 0°C . To explain this phenomenon we could hypothesize that a small layer of water on the plate could cause a conductive resistance between the slush layer and the plate. If we assume the thermal conductivity of water (near freezing) to be 0.569 W/mK a 0.5°C difference could be caused by a 1.2mm thick layer of water (for the 236W/m^2 case). This thickness decreases with increasing heat flux to a minimum value of 0.4mm (for the 789W/m^2 case). This could feasibly explain this temperature differences.

5.2.6 Crystal Size

Crystal size is a primary characteristic for describing snow. To compare the artificial snow with other “real” snow, a value of the grain diameter needed to be found. To observe the crystal size a simple 10X hand lens could be used (Colbeck, 2000). For purposes of recording this process a ruler was used. After using a hand lens, a camera with a macro lens was used to photograph the results and several can be seen in Figure 5.2-6 and Figure 5.2-7.

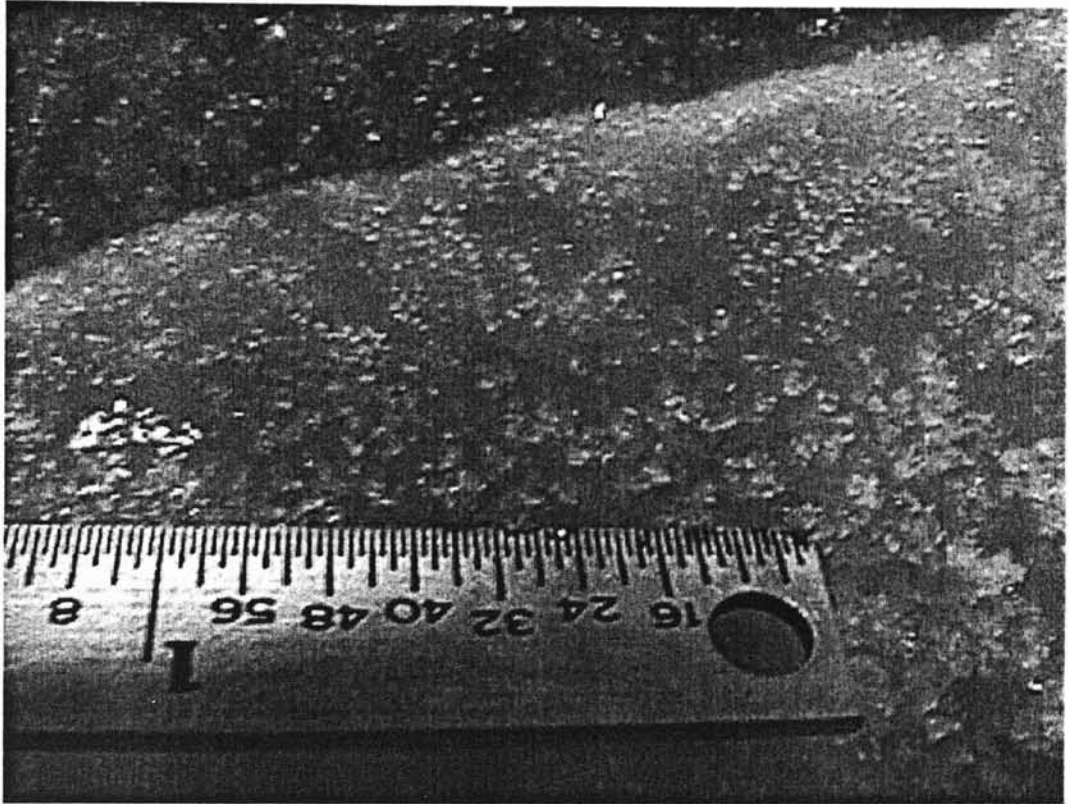


Figure 5.2-6: Crystal size (close up)

From these experiments it was determined that the grain size for the snow made in the environmental chamber had a diameter near 0.2 mm. This value was not used in the numerical model, but was used when describing the snow and finding appropriate correlations for the snow characteristics.

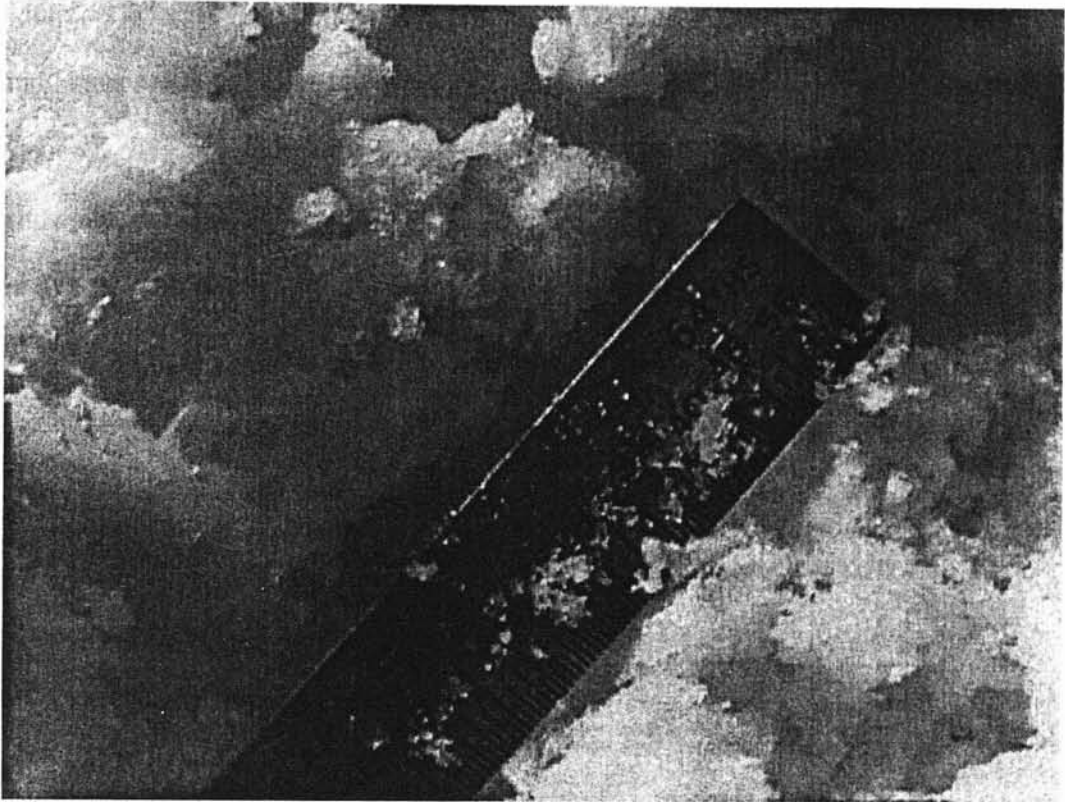


Figure 5.2-7: Crystal size

5.3 Snow Melting Results

As mentioned earlier in the experimental procedure, the height of the snow was measured from visual inspection. A digital camera was set up on a time-lapse setting to take pictures of the snow every 10 minutes. After the experiment was completed, the pictures were downloaded to a PC and a graphics package was used to view the pictures. The height of the snow was then recorded versus the picture number. From the picture number, the time of the picture could be determined. From this data, a plot could be formed to provide the height of snow as a function of time. After the experimental data were collected, the numerical model was run for conditions that matched the experiments. The inputs to the model are the following: initial snow mass, porosity, maximum

saturated layer height, heat flux, and plate area. From the preliminary experiments, the maximum saturated layer height was set as a constant for a particular type of snow. Generally, the density and thus the porosity of the snow varied between the different snowmelt experiments due to variations in the snow making process. The MSLH was set at 3.8 cm. The plate area was a constant for all experiments, and therefore the remaining model inputs were only the initial snow mass, porosity, and the heat flux. The mass of the snow was determined after the experiment was completed from the total mass of water drained from the experiment. The porosity of the snow was determined from the mass of snow and from the volume the snow initially occupied measured by the photographs. Porosity is defined by the equation 5-5:

$$\varepsilon = \frac{\text{Total Volume of Snow} - \text{Volume of Ice}}{\text{Total Volume of Snow}} \quad (5-5)$$

Where:

ε = Porosity, dimensionless

The heat flux was determined from the measured voltage from the FLUKE data logger and the known resistance of the heated plate. From the mass, porosity, and the plate area the model back-calculates the initial height of the snow. The time step of the model was set to 5 minutes to correlate with the experimental data. A comparison of the model predicted snow height (for a particular heat flux case) and the experimental data is shown in the Figure 5.3-1.

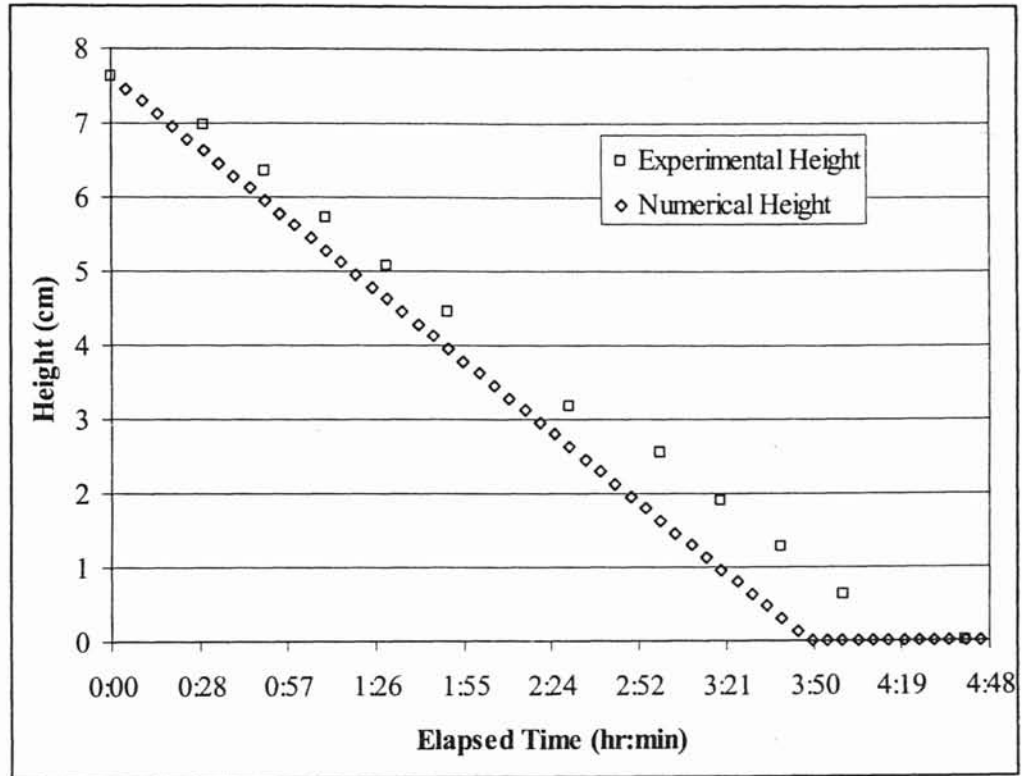


Figure 5.3-1: Model vs. Experimental Height Validation (789 W/m^2)

This figure presents several noteworthy items. The initial height predicted by the model was equal to the experimental known value. This must be true if the porosity and density calculations were done consistently in the numerical model and the experimental calculations. Experimentally, the initial snow height was measured and, with the plate area and snow mass, the density of the snow could be calculated. The density was then converted into porosity and input to the numerical model. The numerical model then takes the porosity and initial snow mass and calculates the snow density and the initial snow height.

The main deviation between the experimentally determined snow height and the numerical snow height occurs during the last hour of the melt experiment. During this

time (3:40-4:40), the snowmelt rate seems to decelerate. i.e., it deviates from the linear melt rate predicted from the numerical model. This phenomenon has been described as inhomogeneous melting. One explanation for this phenomenon is the densification of the snow crystals. As mentioned earlier in the literature review section, Colbeck (1973) reported that snow in contact with water would densify, the individual grains would rapidly grow, and the grains would lose mechanical strength. If the snow were to “reorganize” itself into a more efficient packing manner the effect of would be a reduction in the overall snow height, which can be seen, in Figure 5.3-1. This densification can be viewed as a type of inhomogeneity in the snow melting.

The individual experimental and model results for each heat flux case are summarized in Table 5.3-1. The actual data collected can be seen in Appendix D.

Heat Flux (W/m ²)	Model Melt Time (hr:min)	Experimental Melt Time (hr:min)	Difference (min)
236	11:45	13:19	94
315	8:40	10:50	130
473	6:55	8:15	80
631	4:33	5:20	47
789	3:50	4:40	50

Table 5.3-1: Melt Time Comparison

The melt time (end result) of the model prediction is fairly good. The overall trend matches fairly well. The uncertainties of the model and the experiments were then evaluated to determine if the differences could be accounted for. Firstly the model uncertainty will be addressed. There were several uncertainties in the model that were

initially investigated. The model uncertainties were split into two main categories: unmodeled phenomena and model inputs. The unmodeled phenomena were phenomena that were not accounted for in the model such as back losses, radial losses and radiant gain from the light source. Because these phenomena were not accounted for in the model, an independent (i.e. not using the model) estimate of the error was made.

The model inputs were parameters in the model such as thermal conductivity, mass of snow, porosity of snow, and convection/radiation coefficients, each of which had some inherent uncertainty. A sensitivity analysis was completed for the model inputs and the resulting uncertainty in the results were then calculated based on the sensitivity analysis. A detailed discussion of the uncertainties is given in Appendix B.

After evaluating the individual contributions of several of the uncertainties and the overall uncertainty (found by adding the individual uncertainties in quadrature) it was found that the uncertainty in the initial snow temperature had the largest effect on the model result. The snow was initially stored in the freezer at -17°C and then transferred to the apparatus where it was left undisturbed for up to 70 minutes. During this time the snow temperature increased but the average snow temperature was not measured. This caused a large uncertainty for example, in the 236 W/m^2 (75 Btu/hrft^2) case, the model uncertainty was $+70/-40$ minutes and in the 789 W/m^2 (250 Btu/hrft^2) case, the model uncertainty was $+22/-8$ minutes.

Just as the model had uncertainties, the experiment also had uncertainties. Two of the significant experimental uncertainties are the sampling time and the inhomogeneous melting of the snow. Near the end of the snow melt experiment it was found that the snow was melted in an inhomogeneous manner. Several different methods to visualize

the inhomogeneity can be found in Appendix B. To estimate this inhomogeneity in the snowmelt experiment two possible methods could be employed. The first would be to record the snowmelt time as the time in which the first sign that the plate had been cleared of snow. This could be done either from photographic evidence or from the plate temperature chart. If the plate temperature begins to increase when could assume the plate was free of snow. The second method would be to utilize the snow height versus elapsed time figure. For the most part the slope of the snow height versus time is linear except near the completion of the experiment. If we were to assume the melting was linear throughout the whole experiment we could approximate the melt time. Table 5.3-2 shows the corrected experimental melt time and the resulting difference with the model predicted melt time.

Heat Flux (W/m ²)	Model Melt Time (hr:min)	Corrected Experimental Melt Time (hr:min)	Difference (min)
236	11:45	12:10	25
315	8:40	9:35	55
473	6:55	7:25	30
631	4:35	5:05	30
789	3:50	3:55	5

Table 5.3-2: Corrected Melt Time Comparison

The model and experimental uncertainties can be summarized in the following Figure 5.3-2, which depicts the uncertainties in the form of error bars.

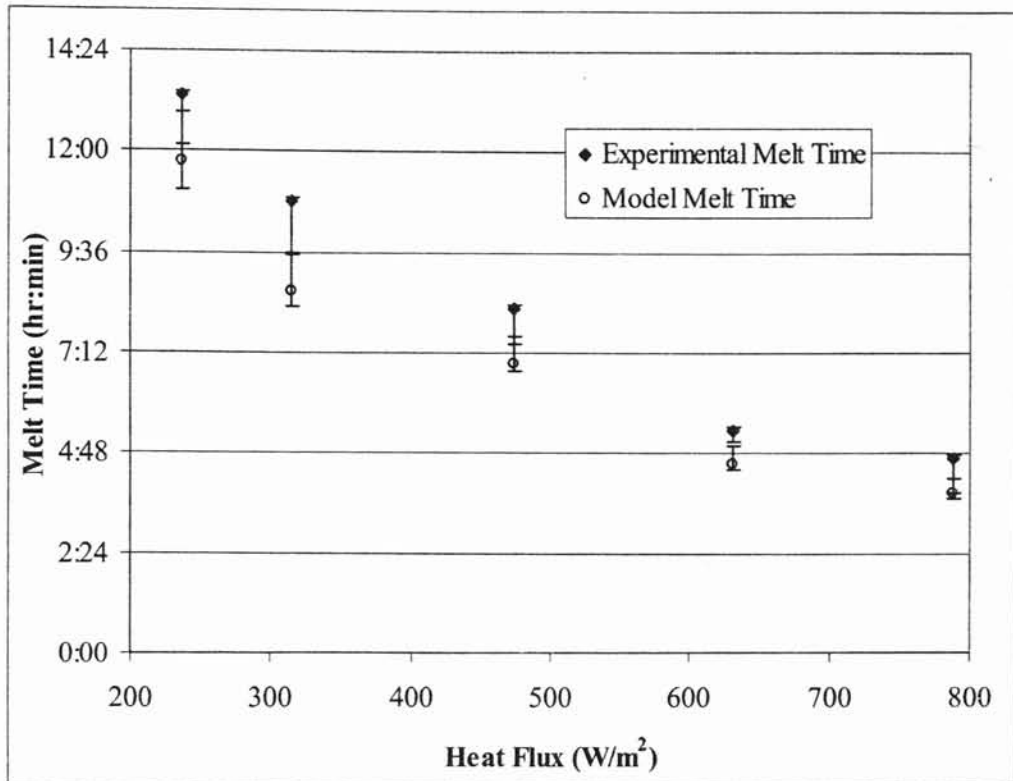


Figure 5.3-2: Model Melt Time Comparison

The individual experimental and model results for each heat flux case can be seen in Appendix D. The uncertainty in the model melt time was dependent upon the heat flux (the smaller the flux and the longer the melting time, the larger the uncertainty). Note: the overall mass of snow in the 5 experiments was not the same. Because the error bars overlap it may be said that the model and the experiment agree within the estimated uncertainty. The error bars are quite large which, as discussed in Appendix B, are due for the most part to the following two causes:

- The initial snow temperature could have been as low as -17°C . Although some attempts at measuring the snow temperature were made no feasible method was found for obtaining a good average value

- The inhomogenous melting of the snow possibly due to densification or water surface tension effects.
- Both of these errors tend to cause the model to under predict the melt time relative to the experiment.

In Figure 5.3-3 the model melt time is plotted against the experimental melt time.

The data points labeled “actual” represent the model melt time for each experiment, plotted against the experimental melt time. The line labeled “theoretical” would represent an exact match between the model and the experiment. The dashed line, labeled “-15%” represents the model under predicting, by 15%, the experimental melt time.

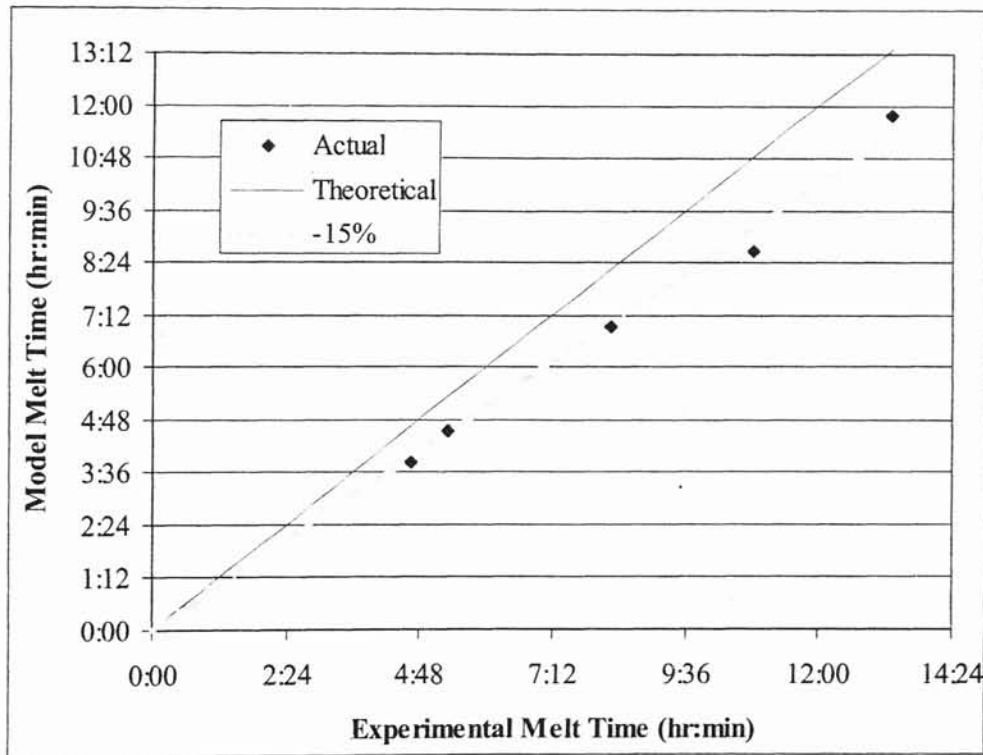


Figure 5.3-3: Model vs. Experimental Melt Time

From this figure it appears that the model systematically under predicts by about 15%. One systematic error in the experiments was the inhomogeneous melting when the slab was free of dry snow (i.e. the only remaining layer was slush). Using the information above and in Appendix B we have estimated the inhomogeneous effect and if we remove it from the data and we arrive at the following Figure 5.3-4.

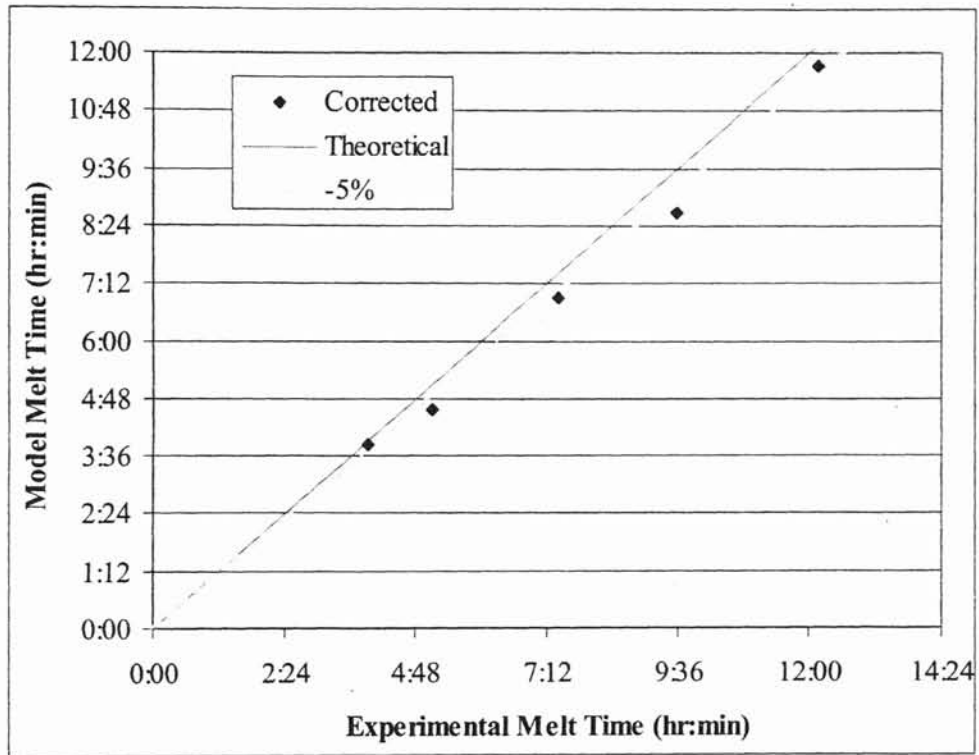


Figure 5.3-4: Model vs. Experimental Melt Time Modified for Inhomogeneity
 Removing the inhomogeneous effect reduced the systematic error by 10%. The remaining uncertainty is presumably due primarily to the uncertainty in the initial snow temperature.

5.4 Thermodynamic Melt Time

The melt times can also be compared to a thermodynamically determined melt time or the time required to melt the snow if it is initially ice at 0°C and is melted only by

heat input from the plate (In actuality, convective and radiative heat gains also contribute to the melting). The thermodynamic melt time will be defined as:

$$t = \frac{H_L m}{q'' A} \quad (5-7)$$

Where:

t = Melt time (s)

H_L = Latent heat of fusion (333.3 J/g)

m = Mass of ice (g)

q'' = Heat flux (W/m^2)

A = Plate area (m^2)

The thermodynamic melt time is not dependent on any porous media effects nor environmental effects, and we will assume the heat flux is that supplied by the plate and the environment plays no part in the melting. Figure 5.4-1 shows the model melt time, the experimental melt time and the thermodynamic melt time.

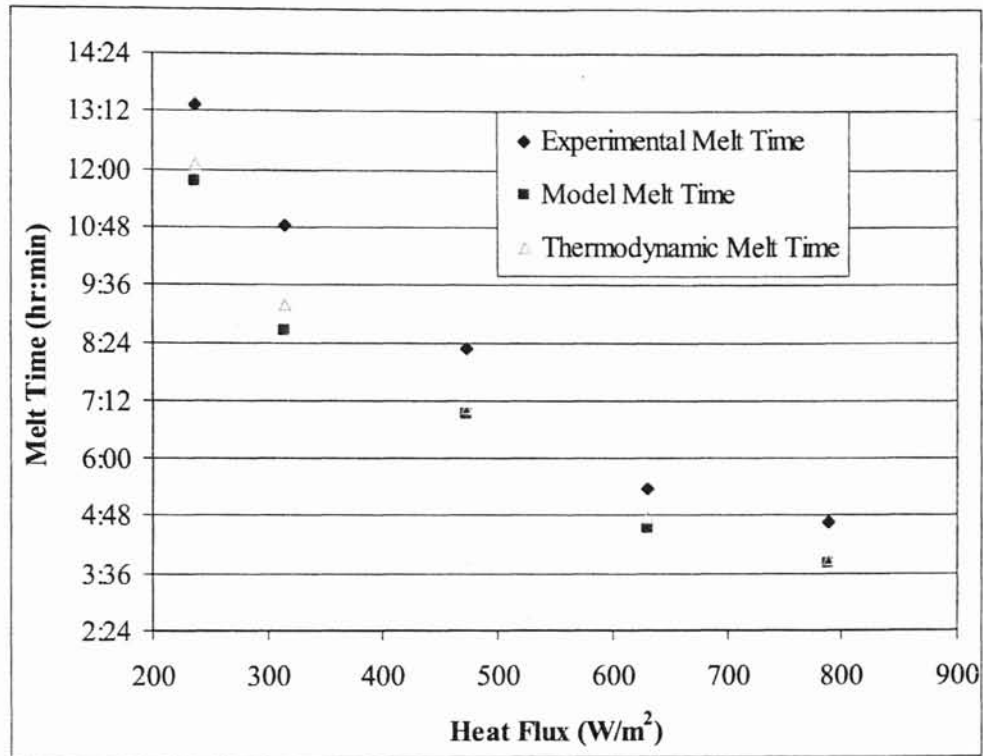


Figure 5.4-1: Thermodynamic, Model, and Experimental Melt Time vs. Heat Flux

In every case the experimental melt time was greater than the thermodynamic melt time. This would tend to signify that something occurred that extended the melting time. It is hypothesized that the two main factors that contributed to this effect were the initial snow temperature and the inhomogeneous melting. If the initial snow temperature was less than freezing (i.e. sub-cooled) the experimental time would be greater than the thermodynamic melt time. Similarly if there were inhomogeneous melting effect then the experimental melt time would be greater.

In every case the model melt time was shorter than the thermodynamic melt time. This is expected because the model included additional heat gains (i.e. convection and radiation) and the plate power drift. It is interesting to note that the difference between the thermodynamic and the model melt time was at most 31 minutes (316 W/m²) and in

the best case the difference was 3 minutes (789 W/m^2) with an average difference of 14 minutes.

5.5 Melt water Runoff

The melt water runoff as mentioned earlier was measured using an electronic balance, which reported the mass via a communications link to a PC. Each experiment was completed with different snow. In each case, the porosity/density varied and, as stated earlier, the MSLH varied. The numerical model was run with conditions matching the experiment. In the snow height case the saturated layer height had no effect on the results of the model conversely the porosity of the snow had no effect on the model predicted melt water runoff data. The maximum saturated layer height significantly affected the results of the water runoff model. From the experimental results, a time delay for the water to runoff was noticed. It was determined that during this early period the melt water was wicked up into the pores of the snow to form a slush layer and did not runoff the plate. Therefore the maximum height of this saturated layer affects the time delay in the melt water runoff. A sample result from the model can be seen in Figure 5.5-1.

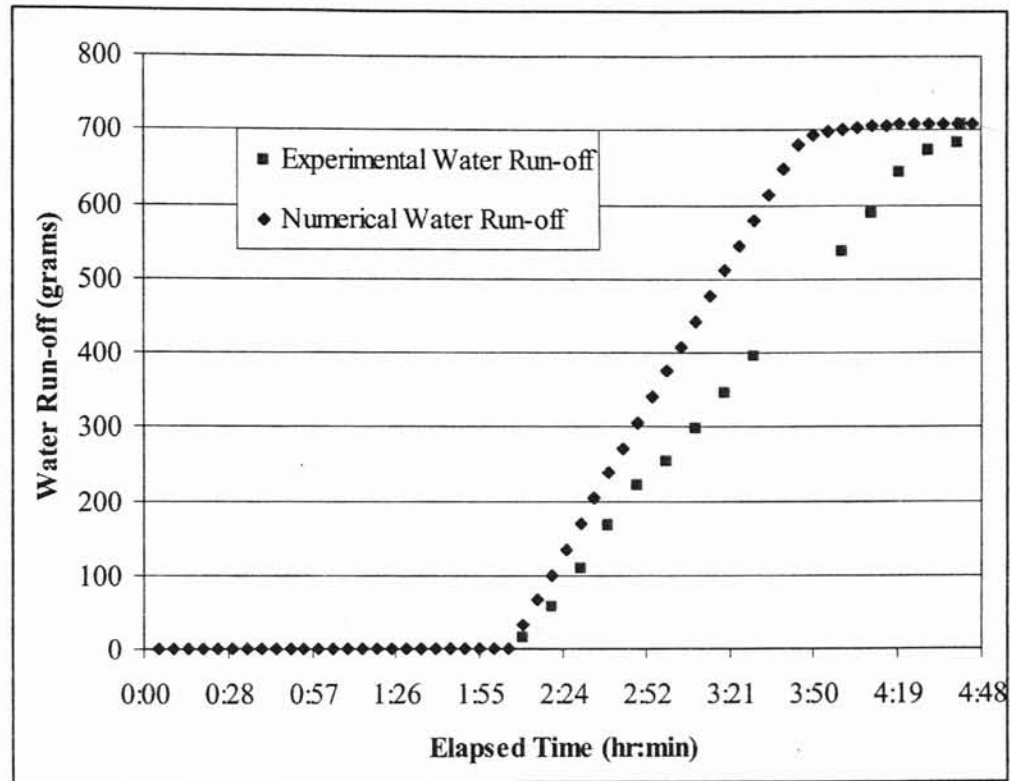


Figure 5.5-1: Experimental vs. Model Melt Water Run-off (789 W/m^2)

The figure presents the results of one experimental trial in which the heat flux was set to 789 W/m^2 (250 Btu/hrft^2). From the experimental data, the time delay was 2 hours and 10 minutes whereas the numerical model predicted a time delay of 2:05 with a maximum saturated layer height (MSLH) of 3.8 cm.

The last 50 minutes of the numerical model, from 3:55 until 4:50, are a result of an inaccurate liquid water drainage model. After the snow has completely melted, the remaining water drains from the plate (slab) according to crowning effects, surface roughness, and orientation. However, since no liquid water drainage model could be found in the literature, a simple model was added to the model. The simplified model used drained water from the slab at a constant rate set arbitrarily. The amount of water

remaining on the plate during the last 40 minutes is approximately 10 grams. The snowmelt time was defined as the time it took the plate to melt all the snow and therefore, this remaining time is neglected. From the numerical model the melt time was found to be 3:50. This value, when compared to the numerical height prediction from the numerical water runoff results, matches within 5 minutes.

5.6 Qualitative discussion of snow melt

As observed from the snowmelt experiments, the snow melted in predictable fashion and each of the common features of the snow melting (both visually and numerically) were grouped together, which resulted in 4 distinct steps or stages. This section will refer back to Figure 5.5-1 and the 789 W/m^2 snowmelt experiment.

In the first stage (time 0:00-2:05), as the water melts due to the imposed heat flux, the water is “wicked” up through the snow due to capillary pressure. As discussed earlier, in porous media, the curvature of the particles causes a capillary pressure, which in turn will draw liquid through the porous media until the pressure due to weight of the fluid offsets that of the capillary pressure. The first stage therefore is characterized by the buildup of the “slush” layer and the end of the first stage occurs when the retained water reaches the maximum saturated height. From an experimental standpoint, the first stage can be characterized by the reduction of snow height (measured with the camera) and the absence of water run-off.

The second stage of snowmelt is characterized by the onset of run-off water (time 2:05-2:50). Physically, this is an indication that the maximum saturated height has been obtained. During the second stage, the snow height continues to decrease and water runs off the plate. After the water has saturated the snow (the maximum saturated height has

been reached), there is no place for excess water to be stored and therefore must run-off the plate. The water runoff is determined numerically by the amount of snow melted, which is a function of heat flux. Therefore, we can conclude that the rate of water runoff is a strong function of the heat flux. The second stage ends when the saturated zone can be seen at the top of the snow via photographs.

The third stage (time 2:50-3:50) of the snowmelt is characterized by the water-saturated zone reaching the top of the snow, i.e. no dry snow remains, only slush. During this stage, the height of the snow is equal to or less than the maximum saturated height that was set as a parameter in the numerical model. Visually, the snow appears to be darker in color; however this may be a function of the color of the plate below the snow. The original snow crystals are no longer present, and have joined to form larger ice crystals. The heat flux still melts the ice crystals and the resulting water drains from the plate. The third stage ends when, for the most part, all the snow has melted. Near the end of the snowmelt experiment there comes a time in which the saturated layer loses the physical appearance of a layer. The ice/slush mixture can be thought of as containing "clumps of slush". Due to the surface tension of water, the plate has a constant layer of water over the entire plate, and the slush/ice remaining on the plate appear as icebergs.

The last stage of the snowmelt occurs after all the snow/ice has been melted and the only remaining substance is water (time 3:50- end). The run-off of the remaining liquid is a function of the run-off properties of the plate (crowning and orientation) and surface tension of the water. The duration of the last stage is quite small compared to the rest of the snowmelt process, and the last stage is not included in the overall snow melt time.

5.7 Practical Guidance

From researching snow melting and performing several snow melting experiments, the author would like to provide the reader with some practical guidance to aid in further snow melting research, and/or using the snow-melting model. First, some guidance for other mechanical engineering researchers who have very little experience in snow melting:

- Samuel Colbeck has performed countless research experiments on snow and snow related topics. The articles written by S. Colbeck have been very helpful and have been used extensively in this thesis.
- Other researchers at the Cold Regions Research and Engineering Laboratory, CRREL, (i.e. Rachel Jordan and Yin-Chao Yen) also provide quality articles that have been used extensively in this thesis.
- Snow metamorphism is talked about in many snow articles. In dry snow, the time scale for snow metamorphism is on the order of weeks and months. In wet snow, metamorphism occurs quite rapidly and the time scale is on the order of hours and days.
- Colbeck, et al. (1990) provides an internationally accepted classification scheme for snow. When dealing with new articles (1990 to present) the type of snow should be reported and therefore correlations and data should be presented with a range of snow classifications.
- Snow can be made in the manner described in the Experimental Apparatus chapter. After the experiments were completed another method was found which might be more economical. This method entail “shaving” ice from an ice block with a deli-style meat saw/shaver (Colbeck, 2000). A HOBART meat saw was

recommended. This method would allow the research to “dial” in the snow diameter desired.

The second section consists of practical guidance for users of the numerical model and its relations to snowmelt experiments and snowmelt scenarios.

- Unless otherwise known, an average value of the MSLH should be 3.5 cm. This value will not affect the height melt time but will not be critical. For the water runoff portion the MSLH is important and should be obtained experimentally or derived with an appropriate model.
- The porosity of the snow should be measured from actual snow. If the model is used for forecasting then a typical snow porosity for dry new-fallen snow might be as high as 0.9 and for wet new-fallen snow might be as low as 0.56.
- If a better liquid water drainage function for a slab is known, this function should be added to the numerical model. Otherwise, the water runoff melt time will be unnecessarily long in duration.
- Use the most accurate weather data that can be obtained.

Although not covered in this thesis there are several possible limitations of the numerical model:

- The model must be run with accurate weather data and actual snow properties, which will be quite hard for someone to obtain before the snow occurs. These limitations will affect accuracy of the numerical model in real life cases.
- The numerical model accepted the recommended convection, radiation, and mass transfer coefficients from Ramsey, et al. (1999), however these coefficients were not validated in this work, as sub models appropriate to the environmental

chamber were used. And was shown that several coefficients had significant limitations.

- The model also does not account for compaction of snow due to actual road conditions, which will affect the snow type and runoff properties.
- The model also does not account for the additions of conventional ice prevention techniques. The addition of salt to a heated bridge would significantly affect the snow melting rate.

5.8 Additional Modeling

An additional model was developed to predict the water runoff rate, however did not result in any positive conclusions and therefore is not included in the main document. However it is described in Appendix C.

CHAPTER 6

CONCLUSIONS AND RECOMMENDATIONS

6.1 Conclusions

As a result of the work described in this thesis, the following conclusions can be drawn:

- Unforeseen uncertainties due to inhomogeneities in the snow melt experiment limit the usefulness of the experimental results.
- Both the inhomogeneous melting effect and the initial snow temperature tend to cause the model to under predict the melt time relative to the experiment.
- The environmental chamber and current snow making apparatus can reproducibly make snow with a density near 250 kg/m^3 and grain diameters near 0.2 mm.
- With the current set-up and experimental procedure, the chamber air temperature can be successfully be maintained near 2°C . This significantly reduces unaccounted heat gains (convection, radiation, and heat storage).
- The numerical model currently can predict, with moderate accuracy, the snowmelt time for a wide range of heat fluxes.
- The numerical model can roughly predict the water runoff.
- Dry snow metamorphism can be ignored for the time scales less than 10 hours.
- Although not proved in this thesis, it may be inferred that wet metamorphism had an measurable affect on the snow melt process, which was associated with the “densification” of ice near the completion of the experiment.

- For purposes of melting thin layers (less than 20 cm), from a heated horizontal surface, capillary pressure should be included in the calculation.
- For snow used in the experiments the maximum saturated layer height was approximately 3.6 cm.

6.2 Recommendations

The following recommendations are provided as a result of the experiments and research completed to date, which could be posed as additional research topics that should be investigated to more accurately predict the snowmelt time:

- The mechanical refrigeration device needs to be rearranged so that the coil temperatures can be dropped below freezing without frosting over, so that the chamber air temperature can be maintained very near 0°C.
- If the camera was outfitted with a lens filter the internal flash of the camera might be used so that the fluorescent light could be removed further reducing the experimental uncertainty.
- The melting apparatus should also be tilted or crowned to reduce the effects of surface tension on the plate. This will aid in determining the melt time from the water data.
- To ensure the snow is completely frozen, snow after it is made should be placed in a freezer. If the freezer temperature could be adjusted so that different initial snow temperatures could be obtained further model uncertainties could be removed.
- Develop a method that could reliably measure the initial average snow temperature.

After the numerical model is validated, several additional topics could be discussed to further validate the model:

- For a given snow crystal shape, a correlation possibly could be drawn up to relate density of snow as a function of crystal diameter.
- A water runoff model that takes into account surface roughness, crowning, and orientation of the slab.
- The numerical model should next be compared to results from a slab, and then finally from an actual slab/bridge deck under a range of sky conditions.
- The experiments should be run using “real” new fallen snow.

BIBLIOGRAPHY

- Adams, E.E. and A. Sato (1993). "Model for Effective Thermal Conductivity of a Dry Snow Cover Composed of Uniform Ice Spheres." Annals of Glaciology 18: 300-304.
- Anderson, E. (1976). "A Point Energy and Mass Balance of a Snow Cover." National Oceanic and Atmospheric Administration (NOAA) Technical Report 19: 1-150.
- Aoki, K., M. Hattori, S. Chiba, and Y. Hayashi (1981). "A Study of the Melting Process in Ice-Air Composite Materials." ASME paper 81-WA/HT: 1-7.
- Aoki, K. M. Hattori, and S. Chiba (1986). "A Study of the Melting Process in Ice-Air Composite Materials – In the case where a temperature gradient exists in porous materials-." Bulletin of the Japan Society of Mechanical Engineers 29(5): 2138-2144.
- Aoki, K., M. Hattori, and T. Ujiie (1987). "Snow Melting by Heating From the Bottom." 1987 International Symposium on Cold Regions Heat Transfer, University of Alberta, Edmonton, Alberta, Canada, American Society of Mechanical Engineers (ASME): 189-194.
- Arons, E.M. and S.C. Colbeck (1995). "Geometry of Heat and Mass Transfer in Dry Snow: A Review of Theory and Experiments." Reviews of Geophysics 33(4): 463-493.
- ASHRAE (1997). ASHRAE Handbook – Fundamentals. Atlanta: American Society of Heating, Refrigerating and Air-Conditioning Engineers, Inc.
- Bear, J. (1972). Dynamics of Fluids on Porous Media. New York: Dover Publications.
- Bienert, W. and authors (1974). "Snow and Ice Removal from Pavements using Stored Earth Energy." Federal Highway Administration Publication. FHWA-RD 75-6.
- Brubaker, K., A. Rango, and W. Kustus (1996). "Incorporation Radiation Inputs into the Snowmelt Runoff Model." Hydrological Processes 10: 1329-1343.
- Carman, P.C. (1941). "Capillary Rise and Capillary Movement of Moisture in Fine Sands." Soil Science 52: 1-14.
- Chiasson, A. and J.D. Spitler. 2000. "A Modeling Approach To Design Of A Ground-Source Heat Pump Bridge Deck Heating System". Proceedings of the 5th International Symposium on Snow Removal and Ice Control Technology. Roanoke, VA. September 5-8, 2000. This paper can be seen in its entirety at www.hvac.okstate.edu/pdfs/Bridge_deck_design_paper.pdf.

- Colbeck, S. (1972). "A Theory of Water Percolation in Snow." Journal of Glaciology 11(63):369-385.
- Colbeck, S. (1973). "Theory of Metamorphism of Wet Snow." U.S. Army Cold Regions Research & Engineering Laboratory Report. 73(119).
- Colbeck, S. (1974a). "Water Flow Through Snow Overlying an Impermeable Boundary." Water Resources Research 10(1):119-123.
- Colbeck, S. (1974b). "The Capillary Effects on Water Percolation in Homogenous Snow." Journal of Glaciology 13(67):85-97.
- Colbeck, S. (1975). "A Theory for Water Flow Through a Layered Snowpack." Water Resources Research 11(2):261-266.
- Colbeck, S. (1976). "An Analysis of Water Flow in Dry Snow." Water Resources Research 12(3):523-527.
- Colbeck, S. (1980). "Thermodynamics of Snow Metamorphism Due to Variations in Curvature." Journal of Glaciology 26(94): 291-301.
- Colbeck, S., and E. Anderson (1982). "The Permeability of a Melting Snow Cover." Water Resources Research 18(4): 904-908.
- Colbeck, S. (1982a). "An Overview of Seasonal Snow Metamorphism." Reviews of Geophysics and Space Physics, 20(1): 45-61.
- Colbeck, S. (1982b). "Growth of Faceted Crystals in a Snow Cover." U.S. Army Cold Regions Research & Engineering Laboratory Report. 82(29).
- Colbeck, S. (1983). "Theory of Metamorphism of Dry Snow." Journal of Geophysical Research 88(C9): 5475-5482.
- Colbeck, S. (1986a). "Statistics of Coarsening in Water-Saturated Snow." Acta Metallurgy 34(3): 347-352.
- Colbeck, S. (1986b). "Classification of Seasonal Snow Cover Crystals." Water Resources Research 22(9):59-70.
- Colbeck, S. (1987a). "Theory of Particle Coarsening with a Log-Normal Distribution." Acta Metallurgy 35(7): 1583-1588.
- Christon, M., P. Burns, and R. Sommerfeld (1987b). "2-D Microscopic Simulation of Temperature Gradient Metamorphism in Dry Snow." ASME, Heat Transfer Division (HTD), Publication 76:1-8.

Colbeck, S.; Akitaya, E.; Armstrong, R.; Gubler, H.; Lafeuille, J.; Lied, K.; McClung, D.; Morris, E. (1990). International Classification for Seasonal Snow on the Ground. Int. Comm. Snow and Ice (IAHS), World Data Center A for Glaciology, U. of Colorado, Boulder, CO.

Colbeck, S. (1993). "The Vapor Diffusion Coefficient for Snow." Water Resources Research 29(1): 109-115.

Colbeck, S. (2000). Personal Communication

Colbeck, S. (n.d.). "The Compaction of Wet Snow on Highways." U.S. Army Cold Regions Research & Engineering Laboratory Report.

Coleou, C., K. Xu, B. Lesaffre, and J. Brzoska (1999). "Capillary Rise in Snow." Hydrological Processes 13: 1721-1732.

Gubler, H. (1985). "Model for Dry Snow Metamorphism by Interparticle Vapor Flux." Journal of Geophysical Research 90(D5):8081-8092.

Incropera, F. P. and D.P. DeWitt (1996). Introduction to Heat Transfer. New York: John Wiley and Sons.

Jordan, R. and E. Andreas (1999a). "Heat Budget of Snow-Covered Sea Ice at North Pole 4." Journal of Geophysical Research 104(C4):7785-7806.

Jordan, R.E., J.P. Hardy, F.E. Perron, and D.J. Fisk (1999b). "Air Permeability and Capillary Rise as Measures of the Pore Structure in Snow: An Experimental and Theoretical Study." Hydrological Processes 17: 1733-1753.

Kays, W.M. and M.E. Crawford (1993). Convection Heat Transfer. New York: McGraw Hill.

Kondo, J. and T. Yamazaki (1990). "A Prediction Model for Snowmelt, Snow Surface Temperature and Freezing Depth Using a Heat Balance Method." Journal of Applied Meteorology 29:375-384.

Leverett, M.C. (1941). "Capillary Behavior in Porous Solids." American Institute of Mining and Metallurgical Engineers Transactions 142: 153-169.

Longwill, M., B. Schultz, and D. Thompson (1999) "Lab-Scale Snowmaking Machine." Senior Design Report, Oklahoma State University, Stillwater, OK. Can also be found electronically at http://www.hvac.okstate.edu/pdfs/snow_making.pdf.

Kustas, W., A. Rango, and R. Uijlenhoet (1994). "A Simple Energy Budget Algorithm for the Snowmelt Runoff Model." Water Resources Research 30(5):1515-1527.

- Mantis, H. (1951). "Review of the Properties of Snow & Ice." SIPRE Report 4, Snow, Ice and Permafrost Research Establishment: 64-70.
- Marbouty, D. (1980). "An Experimental Study of Temperature-Gradient Metamorphism." Journal of Glaciology 26(94): 303-312.
- McQuiston, F.C., J.D. Parker, and J.D. Spitler (2000). Heating, Ventilating, and Air Conditioning: Analysis and Design-5th edition. New York: John Wiley and Sons.
- Minkowycz, W.J. and E. M. Sparrow Editors, (1997). Advances in Numerical Heat Transfer: Volume 1, Washington: Taylor and Francis.
- Munson, B.R., D.F. Young, and T.H. Okiishi (1994). Fundamentals of Fluid Mechanics. New York: John Wiley and Sons.
- Ohtani, S. and S. Maeda (1964). "Mechanism of Water Movement in Moist Granular Material – Study evaporation under uniform temperature-." Kagaku Kogaku 28(5): 362-367 (in Japanese).
- Powers, D. J., S.C. Colbeck, and K. O'Neill (1985). "Thermal Convection in Snow." U.S. Army Cold Regions Research & Engineering Laboratory Report. 85(9).
- Ramsey, J., H. Chiang, and R. Goldstein (1982). "A Study of the Incoming Long-wave Atmospheric Radiation from a Clear Sky." Journal of Applied Meteorology 21: 566-578.
- Ramsey, J., M. J. Hewett, T.H. Kuehn, and S. D. Petersen (1999). "Updated Design Guidelines for Snow Melting Systems." ASHRAE Transactions 105(1): 1055-1065.
- Sharp, R. (1952). "Meltwater behavior in firn on upper Seward Glacier, St. Wlias Mountains." Union Geodesique et Geophysique Internationale. Association Internationale d'Hydrologie Scientifique. Assemblée generale de Bruxelles: 246-53.
- Shea, E. (1999). "Calibration of Snowmaking Equipment for Efficient Use on Virginia's Smart Road." M. Sc. Thesis, Virginia Polytechnic Institute and State University, Blacksburg, VA.
- Shimizu, H. (1970). "Air Permeability of Deposited Snow." Low Temperature Science, Series A (Part 22):1-32.
- Sommerfeld, R.A. and E. LaChapelle (1970). "The Classification of Snow Metamorphism." Journal of Glaciology 9(55): 1-17.
- Spitler, J. (1996). Annotated Guide to Load Calculation Models and Algorithms, (Atlanta, Georgia: ASHRAE).
- Spitler, J., S. Rees, X. Xia, and M. Chulliparambil (2001). "Development of a Two-Dimensional Transient Model of Snow-Melting System and Use of the Model for

Analysis of Design Alternatives.” ASHRAE 1090-RP Final Report, Oklahoma State University School of Mechanical and Aerospace Engineering.

Tarboton, D. G. and C. H. Luce (1996). “Utah Energy Balance Snow Accumulation and Melt Model (UEB).” Utah Water Research Laboratory and USDA Forest Service Intermountain Research Station.

Tseng, P., T. H. Illangasekare, and M. Meier (1994). “A 2-D Finite Element Method for Water Infiltration in a Subfreezing Snowpack with a Moving Surface Boundary During Melting.” Advances in Water Resources 17:205-219.

Unkown (1998). “Runoff from Snowmelt.” U.S. Army Corps of Engineers Engineering Manual 1110-2-1406:1-100.

Yazdanian M. and J. Klems (1994). “Measurement of the Exterior Convective Film Coefficient for Windows in Low-rise Buildings.” ASHRAE Transactions 100(1):1087-1096.

Yen, Y. (1981). “Review of Thermal Properties of Snow, Ice and Sea Ice.” U.S. Army Cold Regions Research & Engineering Laboratory Report. 81(10).

Yen, Y. (1989). “Approximate Solutions of Heat Conduction in Snow with Linear Variations of Thermal Conductivity.” Cold Regions Science and Technology 17(1): 21-32.

Yen, Y., K.C. Cheng, and S. Fukusako (1991). “Review of Intrinsic Thermophysical Properties of Snow, Ice, Sea Ice, and Frost.” Northern Engineer 23(1): 187-218.

Wilkes, G. B. and C. M. Peterson (1938). “Radiation and Convection from Surfaces in Various Positions.” ASHVE 44: 513.

APPENDIX A

INSTRUMENT CALIBRATION

The experiment included three measured variables, temperature, weight, and snow height. Each of these variables were measured using an instrument that had some error associated with the device. To minimize their error, the instruments were calibrated. The weight was measured using an electronic balance and a graduated cylinder. The electronic balance was purchased from the factory and came from the factory calibrated to $\pm 0.1\text{g}$. The snow height was measured using a ruler that was scribed on the wall of the Plexiglas tube. The ruler had divisions of 6.0 mm. It is possible to estimate the snow height with an uncertainty of 3.0 mm (one half the ruler division).

The temperature was recorded using a FLUKE data logger. Each of these thermocouples were calibrated before they were used in the experiments, although the temperature was not directly used in the numerical model. Because the temperature range of the experiments were near freezing, the thermocouples were calibrated over a range of temperatures from -5.0°C to 0°C . Ethylene glycol was used to achieve temperatures below 0°C . A 10% by volume solution of ethylene glycol was premixed and then placed inside a chest freezer, which reaches temperature near -15°C . The chest freezer froze the EG solution which occurred at -5°C . This frozen EG cubes were then mixed with a chilled 10% solution of EG (approximately 8 liters), which resulted in an EG solution at -5°C . This solution was mixed in a standard household portable “ice”

chest. This “ice” chest was then covered with 20 cm of Styrofoam insulation. The thermocouples were then placed in the in the EG solution and the data logger recorded the temperature. An ASTM certified thermometer was used to measure the temperature. The thermometer was certified over the temperature range of -8°C to 32°C and had temperature divisions of 0.1°C . The solution was stirred occasionally and the temperature was recorded from the thermometer every half hour. Data was collected for several hours.

On another occasion, a standard ice bath was created and the temperature was recorded. The temperature of the ice bath was recorded with the ASTM thermometer, which recorded a temperature of 0°C . Both the ice bath and the EG solution data were collected and plotted. A linear regression of the data was completed and a representative plot can be seen in the following Figure A: Thermocouple Calibration 1.

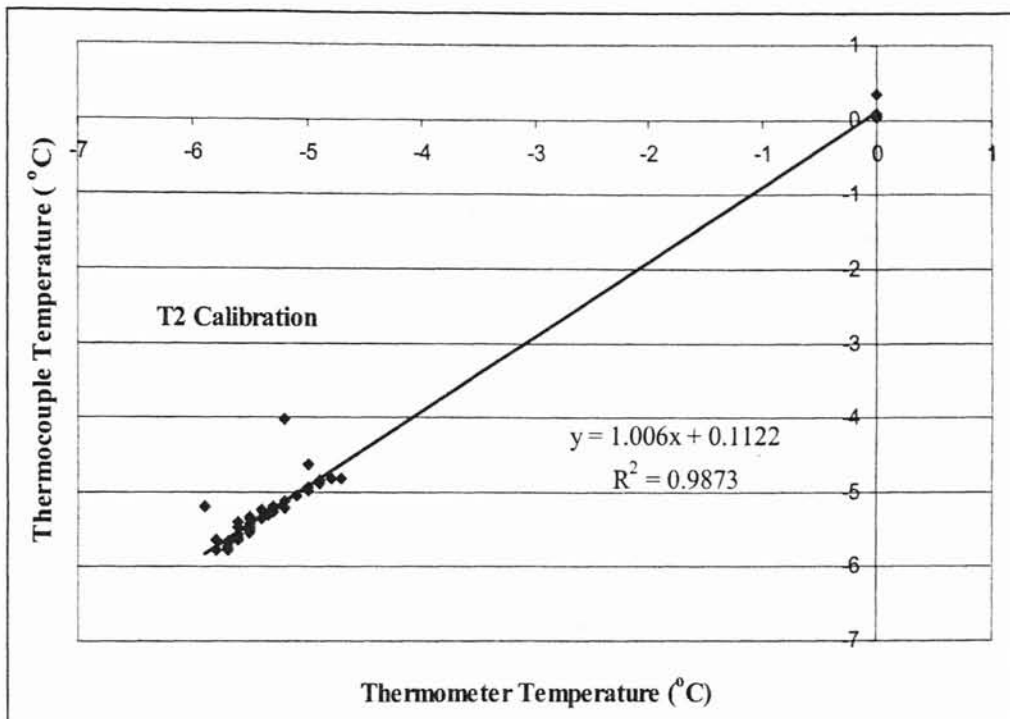


Figure A: Thermocouple Calibration 1

This was completed for all of the thermocouples. After further investigation it was noted that the data matched fairly closely and because the thermometer had division of 0.1°C the thermocouples matched the recorded data with this range. For this reason, the thermocouple data was not corrected in any manner. Because the temperature data was used explicitly the uncertainty associated with the thermocouple data was $\pm 0.1^{\circ}\text{C}$.

APPENDIX B

ERROR ANALYSIS/ UNCERTAINTY ANALYSIS

B.1: Overview

This appendix contains the mathematical calculations and explanations of the uncertainty analysis on the experimentally collected data and the results of the numerical model. The results of this uncertainty analysis can be seen in chapter 5 of the thesis.

B.2: Model Uncertainty

The following subsections describe the uncertainty in the model. The model uncertainty was broken down further into two main sections: uncertainty in model inputs and uncertainties in the model implementation. The uncertainty in melt time due to the uncertainty in the model inputs was determined from a sensitivity analysis. The uncertainties due to phenomena not accounted for in the numerical model were estimated with separate analysis.

B.2.1: Uncertainty in Model Inputs

Each of the inputs to the numerical model are addressed below and the sensitivity of the inputs is discussed. Some of the inputs were a result of direct measurement from the experimental parameters such as the mass of snow. Other model inputs are due to physical property data taken from literature (i.e. thermal conductivity). The remaining inputs are estimated physical phenomenon, convection and radiation, which were modifications to the model as explained in Chapter 3.

B.2.1.1: Mass of Snow

For all of the experiments, the mass of the snow was measured (after it melted) with an electronic balance. The balance was bought new from the factory and was calibrated by the factory. The uncertainty of the balance is ± 0.1 grams.

In the numerical model, uncertainty in the mass of the snow shows up in two places; initial mass of snow and snow porosity (the snow density is linked to snow porosity in the numerical model). A typical total mass of snow was around 600 grams and with uncertainty of 0.1 grams that would result in less than 0.002% change in the total mass of the snow. To validate that the mass of the snow was not a large factor in the uncertainty of the results, the initial snow mass for one specific run was varied by 0.1 gram. Both the porosity and the initial mass of snow were varied and this resulted in less than 1-minute time difference in the numerical melt time interpolating between time steps. It was thus assumed that uncertainty in the mass of the snow had a negligible effect in the model melt time.

B.2.1.2: Thermal Conductivity

The thermal conductivity of snow initially utilized by the model was the value recommended by Ramsey, et al. (1999) of 0.8 W/mK. From literature sources (Yen, et al. 1991; Yen, 1981), this value was determined to be associated with a density of snow near 550 kg/m^3 , which is quite high for new fallen snow. Yen, et al. (1991) provides a review of several correlations that relate thermal conductivity to density and on the average 200 kg/m^3 snow corresponds to a thermal conductivity below 0.3 W/mK. Based on a density of 300 kg/m^3 (representative density made in the environmental chamber) the thermal conductivity should be between 0.2 and 0.4 W/mK. Therefore, the model was modified to use a conductivity of 0.3 W/mK. Because this value was not measured,

and the value was taken from a correlation developed for a type of snow, a relatively high uncertainty was associated with thermal conductivity. To check the sensitivity of the model, the thermal conductivity was changed +20% and -20% from the value of 0.3 W/mK (used in the model) and the resulting melt time changed less than 1 minute. It was concluded that although there seems to be a high uncertainty in thermal conductivity, the overall effect was not significant, probably due to the time scale. Therefore, the uncertainty due to thermal conductivity was concluded to be negligible.

B.2.1.3: Slab Area

The slab was constructed from an aluminum plate and inserted in a Plexiglas tube. Using calipers the diameter of both were measured. The measured value had an uncertainty of ± 0.25 mm. The radius was measured at 8.255 cm resulting in a plate area of 0.021408 m^2 . Using an uncertainty of ± 0.25 mm the resulting difference in area is less than $\pm 0.1\%$, and therefore it was concluded that uncertainty in plate area had no significant effect on the uncertainty in the melt time.

B.2.1.4: Porosity/Snow Density

The density of snow and the snow porosity are coupled parameters and therefore will be discussed together.

$$\rho_s = (1 - \varepsilon)\rho_i \quad (\text{B-1})$$

Where:

ρ_s = Density of snow (kg/m^3)

ε = Porosity of snow

ρ_i = Density of ice (kg/m^3)

The numerical model required the input of the snow porosity; however, the snow density was measured experimentally. As mentioned earlier, the initial snow mass and the plate area had very small contributions to the overall uncertainty of the experiment and therefore the only remaining variable is the initial snow height. The initial snow height measurement uncertainty was estimated to be ± 3.2 mm. Typical snow heights were near 11 cm. The initial snow height was changed +3.2 mm (+3.0%) and -3.2 mm (-3.0%) resulting in a change in the snow density, which resulted in a change in the snow porosity. When the model was changed to reflect the new porosity the overall melt time was changed by less than 1 minute.

The snow used in the experiments all came from the same batch of snow made in the snow making process. It was determined that the snow should have the same porosity. The average porosity for the five different cases run was 0.535 ± 0.03 . This results in a 4% variation in the porosity of the snow. With this uncertainty and the sensitivity of the model to a similar porosity change it was determined the uncertainty was negligible.

As a side note, when the snow porosity was changed (for the uncertainty analysis) it was noticed that the numerically calculated initial snow height did change, however the melt time did not change.

B.2.1.5: Maximum Saturated Layer Height (MSLH)

The MSLH was determined from the experimental results due to the high dependency on the snow density and type. From literature (Jordan, et al. 1999), it was found that the MSLH was highly dependent on the crystal size, crystal shape, density, and age of the snow. Jordan, et al. (1999) reported the MSLH ranged from 1.5-8 cm. As

mentioned earlier, changes in the MSLH had no effect on the melt time nor the initial snow height and only affected the time delay for water runoff.

The MSLH could be viewed in the photographs of the snow height. When the snow height dropped to near the MSLH, the snow texture and contrast changed. The presence of water changed the contrast of the snow and there appeared “dark” spots within the snow. The texture of the snow also changed and although difficult to view in the photographs, from visual inspection, the crystal shape became rounded and increased in size.

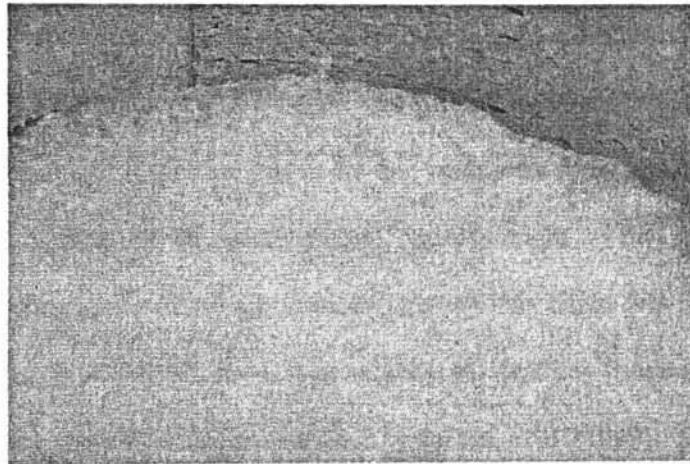


Figure B-1: Picture of Melting Snow Before the MSLH has Been Reached

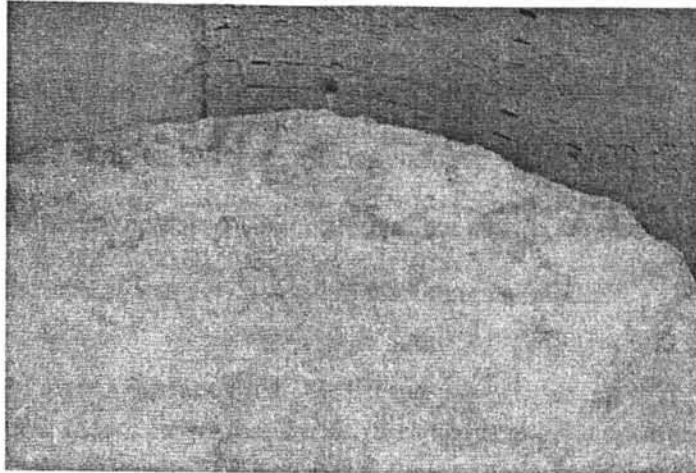


Figure B-2: Picture of Melting Snow After the MSLH has Been Reached

The corresponding height of the MSLH could then be measured from the photograph. The measurement of this height was difficult because of the capillary fringe. From the above pictures it can be said that in the first picture the snow appears to be completely homogenous. In the second picture, one also might say that the snow is not homogenous, taking on a mottled appearance. This capillary fringe was discussed in literature (Jordan, et al. 1999b). It could be said that the capillary fringe in the heat flux experiments had a sharp interface as described by Jordan, et al. (1999). This directly conflicts with the preliminary MSLH experiments and the photographs. This may have been due to the plastic wall effects.

From the experiments completed and the photographs of the different snow melt experiments, an average value of the MSLH was determined to be $3.8\text{cm} \pm 0.6\text{cm}$. This value was used in the numerical model. The results of this can be seen in Appendix D. Each of the five heat flux experiments had a delay before water ran off the plate. In the 236 W/m^2 case the difference between the experimental and numerical delay time was 35 minutes. In the remaining four cases the difference in the delay time was less than or

equal to 5 minutes. If we change the MSLH in the numerical model to 3.25cm and rerun the 236 W/m² case we find the delay time between the numerical and experimental water run off is less than 5 minutes, which would be consistent with the other heat flux cases. Changing this MSLH in the numerical model does not change the overall melt time and for that reason the MSLH was not changed in the numerical model.

B.2.1.6: Heater Power / Surface Flux / Heat Flux

Note: it was shown earlier that the slab area had negligible uncertainty and thus heater power and heat flux will have the same uncertainty. The 24V DC power source seemed to provide a constant voltage to the plate, however, on further inspection, it was found that over the course of a typical experiment the voltage dropped on average 0.3 Volts. The FLUKE data logger measured voltage down to ± 0.01 Volts, which resulted in a fractional uncertainty of 0.06%. The heater was made of nichrome wire and the resistance was measured by the same FLUKE data logger and had a measured uncertainty of 0.001 Ohms. The resistance was measured during working conditions and when the heater was turned off. In both cases the resistance measured 56.90 Ohms, and the fractional uncertainty was calculated to be 0.017%. The voltage drift significantly affected the power to the heater and therefore to accurately predict the effect, the a 4th order polynomial was found for each power curve to predict the heater power drift. This polynomial was then added to the numerical model. Since we altered the numerical model to use the actual heater power, the uncertainty in the heater power was found to have negligible uncertainty.

B.2.1.7: Convection Heat Flux

The convection heat flux was estimated using tabulated data from ASHRAE (1997). A typical value of the convection coefficient for retarded flow over a horizontal surface was found to be $1.50 \text{ W/m}^2\text{K}$ (Wilkes and Peterson, 1938). In order to estimate the uncertainty, we will assume the snow surface layer is constant at 0°C and the chamber air temperature is also constant at 2°C . Wilkes and Peterson (1938) did not estimate uncertainty of the experimental results nor did we measure the convection coefficient. Therefore we might roughly estimate the uncertainty by bounding the convection coefficient.

As an absolute lower bound on the convection we might consider a convection coefficient of $0.0 \text{ W/m}^2\text{K}$, which results in a +7 minute uncertainty for the 236 W/m^2 case and a +1 minute uncertainty for the 789 W/m^2 case. As an upper bound we might consider the convection coefficient of an enhanced natural convection over a horizontal surface. Wilkes and Peterson (1938) state that for enhanced natural convection a typical value of the convection coefficient is $6.6 \text{ W/m}^2\text{K}$. This results in a -36 minute uncertainty for the 236 W/m^2 case and a -4 minute uncertainty for the 789 W/m^2 case. In conclusion, uncertainty in the convection coefficient has a significant effect on the estimated melt time, however most of the uncertainty would tend to say the model over predicts the experimental results where in reality the model under predicts the experiments. This would suggest that a convection coefficient of $6.6 \text{ W/m}^2\text{K}$ might be an unnecessarily high value and that the real convection coefficient would be closer to the estimated value of $1.5 \text{ W/m}^2\text{K}$.

B.2.1.8: “Sky” Temperature / Chamber Temperature

The numerical model was modified to accept the measured “sky” temperature, which was then used to estimate the radiation exchange from the snow surface to the ceiling of the environmental chamber. The chamber temperature was directly input into the numerical model with no modification. There are two types of uncertainty associated with the temperatures: measurement and spatial/temporal averaging.

The “sky” temperature and the chamber temperature were measured with thermocouples attached to the surfaces. The uncertainty in the measured temperatures was $\pm 0.1^{\circ}\text{C}$. This uncertainty resulted in less than 1-minute difference in the overall melt time for both the “sky” and chamber temperatures.

The second type of uncertainty was the spatial/temporal averaging effect. The “sky” temperature was measured with one thermocouple. The thermocouple was placed in a position in which an average value of the ceiling temperature should be measured, however no measurement was completed to substantiate this claim. Also, the fluorescent light was turned on for 30 seconds every 10 minutes which would lead to temporal averaging effects. These effects are difficult to quantify without extensive measurement. A conservative estimate of these effects might be $\pm 0.5^{\circ}\text{C}$. This uncertainty in the “sky” temperature results in a 1 minute difference in the melt time for the 236 W/m^2 heat flux case and less than a minute difference for the 789 W/m^2 case.

B.2.1.9: Surface Emissivity

In the current modified numerical model there are two surface emissivities, snow emissivity and ceiling emissivity. As stated in Chapter 4 the ceiling surface was constructed with a sheet of plastic coated covering material. Since the surface was made from plastic it was water resistant. The emissivity of this product was not found and

B.2.1.8: “Sky” Temperature / Chamber Temperature

The numerical model was modified to accept the measured “sky” temperature, which was then used to estimate the radiation exchange from the snow surface to the ceiling of the environmental chamber. The chamber temperature was directly input into the numerical model with no modification. There are two types of uncertainty associated with the temperatures: measurement and spatial/temporal averaging.

The “sky” temperature and the chamber temperature were measured with thermocouples attached to the surfaces. The uncertainty in the measured temperatures was $\pm 0.1^{\circ}\text{C}$. This uncertainty resulted in less than 1-minute difference in the overall melt time for both the “sky” and chamber temperatures.

The second type of uncertainty was the spatial/temporal averaging effect. The “sky” temperature was measured with one thermocouple. The thermocouple was placed in a position in which an average value of the ceiling temperature should be measured, however no measurement was completed to substantiate this claim. Also, the fluorescent light was turned on for 30 seconds every 10 minutes which would lead to temporal averaging effects. These effects are difficult to quantify without extensive measurement. A conservative estimate of these effects might be $\pm 0.5^{\circ}\text{C}$. This uncertainty in the “sky” temperature results in a 1 minute difference in the melt time for the 236 W/m^2 heat flux case and less than a minute difference for the 789 W/m^2 case.

B.2.1.9: Surface Emissivity

In the current modified numerical model there are two surface emissivities, snow emissivity and ceiling emissivity. As stated in Chapter 4 the ceiling surface was constructed with a sheet of plastic coated covering material. Since the surface was made from plastic it was water resistant. The emissivity of this product was not found and

therefore an estimate was made with regards to its composition. A typical value of emissivity for similar materials was found to be near 0.9 (Incropera and Dewitt, 1996). For a conservative estimate in the model it was assumed the ceiling acted as a black body and therefore had an emissivity of 1.0. The uncertainty therefore was +0.0/-0.1, which resulted in an uncertainty for the 236 W/m² case to be +1 minute, and for the 789 W/m² case less than 1 minute. From this analysis it was determined that the uncertainty due to the ceiling emissivity was negligible.

The snow emissivity was also input to the numerical model. The snow emissivity was not measured and an estimated value from literature was used. In the literature there was a varying range for snow emissivities. Also the type of snow was not stated. Anderson (1976) stated that snow is could be approximated as a black body with minimal error. Anderson (1976) used an emissivity of snow of 0.99. Incropera and Dewitt (1996) provided a range of emissivities for snow from 0.82 to 0.90. Because of this wide range the model emissivity used in the model was 0.9, which from the literature data had an uncertainty of ±0.1. This resulted in a ±1 minute uncertainty for the 236 W/m² case. From this analysis it was determined that the snow emissivity uncertainty had a negligible effect.

B.2.1.10: Model Input Uncertainty Summary

A summary of the model input uncertainties can be seen in the following Tables B.2-1, 2, 3, 4, and 5.

236 W/m²		
Uncertainty	- Melt Time (min)	+ Melt Time (min)
Mass of Snow	<1	<1
Thermal Conductivity	<1	<1
Slab Area	~0	~0
Snow Porosity	<1	<1
MSLH	<1	<1
Convection Coefficient	36	7
“Sky”/Chamber Temperature	<1	<1
Surface Emissivity	1	2
Total	36.1	5.8

Table B.2-1: Model Input Uncertainty (236 W/m²)

316 W/m²		
Uncertainty	- Melt Time (min)	+ Melt Time (min)
Mass of Snow	<1	<1
Thermal Conductivity	<1	<1
Slab Area	~0	~0
Snow Porosity	<1	<1
MSLH	<1	<1
Convection Coefficient	18	3
“Sky”/Chamber Temperature	<1	<1
Surface Emissivity	<1	2
Total	18.2	4.8

Table B.2-2: Model Input Uncertainty (315 W/m²)

473W/m²		
Uncertainty	- Melt Time (min)	+ Melt Time (min)
Mass of Snow	<1	<1
Thermal Conductivity	<1	<1
Slab Area	~0	~0
Snow Porosity	<1	<1
MSLH	<1	<1
Convection Coefficient	6	2
“Sky”/Chamber Temperature	<1	<1
Surface Emissivity	<1	1
Total	6.5	4.2

Table B.2-3: Model Input Uncertainty (473 W/m²)

631 W/m²		
Uncertainty	- Melt Time (min)	+ Melt Time (min)
Mass of Snow	<1	<1
Thermal Conductivity	<1	<1
Slab Area	~0	~0
Snow Porosity	<1	<1
MSLH	<1	<1
Convection Coefficient	5	1
“Sky”/Chamber Temperature	<1	<1
Surface Emissivity	<1	1
Total	5.6	2.6

Table B.2-4: Model Input Uncertainty (631 W/m²)

789 W/m ²		
Uncertainty	- Melt Time (min)	+ Melt Time (min)
Mass of Snow	<1	<1
Thermal Conductivity	<1	<1
Slab Area	~0	~0
Snow Porosity	<1	<1
MSLH	<1	<1
Convection Coefficient	4	1
“Sky”/Chamber Temperature	<1	<1
Surface Emissivity	<1	1
Total	4.7	2.6

Table B.2-5: Model Input Uncertainty (789 W/m²)

B.2.2: Uncertainties in Model Implementation

There were several phenomena not accounted for in the numerical model that could significantly effect the overall melt time. The numerical model did not include these phenomena and therefore estimates had to be made of the resulting heat flux. In the following subsections these phenomena will be investigated and model uncertainty will be estimated.

B.2.2.1: Time Step

When determining the melt time numerically, this time was defined as the time in which the last crystal of ice disappeared. From the numerical model results, this was taken as the time when the snow height went to zero. Because the numerical model time step was set at 5 minutes there was an uncertainty associated with the melt time -- +0/-5 minutes. From the numerical model results, the time step for which the snow height was

zero was determined to be the model melt time, however, due to the 5 minute time step the actual model melt time could fall somewhere in between the last two points.

B.2.2.2: Radiant Heat Gain from Light

Two four foot shop fluorescent lights were used to provide enough light so that the camera could take pictures of the snow surface. The light was installed in the roof of the chamber. The light was mounted outside the chamber and the light was directed through a double pane Plexiglas window. This was done to isolate the heat generated from the ballast (40 watts) from the chamber environment. The light provided by the flash installed on the camera whitewashed the picture so that no information could be gleaned from the picture. This was the reason an external light was added. The light was turned on approximately 15 seconds before the camera was set to take the picture. The camera requires light before the picture is taken to auto focus the lens and adjust the f-stop to produce the best quality picture. To ensure the picture was taken, the light was kept on for 15 seconds after the camera was scheduled to take the picture. Since pictures were taken every 10 minutes, the light was on for 30 seconds for every 10 minutes. For the 789 W/m^2 case (4 hours) the light was on for a total of 12 minutes. The light bulb was assumed to be a point source and a simple calculation was completed to determine the amount radiation that reached the plate using the following equation. It was assumed the fluorescent bulbs were equivalent to a 40-watt point source.

$$q_{plate} = C_{ontime} \frac{q_{light} A_{plate}}{r^2} \quad (\text{B-1})$$

Where:

q_{plate} = Radiation absorbed by the plate (W)

q_{light} = Power of the light bulb (40W)

A_{plate} = Area of the plate (m^2)

r = Distance from the light to the plate (2.3 m)

C_{ontime} = Fraction of time the light is on (30 second for every 10 minutes)

The additional amount of radiation the light provided was determined to be 0.04 Watts. To determine the melt time, this power was added to the plate power for each case. For the 236 W/m^2 case this resulted in a 40 second uncertainty, and for the 789 W/m^2 case this resulted in a 10 second uncertainty. This was considered small and therefore neglected.

B.2.2.3: Radiation Model

The numerical model included a model to estimate the radiation heat gain using a correlated sky temperature. This model was not appropriate for the environmental chamber validation and therefore, another model had to be found. In the experiment, the ceiling was at a higher temperature than the snow. The radiation from the ceiling to the snow needed to be estimated, and a simple network model, described in Chapter 3, was implemented. The network model represented the cylinder walls as a reradiating surface. Incropera and Dewitt (1996) describe a reradiating surface as a surface that has zero net radiation and is commonly used for surfaces that are well insulated on one side and where convection effects may be neglected.

Because a model was used to estimate the radiation there will be some uncertainty built into the model because it is itself an estimation of reality. We can estimate the uncertainty of the parameters in the numerical model but there is no straightforward way to estimate the uncertainty in the model itself.

In the previous section, the surface emissivities, “sky” temperature, and slab area uncertainties were discussed. The remaining model parameters not discussed are the ceiling area, and ceiling view factor. As discussed in the slab area section, we know the ceiling area fairly well. The uncertainty in the measurement device was 2mm. The dimensions of the ceiling were found to be 91cm square. This resulted in a ceiling area of 0.83m^2 . Using an uncertainty of $\pm 2\text{mm}$ the resulting difference in area is less than $\pm 0.4\%$ of the total area, and therefore it was concluded that uncertainty in ceiling area had no significant effect on the uncertainty in the melt time.

To estimate the view factor of the plate to the ceiling, it was assumed that the plate and ceiling were coaxial parallel disks. The plate itself was a disk, however the ceiling was in reality a square. The area of the ceiling was preserved, however the shape was changed. Again this estimation made it difficult to quantify the uncertainty.

One major assumption of the model was the reradiating surface. The Plexiglas cylinder was insulated with 12cm of Styrofoam insulation and temperature difference between the snow and the chamber was 2°C . These two facts were assumed to satisfy the requirement that the surface was well insulated on one side. The second requirement for the reradiating surface was that the convection effects may be neglected. Due to the setup of the experiment convection effects were minimized.

The last source of uncertainty is the simplified radiation model itself. The model included 3 nodes: ceiling, Plexiglas cylinder walls, and snow surface. The snow surface could have also seen part of the chamber walls. This would have significantly increased the complexity of the radiation network. Because the plate was recessed in the Plexiglas

cylinder it was thought that the cylinder walls would in fact “shade” the chamber walls and thus the three-node network would be sufficient to estimate the radiation heat gain.

After investigating each of the parameters in the radiation model there had to be some estimate of the model uncertainty itself. With our limited knowledge, a conservative estimate was made which was then input into the model to determine the sensitivity of the model. The conservative estimate of the uncertainty of the radiation coefficient was $\pm 50\%$. For the 236 W/m^2 case, an increase in the radiation coefficient by 50% resulted in a 8 minute drop in the melt time, whereas for the 789 W/m^2 case the same change in the convection coefficient resulted in less than a 1 minute drop in the melt time. In other words, the radiation model is thought not to have a significant effect on the melt time.

B.2.2.4: Apparatus Radial Heat Gain

Another area of potential uncertainty is the heat gained by the snow radially through the wall of the Plexiglas tube. To estimate the heat gain, a simple heat conduction analysis was completed. This heat gain will decrease as time goes on because the height of the snow drops. We will assume a 2°C temperature difference between the snow and the chamber air and an initial snow height of 0.1 m. The insulation had a thermal conductivity of 0.075 W/mK . It was assumed that the Plexiglas had a minor effect on the overall insulative value of the wall. When the snow is at the initial height of 10 cm, the heat gain by the snow from the wall is approximately 0.05 Watts. Adding this power to the plate power, the effect on the melt time could be determined. For the 236 W/m^2 case, this resulted in a 7-minute uncertainty, whereas for the 789 W/m^2 , this resulted in a 50-second uncertainty.

B.2.2.5: Heat Gain from Backside of Plate

Heat gain from the backside of the plate may slightly decrease the melt time. On the backside of the plate there is a 5mm layer of epoxy and 5 cm of insulation. The air temperature directly under the plate was not measured but was estimated to be 2°C. A simple multiple-layer conduction analysis was completed which showed a possible heat gain of 0.013 Watts. At most this affected the model melt time by less than 2 minutes.

B.2.2.6: Initial Conditions

As described in the experimental setup section, after the snow was made it was placed inside the chest freezer. This froze all of the water (therefore the snow did not have an initial fraction of liquid), and it cooled the snow down to a constant temperature. After the snow had set for several days the snow was removed from the freezer and placed inside the chamber to complete the snowmelt experiment. The chamber was cooled down to 2°C and therefore when the snow was placed inside the snowmelt apparatus it was exposed to the chamber air temperature for up to 5 minutes. This could have reduced the overall snowmelt time. The freezer temperature cooled the snow to –17°C (the lowest temperature the chest freezer can achieve). This would sub-cool the snow thereby increasing the melt time. To evaluate this uncertainty the two extremes were calculated. For the first case, it was assumed that the snow was sub-cooled to –17°C. The specific heat of ice was found to be 2040 J/kgK. Using the following equation the amount energy needed to heat the ice from –17°C to 0°C could be determined.

$$Energy = mc_p(T_{freezer} - 273.15K) \quad (B-2)$$

Where:

m = Mass of snow (kg)

c_p = Specific heat of ice (2040 J/kgK)

$T_{freezer}$ = Temperature of freezer (K)

To determine the effect on the melt time, the *Energy* is divided by the plate heat flux.

This effect increases the melt time by 70 minutes for the 236W/m² heat flux case.

To determine the other half of the uncertainty, it was assumed that the snow was taken out of the freezer at 0°C and was left in contact with room air for up to 4 minutes (average time it took to fill the apparatus with snow). It was assumed while exposed to chamber air, a 5 W/m²K convection coefficient and a 2°C temperature difference provided the heat gain to the snow. It was also assumed that the amount of snow affected by the convection coefficient was exactly the same size needed to fill the apparatus, and thus the area could be determined by determining the surface area of a cylinder with a diameter of 16.5cm and a length of 10 cm. The energy gained by the snow could be found, which when divided by the heat flux resulted in a change in melt time. This melt time corresponds to a decrease in the melt time between 70 minutes and 22 minutes

For the 236 W/m² case, the overall result is the uncertain is +69/-3 minutes, and for the 789 W/ m² case, the uncertainty was determined to be +22/-0.6 minutes. In other words, the uncertainty in the initial energy of the snow due to subcooling may be quite significant

B.2.2.7: Heat Storage

The final uncertainty evaluated is the heat storage in the apparatus itself. The chamber and apparatus were cooled down to 2°C. This resulted in a certain amount of energy stored in the apparatus. To estimate this uncertainty the specific heat for each of the materials, aluminum, polystyrene insulation, and Plexiglas was determined. From the

experimental temperature measurements it was determined that the plate temperature was typically 2°C. This value was then used to calculate the amount of energy stored. Because the apparatus stored some energy that could be transferred to the snow, this uncertainty resulted in a decrease in the model melt time. For the 236 W/m² case, this resulted in a 10-minute uncertainty and for the 789 W/m² case the uncertainty was calculated to be 2.5 minutes.

B.2.2.8: Model Implementation Uncertainty Summary

Each of the uncertainties in the model implementation have been discussed in the above sections. In each case the uncertainty in the model melt time was estimated and the results can be seen in the following Tables B.2-6, 7, 8, 9, and 10.

236 W/m ²				
Uncertainty	+ Watts	- Watts	- Melt Time (min)	+ Melt Time (min)
Time Step			5	0
Radiant Gain from Light	0.007	0	1	0
Radiation Model			5	5
Radial Heat Gain	0.05	0	7.4	0
Back Side Heat Gain	0.01	0	2	0
Initial Conditions	0.02	0.51	2.7	70
Heat Storage	0.07	0	10	0
Total			14.7	70.1

Table B.2-6: Model Implementation Uncertainty (236 W/m²)

315 W/m ²				
Uncertainty	+ Watts	- Watts	- Melt Time (min)	+ Melt Time (min)
Time Step			5	0
Radiant Gain from Light	0.007	0	0.6	0
Radiation Model			5	5
Radial Heat Gain	0.05	0	4.1	0
Back Side Heat Gain	0.01	0	1.1	0
Initial Conditions	0.02	0.69	2.0	52.3
Heat Storage	0.09	0	7.5	0
Total			11.3	52.5

Table B.2-7: Model Implementation Uncertainty (315 W/m²)

473 W/m ²				
Uncertainty	+ Watts	- Watts	- Melt Time (min)	+ Melt Time (min)
Time Step			5	0
Radiant Gain from Light	0.007	0	0.3	0
Radiation Model			4	3
Radial Heat Gain	0.05	0	2.1	0
Back Side Heat Gain	0.01	0	0.6	0
Initial Conditions	0.03	1.04	1.3	40.3
Heat Storage	0.11	0	5.0	0
Total			8.5	40.5

Table B.2-8: Model Implementation Uncertainty (473 W/m²)

631 W/m ²				
Uncertainty	+ Watts	- Watts	- Melt Time (min)	+ Melt Time (min)
Time Step			5	0
Radiant Gain from Light	0.007	0	.2	0
Radiation Model			3	2
Radial Heat Gain	0.05	0	1.1	0
Back Side Heat Gain	0.01	0	0.3	0
Initial Conditions	0.05	1.4	1	27.2
Heat Storage	0.17	0	3.7	0
Total			7.1	27.4

Table B.2-9: Model Implementation Uncertainty (631 W/m²)

789 W/m ²				
Uncertainty	+ Watts	- Watts	- Melt Time (min)	+ Melt Time (min)
Time Step			5	0
Radiant Gain from Light	0.007	0	0.1	0
Radiation Model			2	2
Radial Heat Gain	0.05	0	0.7	0
Back Side Heat Gain	0.01	0	0.2	0
Initial Conditions	0.05	1.73	0.8	22.2
Heat Storage	0.2	0	3.0	0
Total			6.3	22.3

Table B.2-10: Model Implementation Uncertainty (789 W/m²)

B.2.3: Overall Numerical Uncertainty

If we take all the numerical uncertainties that have been addressed above and add them in quadrature, we can arrive at an overall experimental uncertainty which can be

found in Table B.2-11. The numerical input uncertainty was added in quadrature with the model implementation uncertainty. In every case the dominant uncertainty (increasing the melt time) is the subcooling of the snow or the initial condition of the snow. For the 236 W/m² case the subcooling uncertainty results in 99% of the overall uncertainty.

Heat Flux (W/m²)	- Melt Time (min)	+ Melt Time (min)
236	40	70.3
315	21.4	52.7
473	10.7	40.7
631	9.0	27.5
789	7.9	22.5

Table B.2-11: Model Uncertainty Summary

B.3: Experimental Uncertainty

The following subsections will discuss the experimental uncertainty.

B.3.1: Observation Interval

The experimentally determined melt time was defined as the time it took the last crystal of ice to melt. As discussed throughout the paper, the surface tension of water resulted in a layer of water to collect on top of the plate and would not drain off without user intervention; therefore, from the water runoff data the actual melt time had some uncertainty. From the photographs the presence of water on the plate also hindered the detection of ice. If the presence of ice could not be determined with some precision then the resulting model melt time included some uncertainty. The 5-minute time-lapse interval also contributed to the uncertainty because the melt time could not be defined down to the minute. Therefore, the experimentally determined melt time was estimated to have an uncertainty of ±5 minutes.

B.3.2: Inhomogeneous Melting

Near the end of the snow melt experiment it was found that the snow was melted in an inhomogeneous manner. There are several methods in which this inhomogeneous melting can be quantitatively seen. The 236 W/m^2 case will be examined in this section; however, all of the different cases show the same effect. In the 236 W/m^2 case the experimentally determined melt time was 13 hours and 20 minutes. This time is defined as the time in which the last snow crystal could not be seen in the photographs. However, as can be seen in Figure B.3-1, the plate temperature started to rise well before the last snow crystal was melted

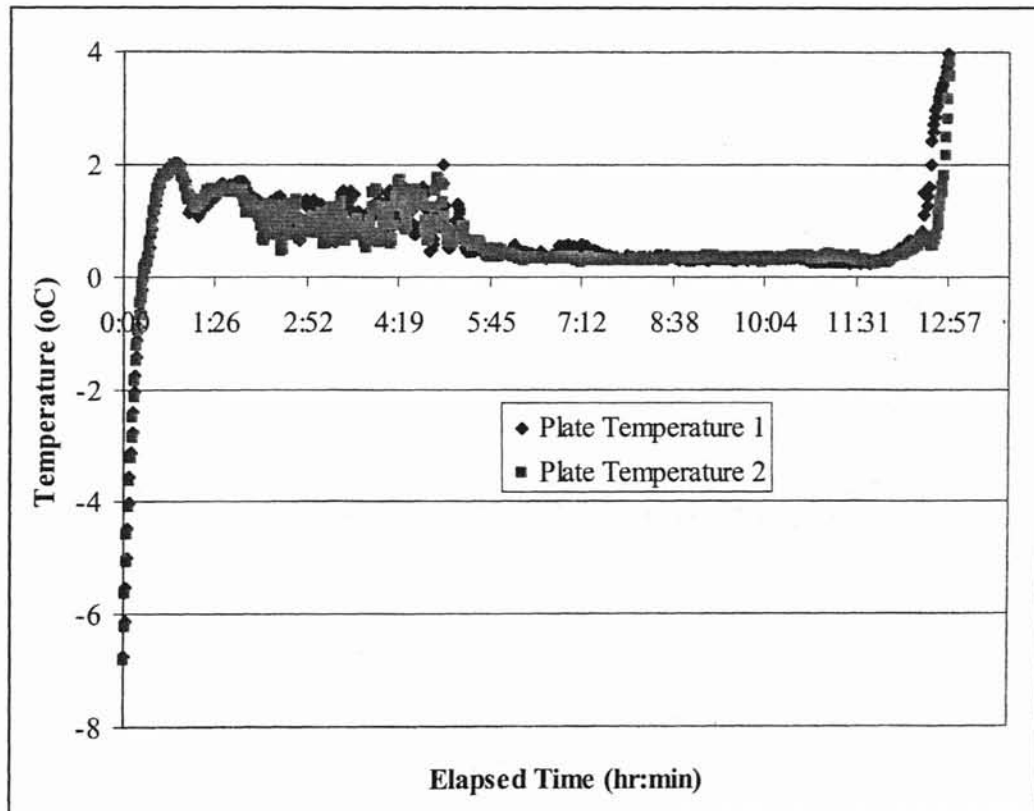


Figure B.3-1: Plate Temperature (236 W/m^2)

In Figure B.3-1 we can see that the plate temperature starts to rise at about 12:10 and dramatically increases about 12:30. During this final hour the heat input does not go only into melting the snow but also into raising the temperature of the plate. As a result of increasing the plate temperature the water could evaporate at a faster rate. The humidity sensor was installed above the snowmelt apparatus. During a few of the snowmelt experiments the humidity sensor did show a sudden rise in the humidity. This did not occur in the 236 W/m^2 case because the heat flux was small and the plate temperature did not rise to an extreme temperature ($>10^\circ\text{C}$). In the 473 W/m^2 case as the plate temperature increased the humidity sensor picked up the increased humidity.

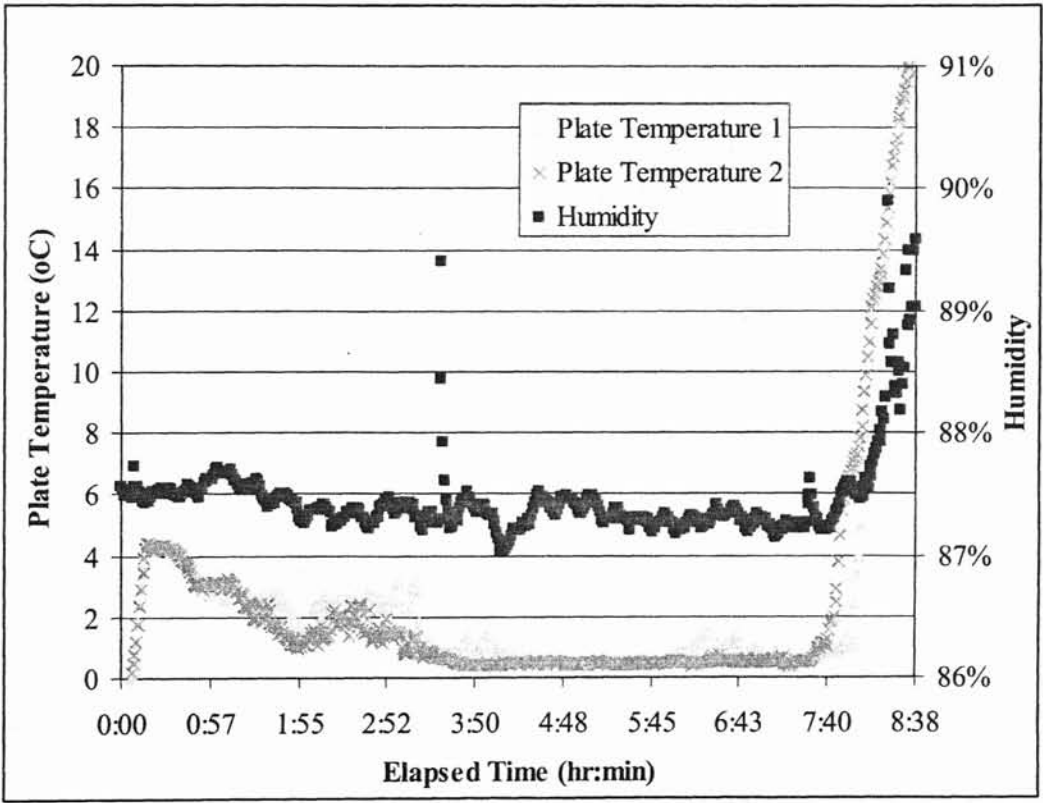


Figure B.3-2: Chamber Humidity and Plate Temperature (473 W/m^2)

In Figure B.3-2, it can be seen that as the plate temperature begins to increase after 7:40 the humidity above the experiment increased as well.

The inhomogeneous melting can also be seen in the snow height measurements. From the snow height charts the slope of the snow height versus elapsed time changes near the completion of the experiment. This effect can be seen in the following Figure B.3-3.

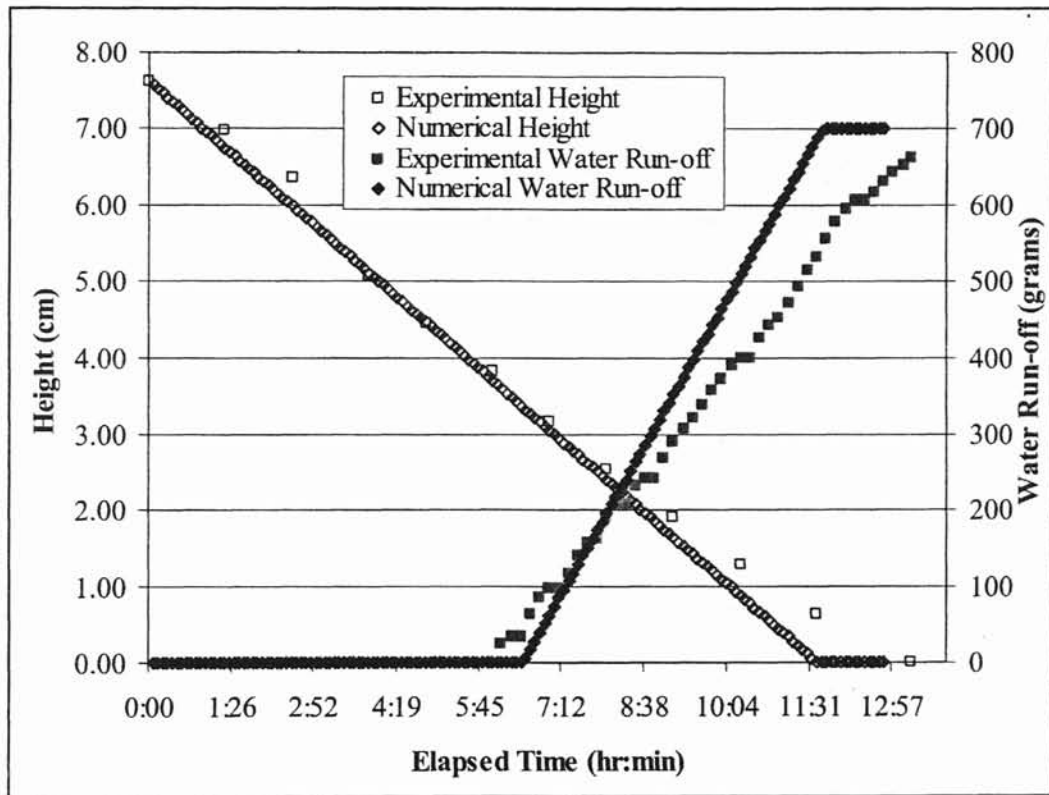


Figure B.3-3: Model vs. Experimental Height Validation and Water Run-off Validation (236 W/m^2)

The snow height data were taken from photographs. Again, the definition of snowmelt time was set as the time in which the last crystal of snow had melted. From the photographs it can be seen that portions of the plate were free of snow where other parts still contained snow. When the plate was free of snow, the plate temperature began to

rise which explains why the two plate temperature do not match near the completion of all of the experiments. In extreme cases this will cause a significant difference in plate temperature as can be seen in the following Figure B.3-4.

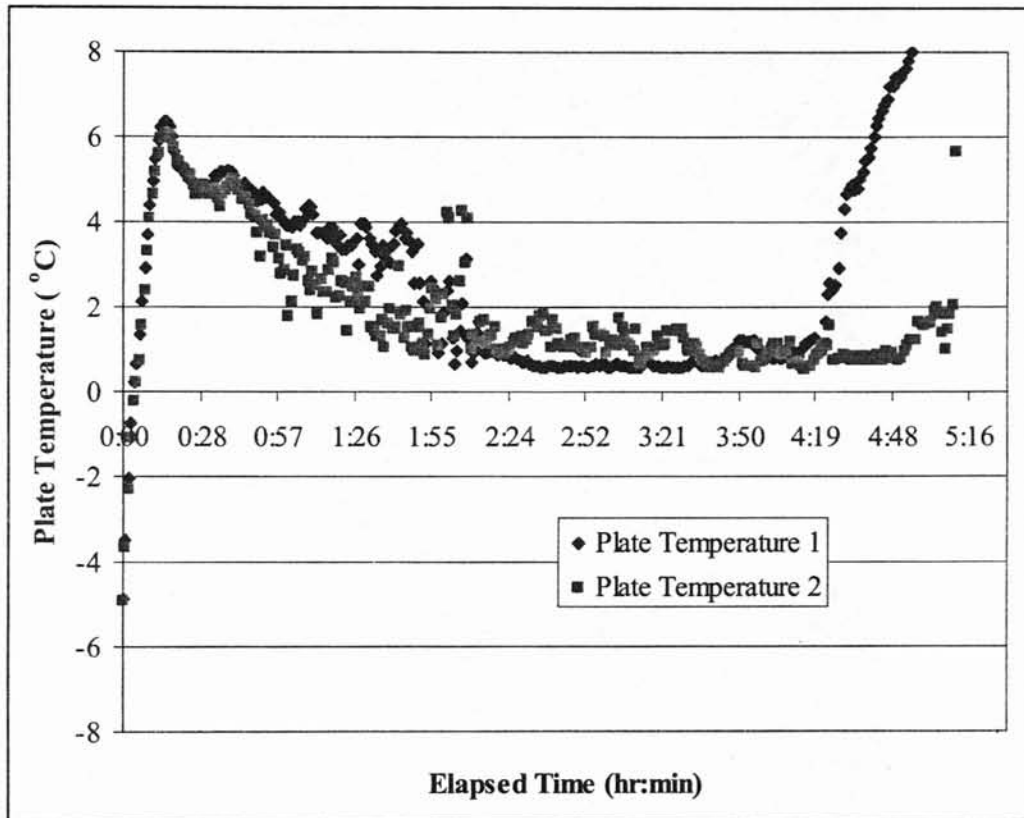


Figure B.3-4: Plate Temperature (631 W/m²)

This can also be seen in the photographs of the experiment. The following Figures B.3-5, 6,7 depict the snow for the 631 W/m² case at specified intervals, which will show how one part of the plate will be free of snow before the rest of the plate. These pictures follow the trend shown in Figure B.3-4.



Figure B.3-5: Snowmelt photograph at 4:40 (631 W/m^2)

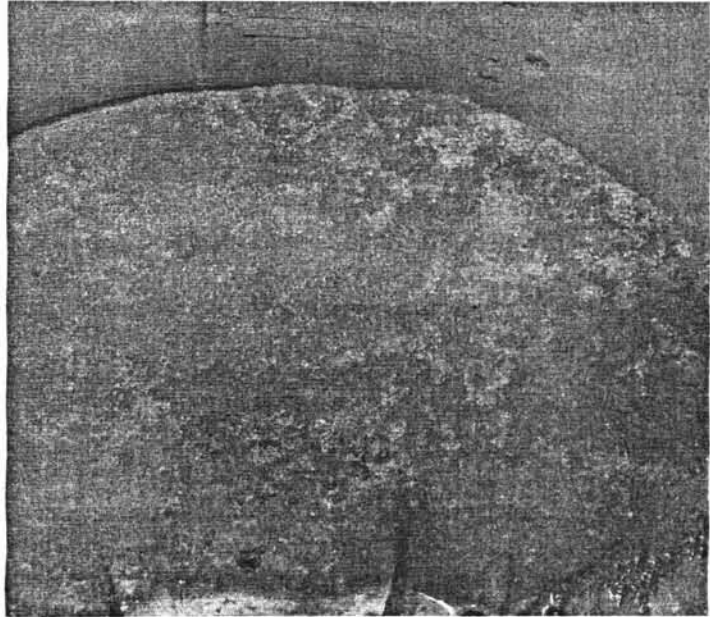


Figure B.3-5: Snowmelt photograph at 4:50 (631 W/m^2)

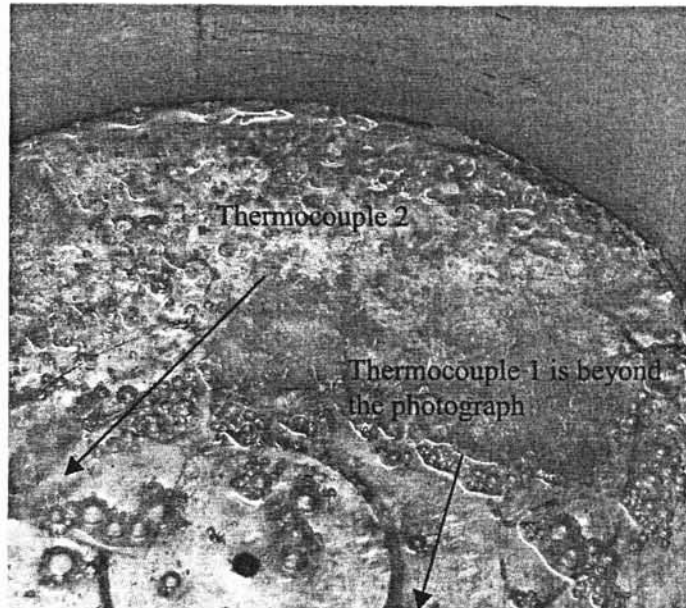


Figure B.3-5: Snowmelt photograph at 5:10 (631 W/m²)

Thermocouple 1 is off the photograph however from the temperature chart we can predict that part of the plate is void of snow.

To estimate this inhomogeneity in the snowmelt experiment two possible methods could be employed. The first would be to record the snowmelt time as the time in which the first sign that the plate had been cleared of snow. This could be done either from photographic evidence or from the plate temperature chart. If the plate temperature begins to increase one could assume the plate was free of snow. The second method would be to utilize the snow height versus elapsed time figure. For the most part the slope of the snow height versus time is linear except near the completion of the experiment. If we were to assume the melting was linear throughout the whole experiment we could estimate this time using the figure. This method can be seen in the following figure B.3-6.

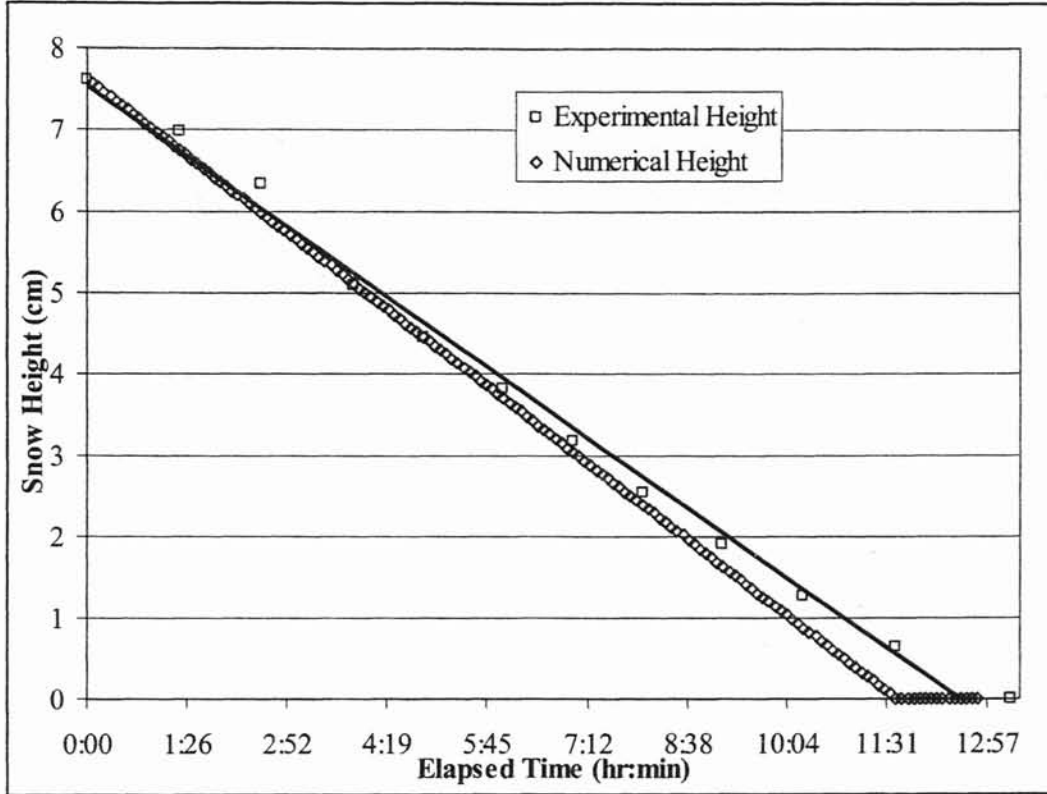


Figure B.3-6: Inhomogeneous Effect on Snowmelt time (236 W/m^2)

In the above figure a linear fit is used with all of the data points. This method reduces the snowmelt time from 13:20 to 12:30, however this is still considerable higher than the estimated model melt time. Because the linear fit used all of the data points, the inhomogeneous effects were included in the estimated melt time. To reduce this affect these last points will be removed from the fit and we will arrive at a better estimate of the snowmelt time.

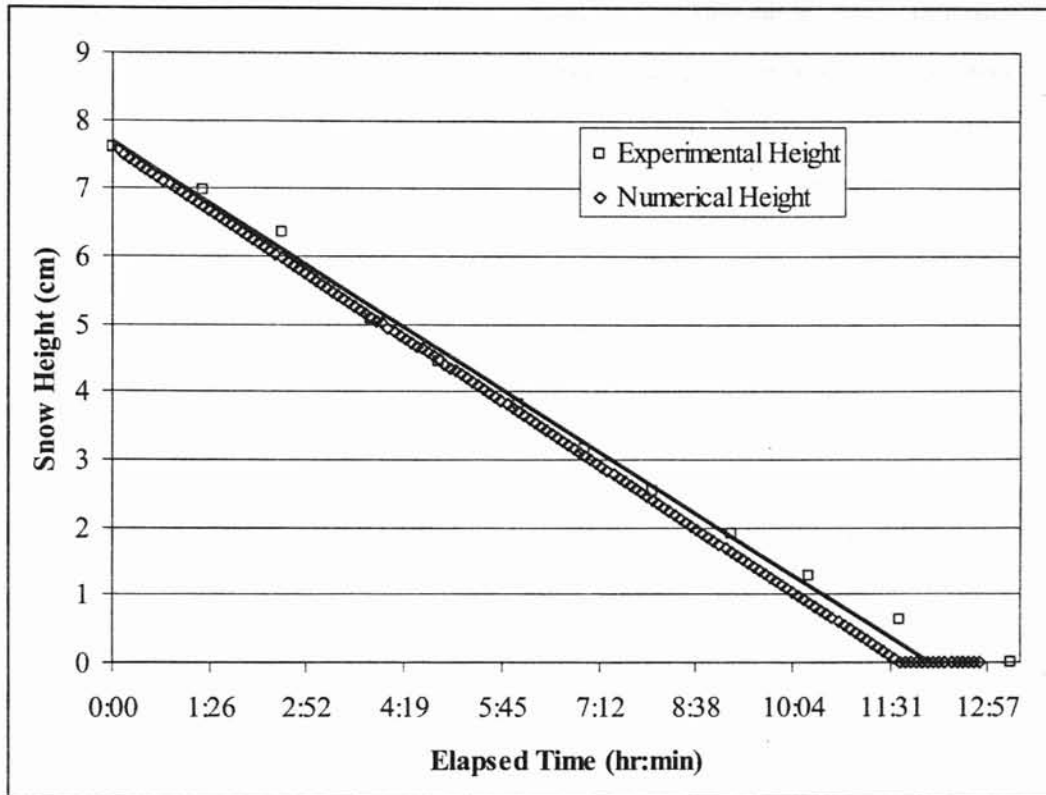


Figure B.3-7: Estimate of Snowmelt time (236 W/m^2)

In Figure B.3-7 the estimated snowmelt time is now 12:10. This method was used for each of the five cases to estimate the inhomogeneous melting effect and is summarized in the following chart.

Heat Flux (W/m ²)	Experimentally Determined Melt time (hr:min)	Modified Melt Time due to inhomogeneous affects (hr:min)	Difference (hr:min)
236	13:20	12:10	1:10
316	10:50	9:35	1:15
473	8:15	7:25	0:50
631	5:20	5:05	0:15
789	4:40	3:50	0:50

Table B.3-1: Inhomogeneous Melting Uncertainty

This inhomogeneous effect will be included in the experimentally uncertainty and thus in the error bars that can be seen in Section 5 of the main part of the thesis.

B.4: Uncertainty Summary

The uncertainty was split into two categories: model and experimental uncertainty. From the above sections there are two main uncertainties: subcooling of the snow prior to the snow melt experiment and the inhomogeneous melting of the snow during the last few hours of the experiment. The subcooling uncertainty for the 236 W/m² case was determined to be 70 minutes. The uncertainty of the inhomogeneous melting was estimated to be 70 minutes as well.

APPENDIX C

WATER SATURATION LAYER MODEL

Overview

During the early stages of the modeling and model verification, the maximum saturated layer height was not known and there was no literature that addressed the subject. Also when reading articles such as Colbeck, (1973) wet snow metamorphism seemed to be on the time scale of the experiments and was stress as very important. Colbeck, (1973) states that rapid metamorphism of snow at high water saturations has been observed many times. Colbeck, (1973) goes on to state that wet metamorphisms results in rapid grain growth, loss of mechanical strength and rapid densification. From preliminary snow melt experiments, it was noticed that a “slush” layer formed on the plate, which by definition is snow with high water saturation.

The maximum saturation layer height is a function of pore radius. The capillary pressure is an indirect function of pore radius, and thus as the pore radius increases the capillary pressure drops and thus the maximum saturated layer height would decrease. The wet metamorphism effects described by Colbeck would seem to effect the overall snow diameter, pore radius, and porosity.

This purpose of this additional model was to predict the change in the maximum saturated layer height as a function of time. We expected be able the decrease in MSLH as time elapsed.

Procedure

The overall algorithm for this model will now be discussed.

Step 1: We must know the initial crystal diameter. For research oriented modeling this step is quite easy. A 10X hand lens and a ruler is sufficient to measure the initial crystal size. The “big picture” is to create a model that a bridge/slab operator could be able to input several parameters into a control box and the bridge/slab deck would turn on/off accordingly. The size of snow crystals would not be a parameter that an ordinary bridge operator would know. This initial problem did not stop the modeling.

Step 2: From the snow crystal size can we calculate the density or porosity of the snow. From literature, there have been no such experiments completed, and in fact due to the ranging crystal types this correlation may not even be possible. As noted in Colbeck, et al. (1990), crystal size, shape, and density are among the fundamental characteristics of snow and from the committees knowledge are not related. This step proved to be the hardest to complete.

Step 3: From the crystal size and density/porosity can the MSLH be determined. As discussed earlier in this appendix, the MSLH is a function of pore radius and thus the crystal diameter/porosity. After searching the literature one such correlation was found. Jordan, et al. (1999b) provides the following correlation:

$$D_{est} = \frac{\sigma_{al} \cos \theta}{\rho_l g h \sqrt{5 \cdot 0.077 \exp(-0.0078 \rho_s)}} \quad (C-1)$$

Where:

D_{est} = Estimated crystal diameter (mm)

θ = Contact angle between solid and liquid (radians)

g = Acceleration due to gravity (m/s^2)

h = MSLH (m)

ρ_s =Density of snow (kg/m³)

ρ_l = Density of liquid water (kg/m³)

σ_{al} = Surface tension of air/water interface (N/m)

This equation could then be solved for h , and used in the manner described above.

Step 4: We have now predicted the MSLH from the diameter of the crystals. The last remaining step is to predict how the diameter of the crystals will change over time due to snow metamorphism. Colbeck, (1986a) presents a correlation developed from experimentally determined diameter. Snow crystals were immersed in water, and through time lapse photography and an image analysis system the crystal diameter could be measured as a function of time. This data was then regressed and the following correlation is presented:

$$\bar{D} = \bar{D}_o + 0.132 * t^{0.362} \quad (C-2)$$

$$D_g = D_{g,o} + 0.117 * t^{0.369} \quad (C-3)$$

Where:

D_g = geometric mean diameter (mm)

$D_{g,o}$ = Initial geometric mean diameter (mm)

\bar{D} = Average mean diameter (mm)

\bar{D}_o = Initial average mean diameter (mm)

t = time (hours)

Results

This section presents the results of this modeling algorithm. However, before we start with the overall results, the problem discussed in step 2 must be addressed. Since no

correlation was found to relate density to diameter one was developed. Jordan, et al. (1999b) also presented a table of physical data from approximately 30 snow samples. As discussed earlier, the crystal size and shape must be matched before the data can be used and therefore several of the samples had to be discarded. This resulted in 3 sample data which then a parameter estimation was completed to determine a suitable correlation for density as a function of diameter, see Figure C-1.

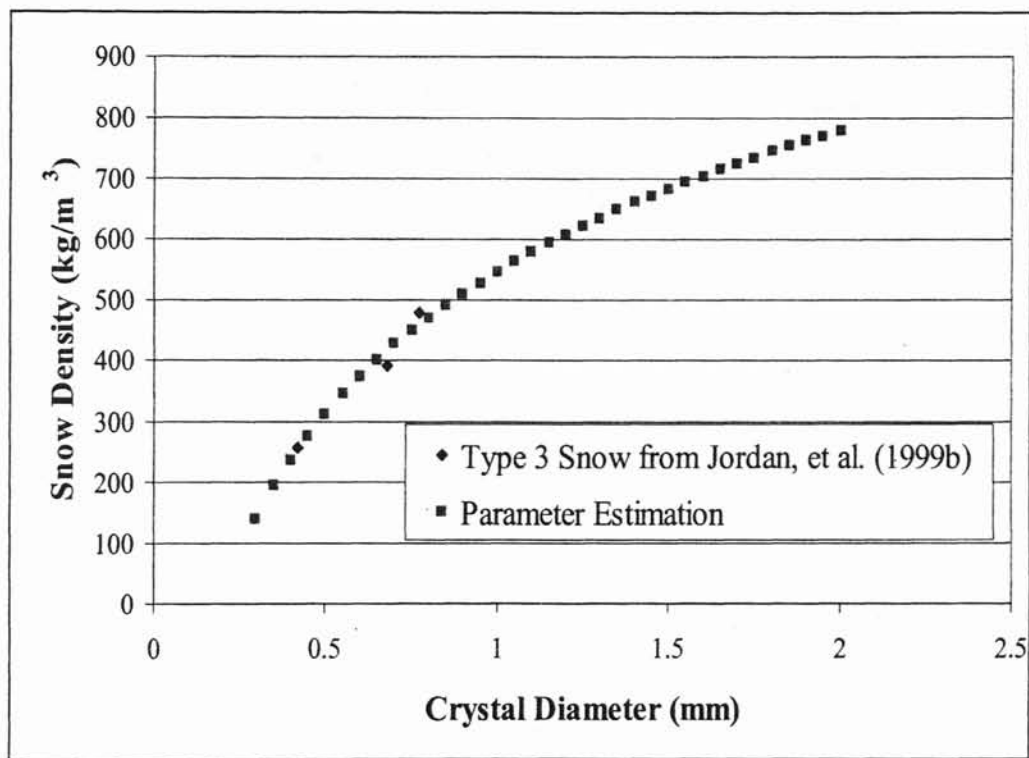


Figure C-1: Density vs. Diameter

This correlation has all the parts to be an appropriate correlation. As the crystal size decreases to zero the density decreases to zero. As diameter increases there is a leveling off of the density. At high crystal diameter the resulting snow would resemble ice, which

has a density of approximately 920 kg/m^3 . The correlation also matches the 3 sample data points fairly well.

Now that we have a correlation for each of the steps, we can begin to put each together. In step 3, a correlation was given by Jordan, et al. (1999b), which related saturation layer height as a function of particle diameter and density. Visually the results of the correlation can be seen in the following figure C-2.

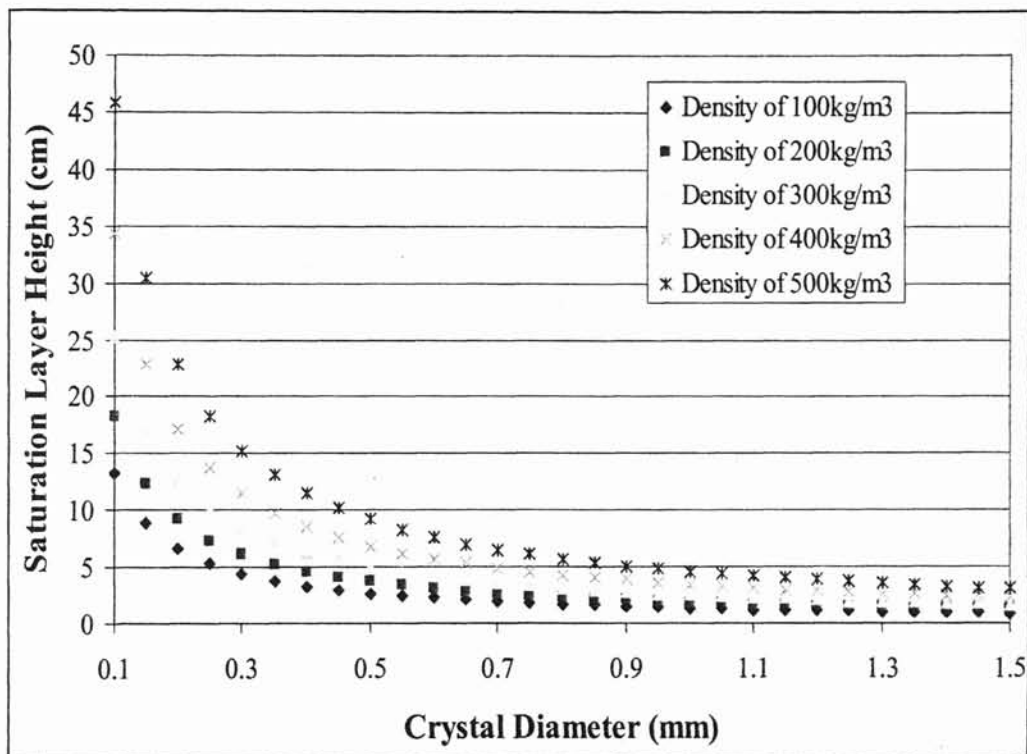


Figure C-2: Saturation Layer Height vs. Crystal Diameter

From Figure C-2 it can be seen that the saturation layer height for a density of 200 kg/m^3 and a particle diameter of 0.2 mm (approximate conditions found in the snow melt experiments) the predicted saturation layer height is 9.5 cm . This value is considerable higher than that found in the actual snow melt case, and in fact in some snow melt experiments the total height of the snow was less than 9.0 cm .

In step 4, Colbeck (1986a) presented a correlation that accounted for the wet metamorphism in snow. This correlation can be seen visually in the following figure C-3. Two initial diameters (1.0 mm and 0.5 mm) were chosen to compare the results.

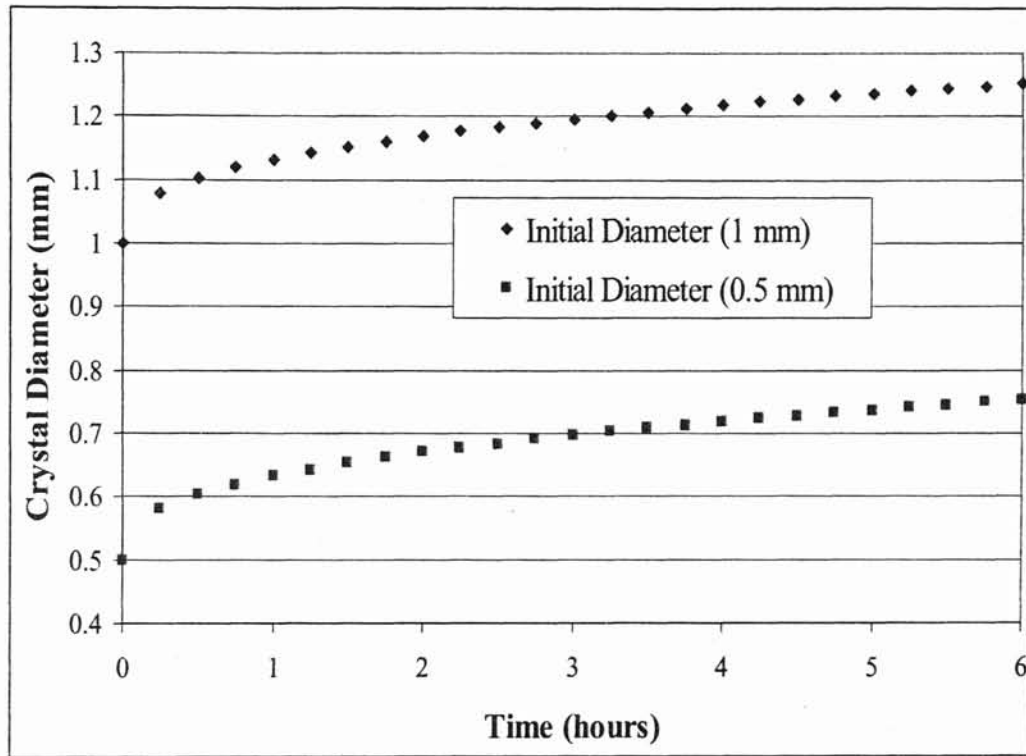


Figure C-3: Effect of Wet Snow Metamorphism over Time

From Figure C-3 it can be seen that over the course of the experimental snow melt experiments (approximately 5 hours) the crystal diameter increases by 0.25 mm in both initial cases.

Now when each of these correlations are put together from step 1, step 2, step 3 and step 4 the result can be seen in Figure C-4.

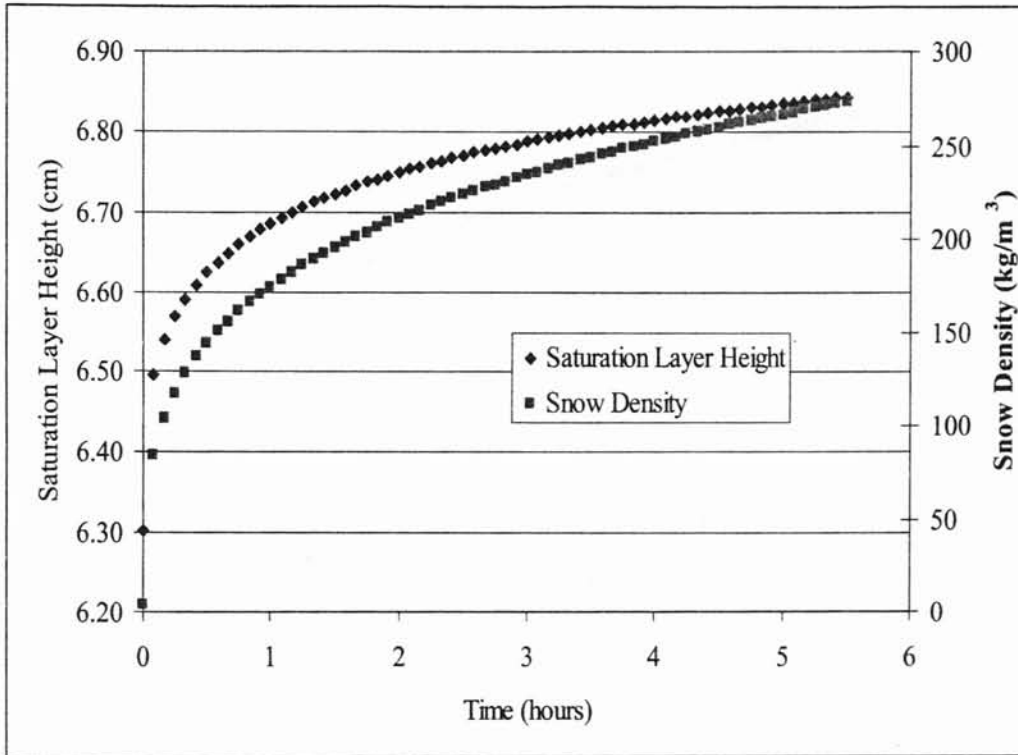


Figure C-4: Saturation Layer Height vs. Time (Initial Diameter = 0.2mm)

From Figure C-4 it can be seen that the predicted saturation layer height changes increases from an initial value of 6.2 cm to a value of 6.85 after 5 hours. This effect is opposite what was initially predicted. If the diameter of the particle increases then the pore diameter should also increase, and decrease the saturation height. The initial diameter of the snow as chosen to be 0.2 mm. It is also interesting to note that the initial density was calculated to be 3.9 kg/m³, which is quite low. After 10 minutes though the density increases above 100 kg/m³ a more realistic value. If the initial diameter is changed to 1.0 mm the resulting trends change significantly and can be seen in Figure C-5.

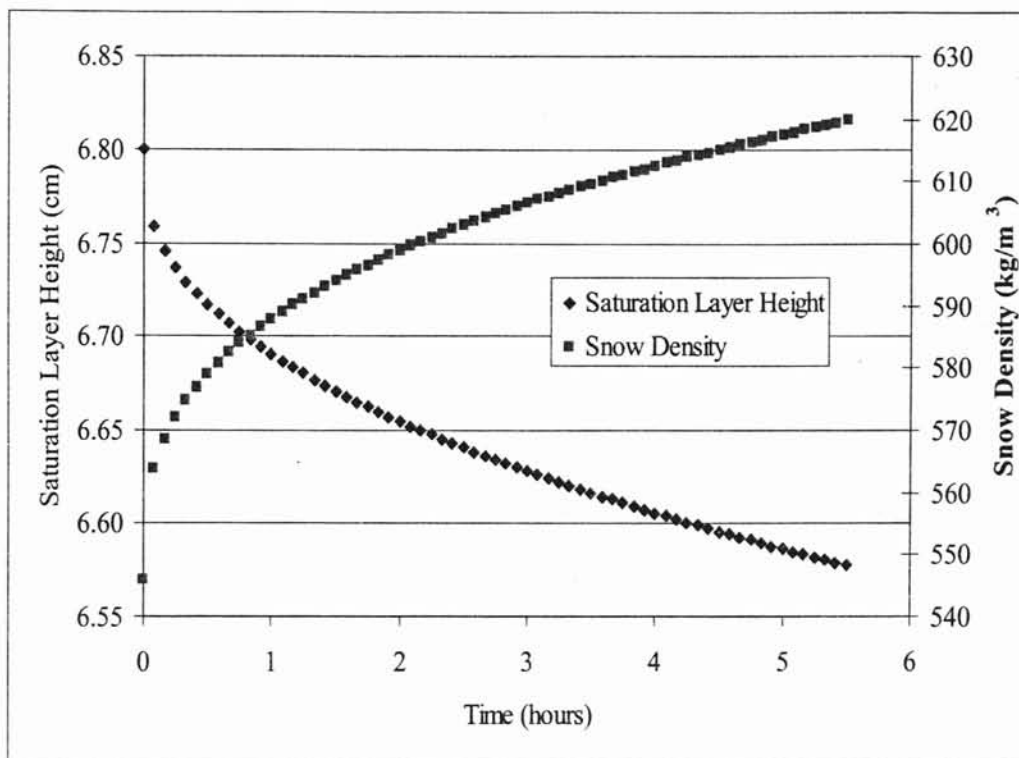


Figure C-5: Saturation Layer Height vs. Time (Initial Diameter = 1.0mm)

From Figure C-5 it can be seen that the saturation layer height actually decreases as time goes on which was initially predicted. The density also increases to on average 550 kg/m^3 , which by all accounts is very dense snow. It is also interesting that the overall saturation height does not significantly change between the two cases (0.2mm and 1.0 mm initial diameter). It would be expected that in the 1.0 mm case the overall saturation layer height would be significantly lower than the 0.2 mm height.

APPENDIX D

OTHER EXPERIMENTAL DATA

Overview

This section includes the data taken from the different snowmelt cases. Included are several figures of the experimental data, and numerical model results. It also includes the porosity and density that was calculated for each case.

236 W/m² Case

Initial Snow Mass = 700.1 grams

Snow Porosity = 0.534266

Snow Density = 429 kg/m³

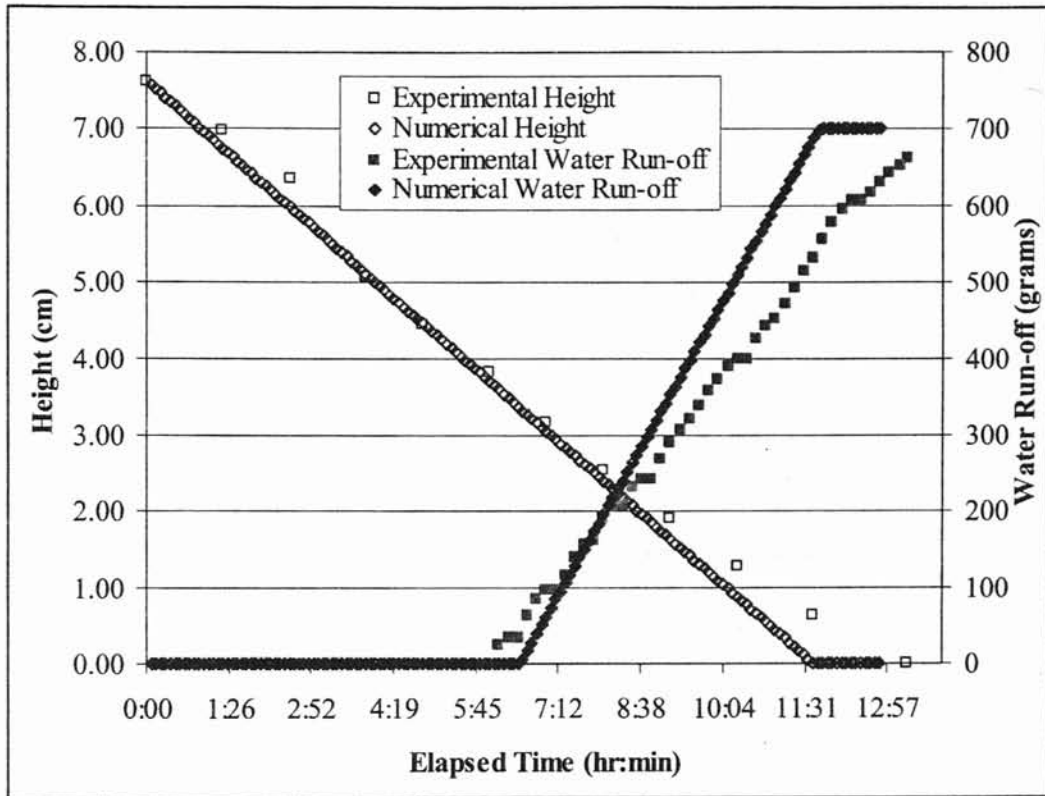


Figure D.1-1: Model vs. Experimental Height Validation and Water Run-off Validation (236 W/m²)

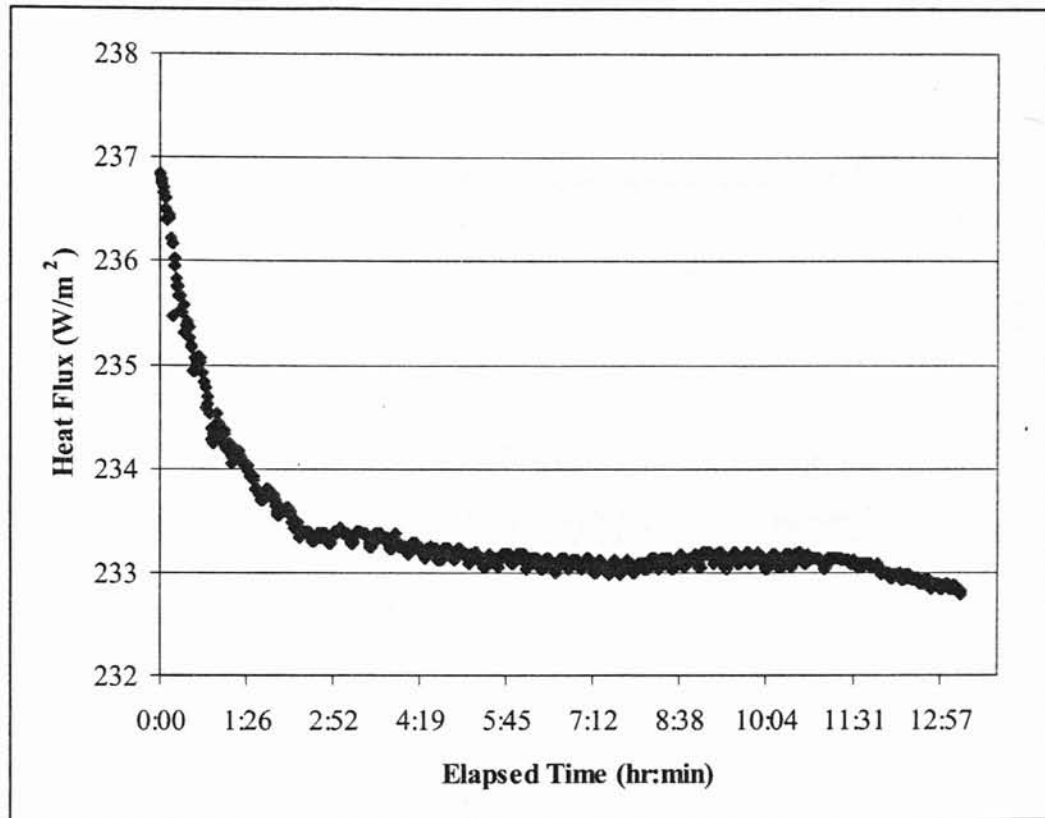


Figure D.1-2: Experimental Power Supply (236 W/m²)

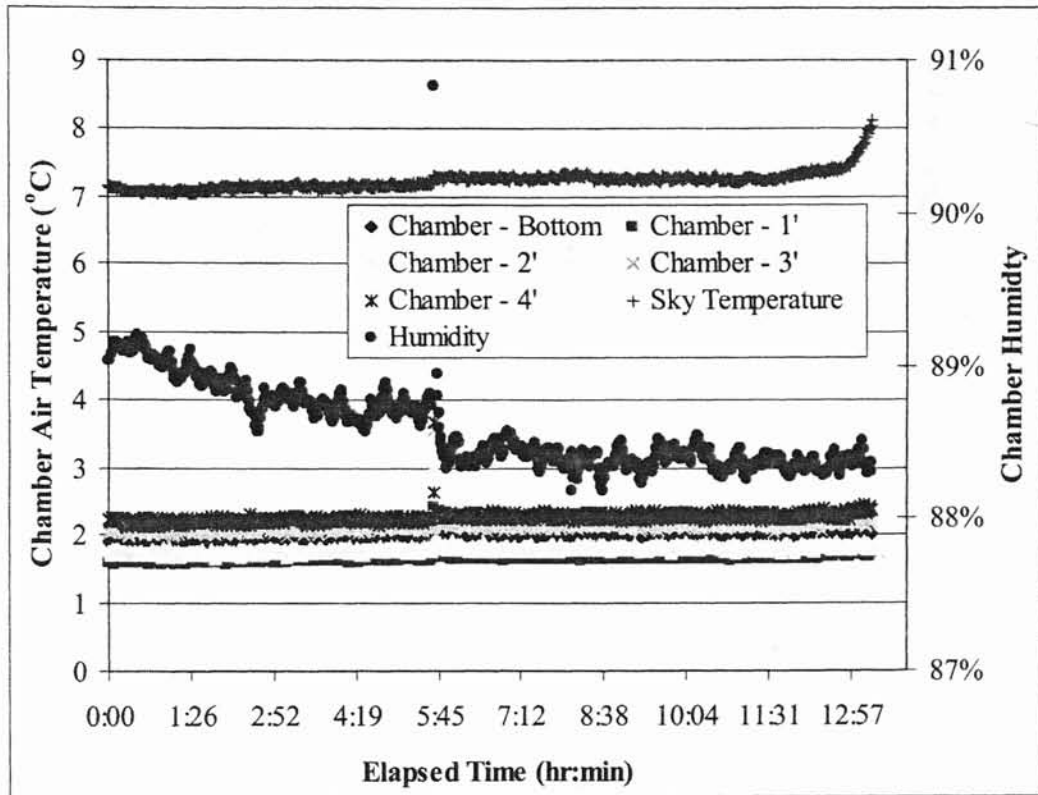


Figure D.1-3: Chamber Air and Sky Temperature and Chamber Humidity (236 W/m²)

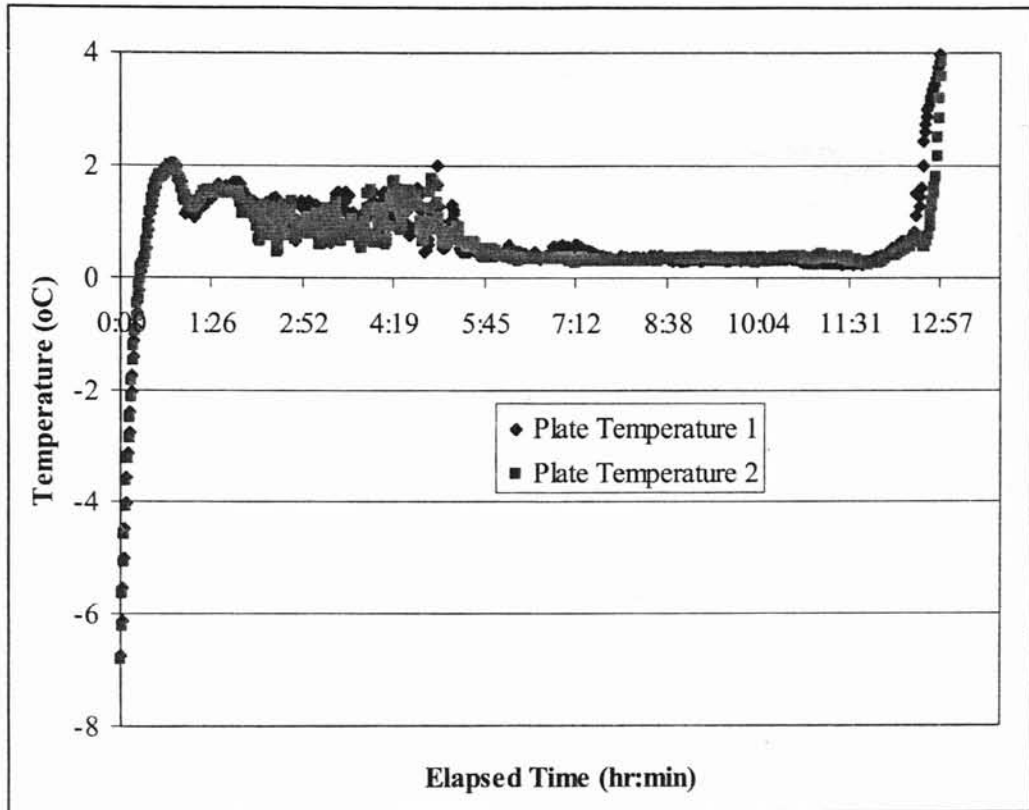


Figure D.1-4: Plate Temperature (236 W/m²)

316 W/m² Case

Initial Snow Mass = 670.3 grams

Snow Porosity = 0.55409

Snow Density = 410.8 kg/m³

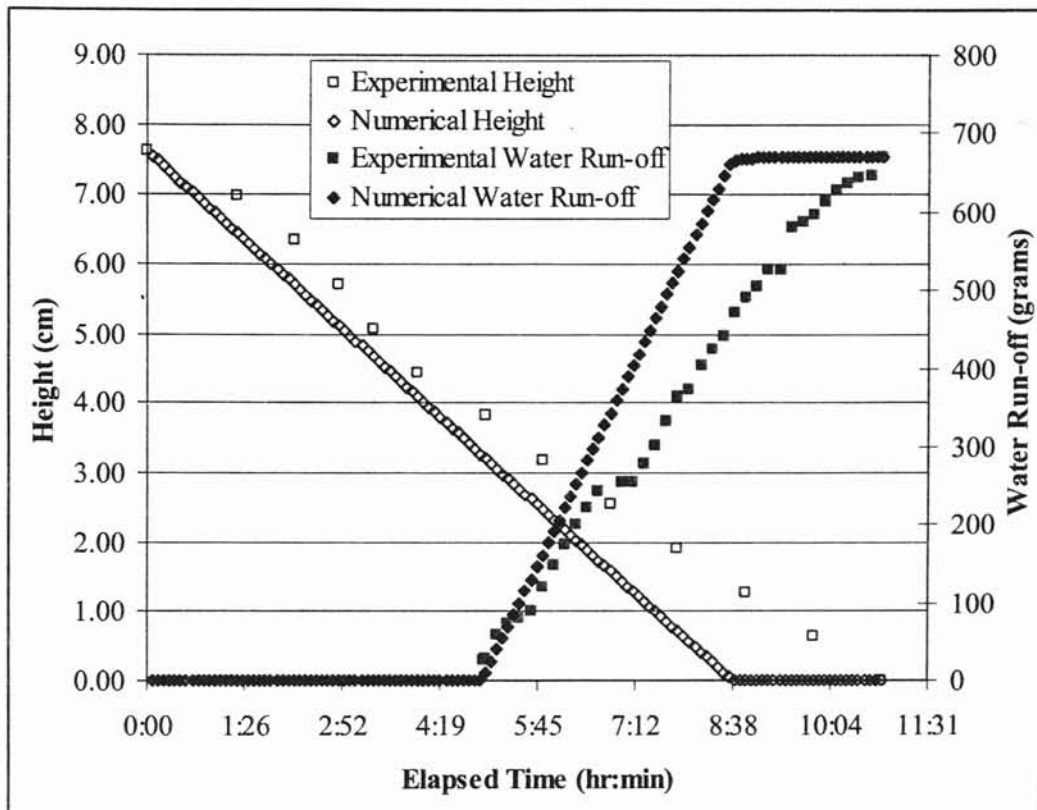


Figure D.1-5: Model vs. Experimental Height and Water Run-off Validation (316 W/m^2)

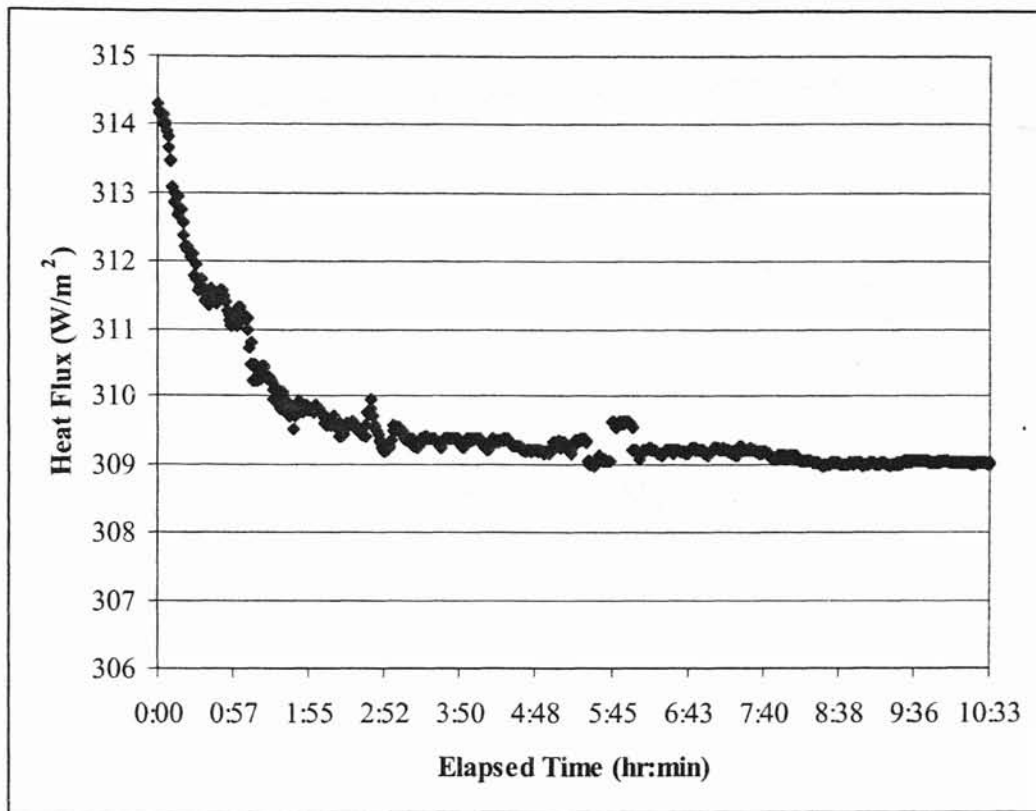


Figure D.1-6: Experimental Power Supply (316 W/m²)

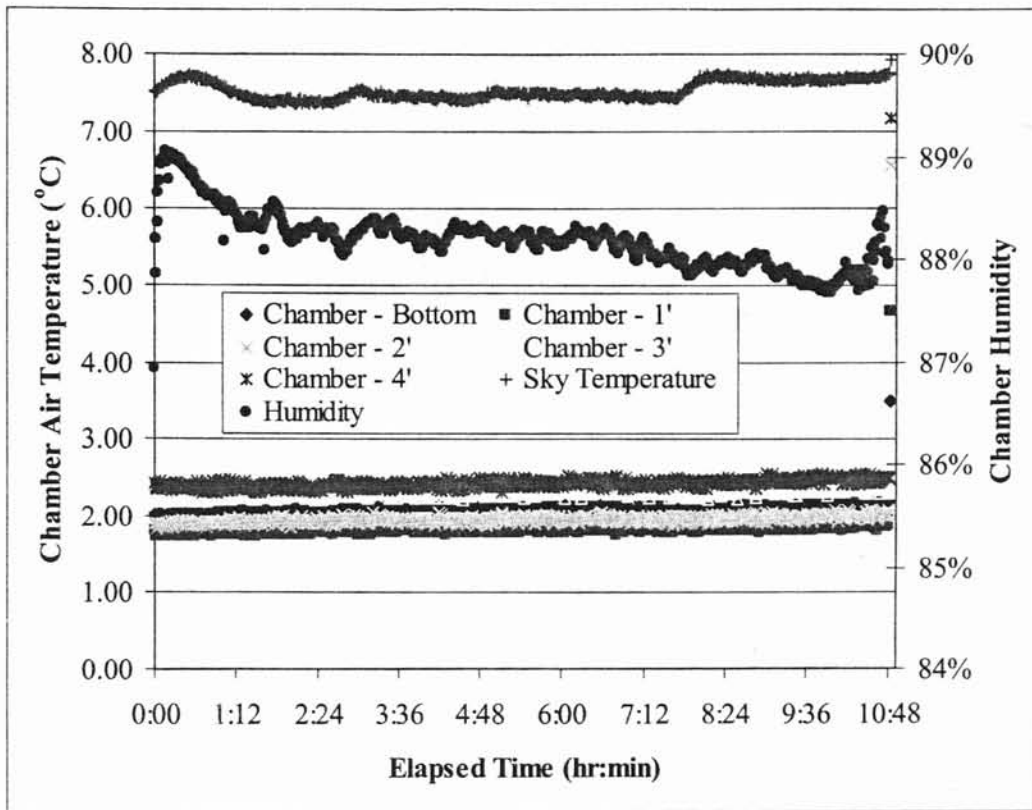


Figure D.1-7: Chamber Air and Sky Temperature and Chamber Humidity (316 W/m²)

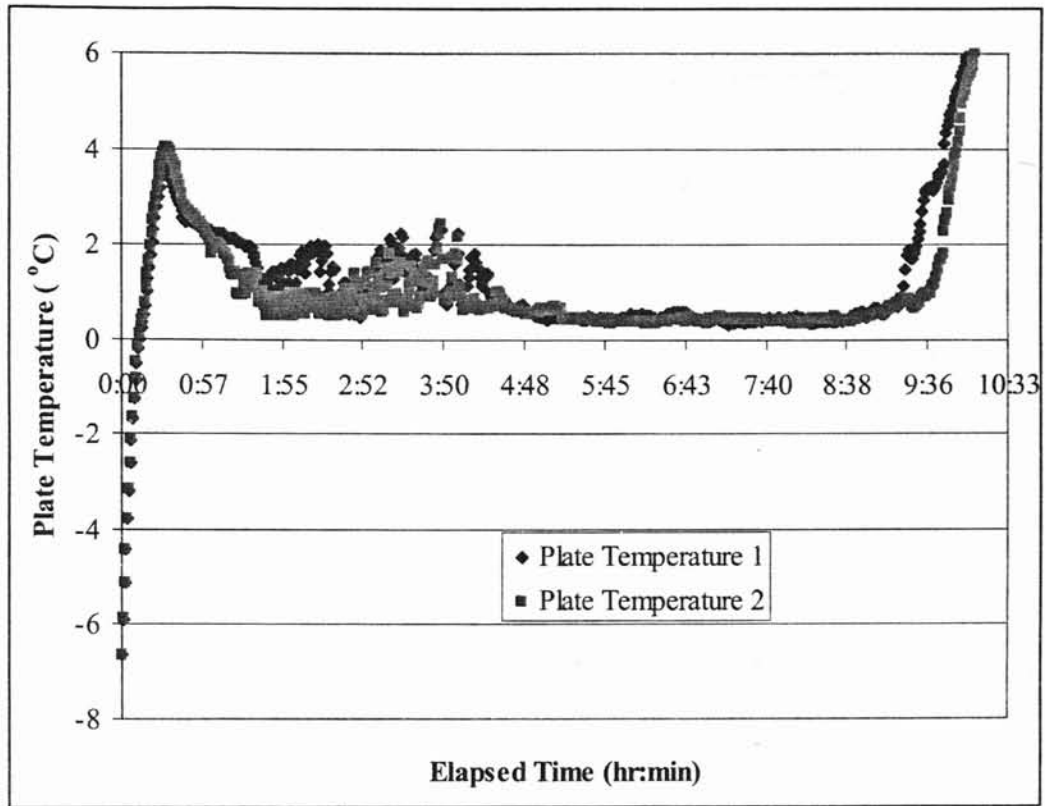


Figure D.1-8: Plate Temperature (316 W/m²)

473 W/m² Case

Initial Snow Mass = 772.3 grams

Snow Porosity = 0.5257

Snow Density = 439.0 kg/m³

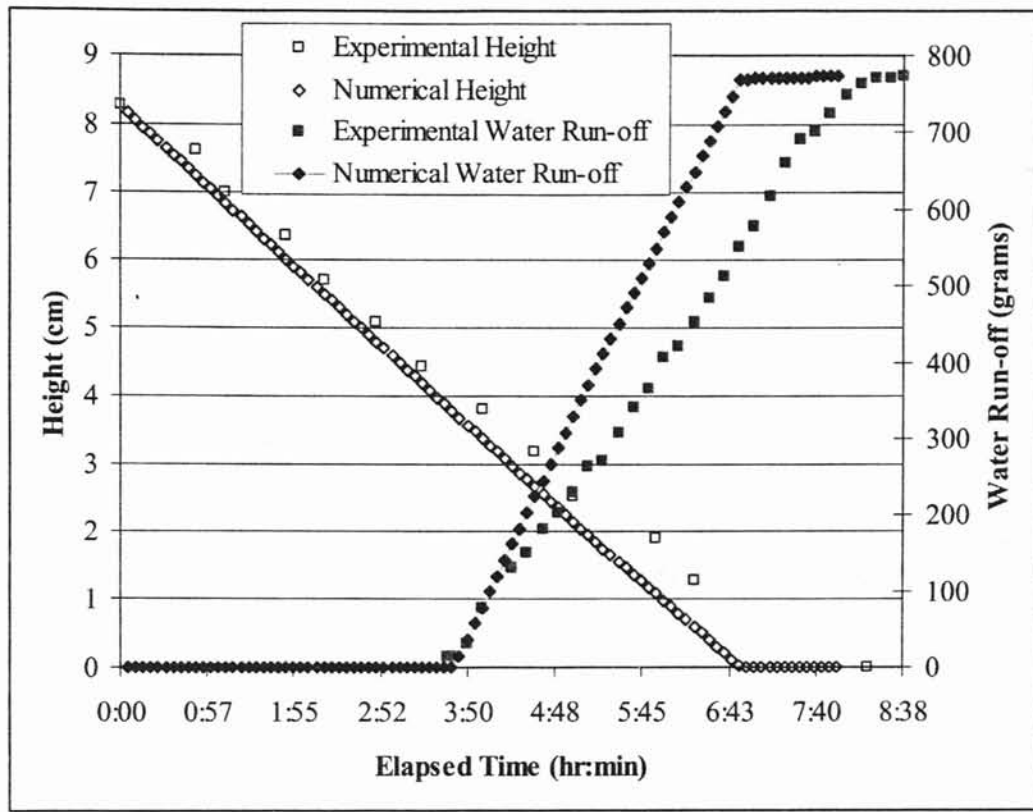


Figure D.1-9: Model vs. Experimental Height and Water Run-off Validation (473 W/m²)

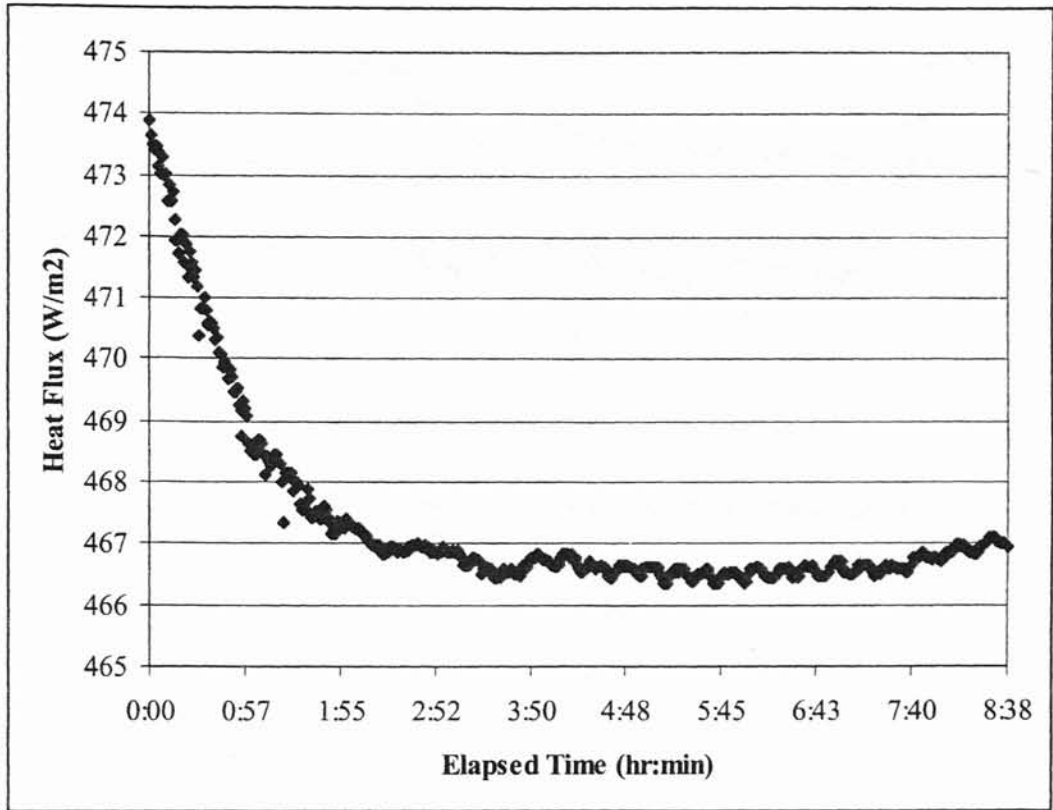


Figure D.1-10: Experimental Power Supply (473 W/m²)

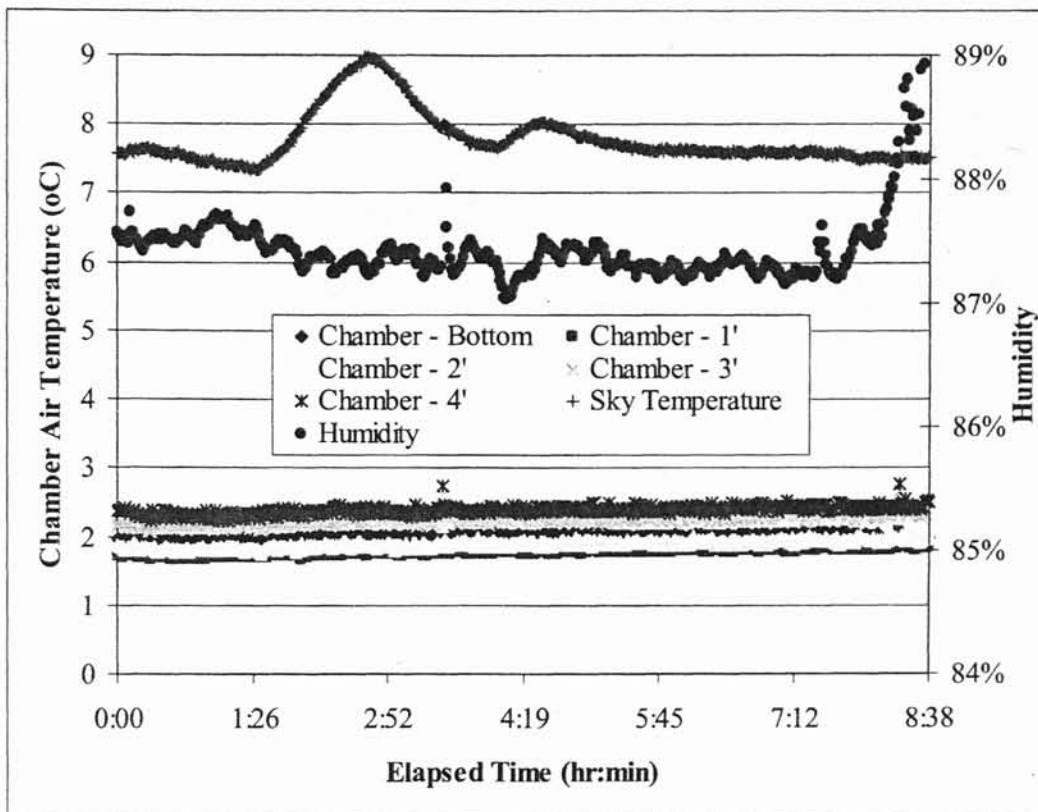


Figure D.1-11: Chamber Air and Sky Temperature and Chamber Humidity (473 W/m²)

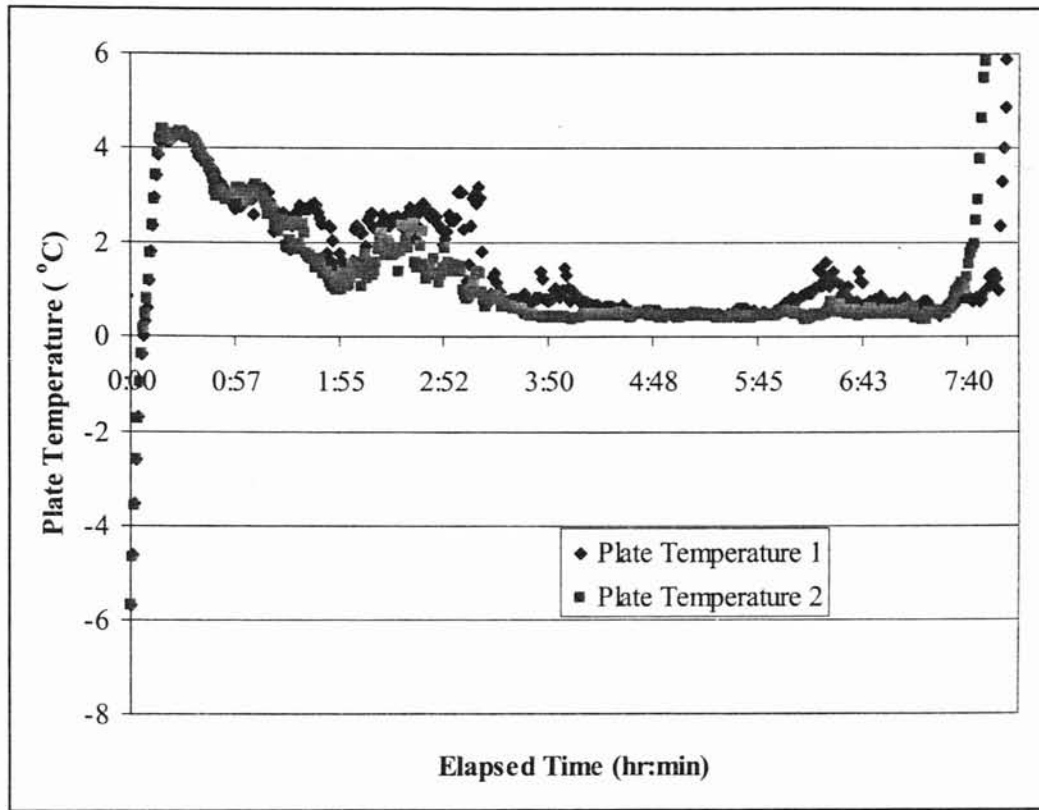


Figure D.1-12: Plate Temperature (473 W/m²)

631 W/m² Case

Initial Snow Mass = 696.0 grams

Snow Porosity = 0.5369

Snow Density = 426.1 kg/m³

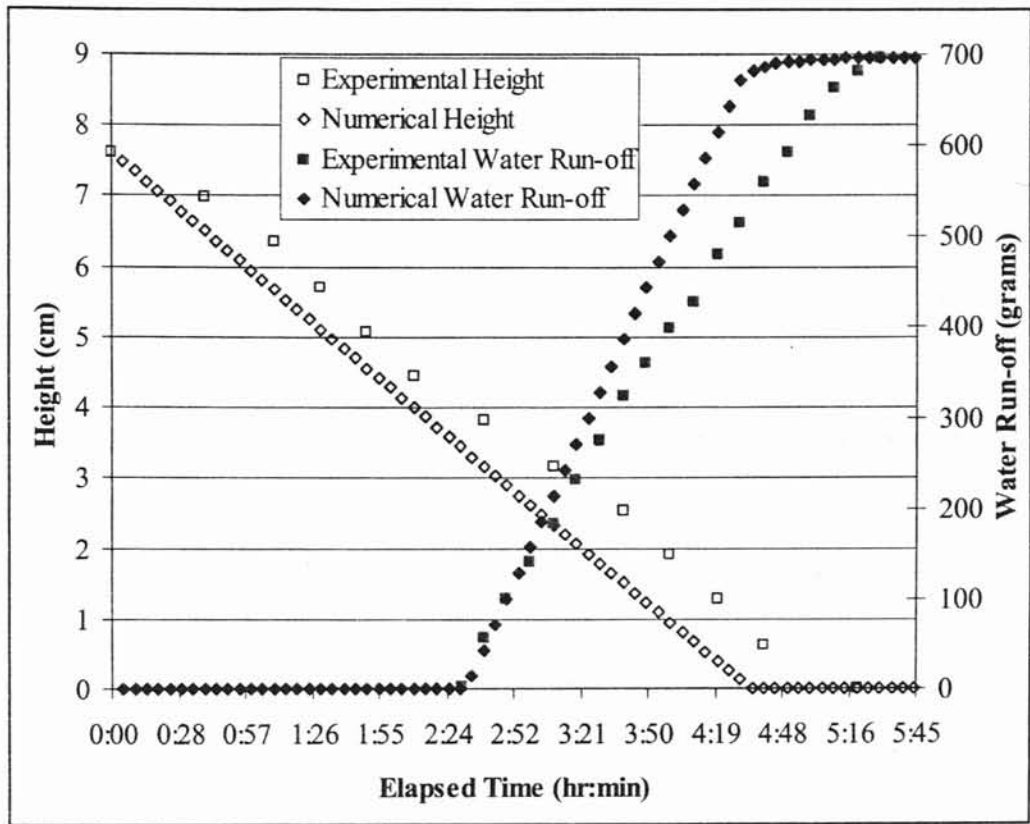


Figure D.1-13: Model vs. Experimental Height and Water Run-off Validation (631 W/m^2)

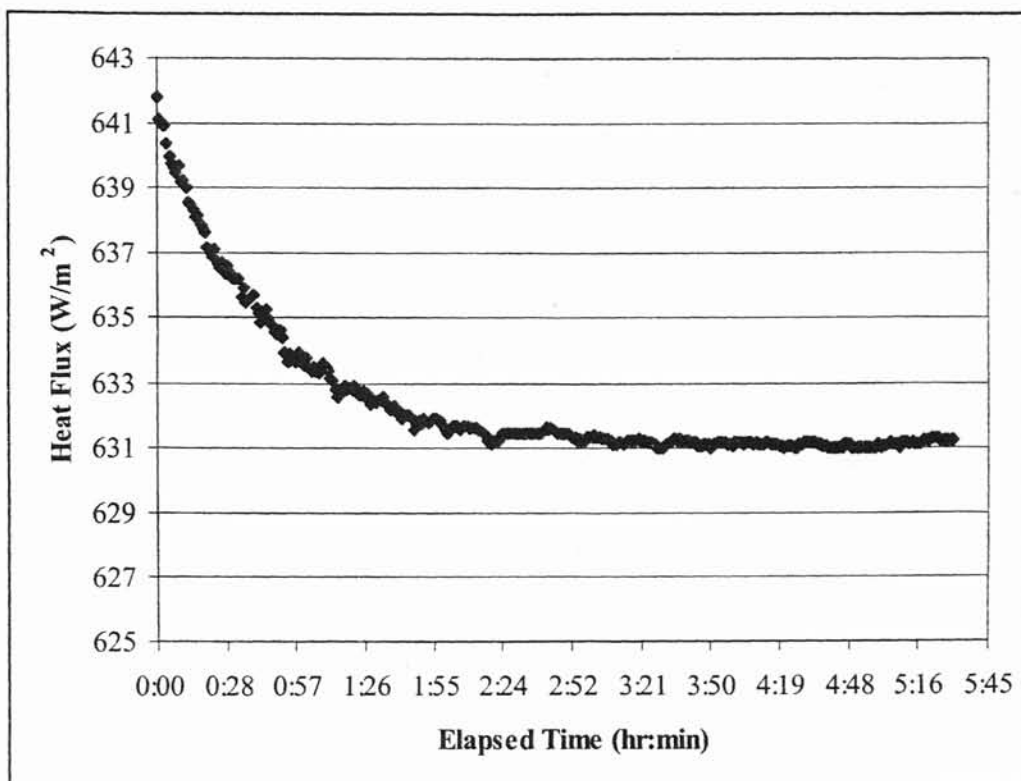


Figure D.1-14: Experimental Power Supply (631 W/m²)

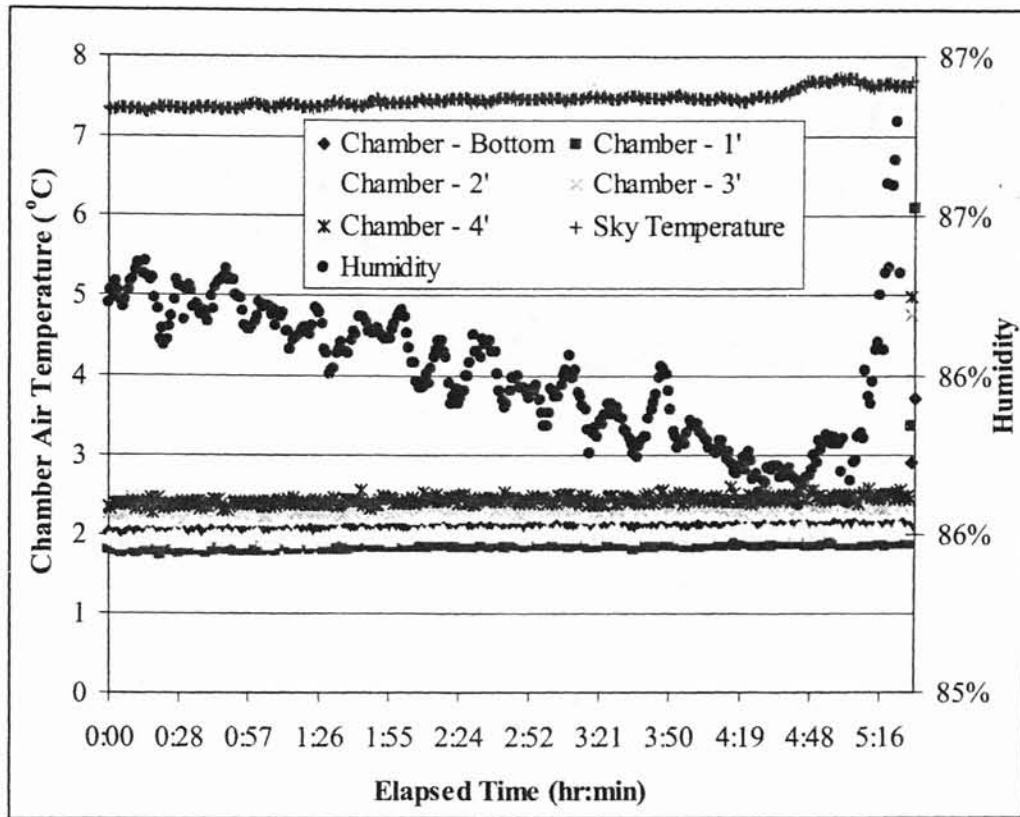


Figure D.1-17: Chamber Air and Sky Temperature and Chamber Humidity (631 W/m²)

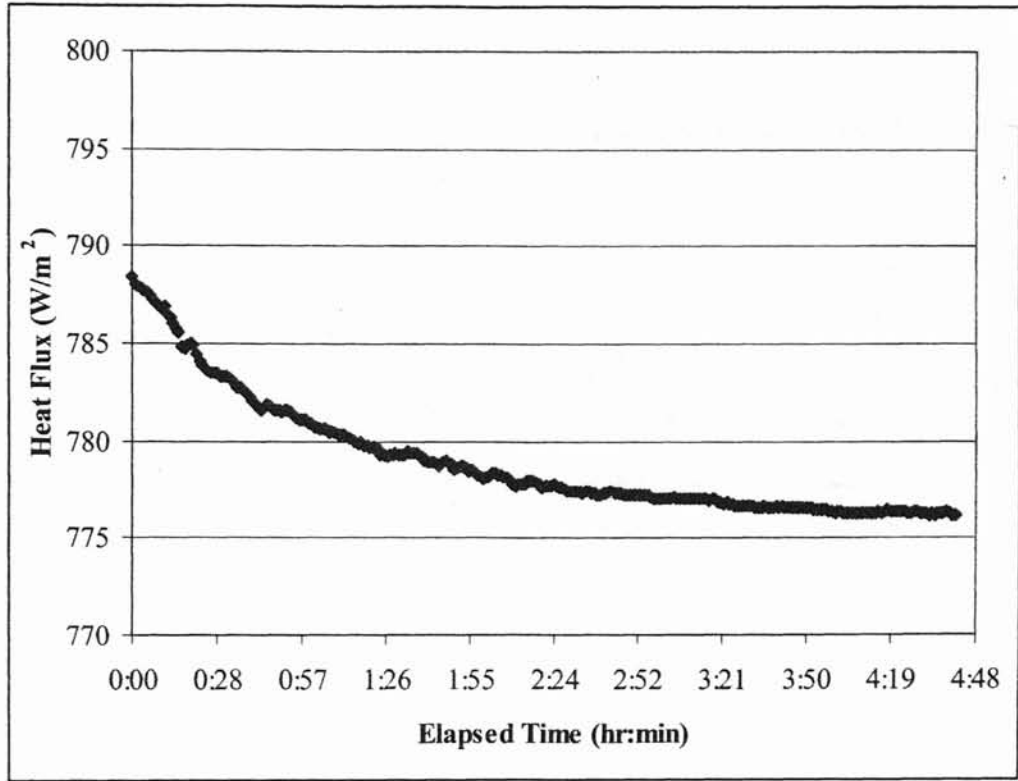


Figure D.1-20: Experimental Power Supply (789 W/m²)

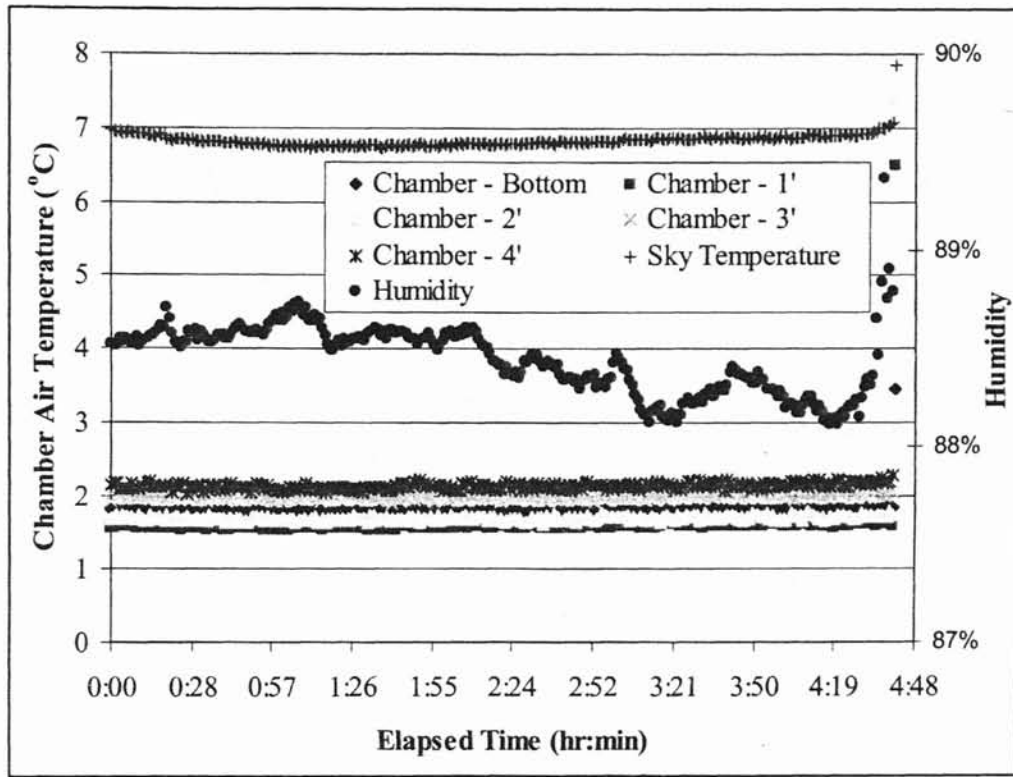


Figure D.1-21: Chamber Air and Sky Temperature and Chamber Humidity (789 W/m²)

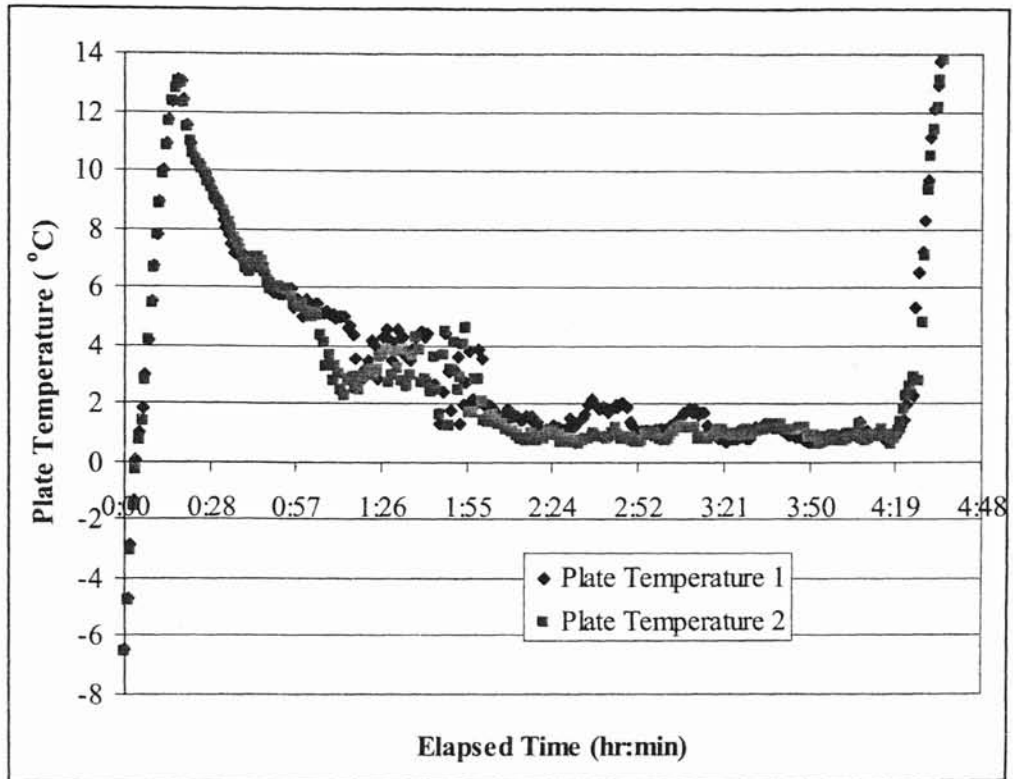


Figure D.1-22: Plate Temperature (789 W/m²)

VITA 2

Sean Lynn Hockersmith

Candidate for the Degree of

Master of Science

Thesis: EXPERIMENTAL AND COMPUTATIONAL INVESTIGATION OF SNOW
MELTING ON HEATED HORIZONTAL SURFACES

Major Field: Mechanical Engineering

Biographical:

Personal Data: Born in Oklahoma City, Oklahoma, June 14, 1976, the son of
Benny D. and Lenita I. Hockersmith

Education: Graduated from Redlands High School, Redlands, California, in June
1994; Received Bachelor of Science Degree in Chemical Engineering
from Oklahoma State University in May, 1999; Completed the
requirements for Master of Science degree at Oklahoma State University
in December 2002.

Experience: Summer Engineer Intern at Schlumberger Wire line, in Enid
Oklahoma, from May 1998 to August 1998; Research Assistant,
Department of Mechanical Engineering, Oklahoma State University,
August, 1999 to 2002

Professional Membership: ASHRAE